



TECHNISCHE
UNIVERSITÄT
WIEN

Vienna University of Technology

MASTERARBEIT

Application of aerogel-based plaster towards thermal retrofit of historical building facades: a computational assessment

ausgeführt zum Zwecke der Erlangung des akademischen Grades einer **Diplom-
Ingenieurin**

unter der Leitung von

Univ.-Prof. Dipl.-Ing. Dr. techn. Ardeshir Mahdavi

E 259-3 Abteilung für Bauphysik und Bauökologie

Institut für Architekturwissenschaften

eingereicht an der

Technischen Universität Wien

Fakultät für Architektur und Raumplanung

von

Olga Proskurnina

Matrikelnr. 1228030

Josef-Baumann Gasse 8a, 1220

Supported by the Erasmus Mundus Action 2 Program of the European Union

Wien, im Januar 2014

KURZFASSUNG

Diese Diplomarbeit befasst sich mit der Auswirkung der Aufbringung von Aerogel-basierten Dämmputzsystemen auf historische / artikulierte Fassaden. Im Rahmen der europäischen 20-20-20 Strategie besteht die Notwendigkeit die thermische Performance nicht nur von neuen Gebäuden, sondern auch des Gebäudebestandes zu verbessern. Weil viele für den Neubau einsetzbare Systeme aus verschiedenen Gründen (Denkmalschutz, Materialkompatibilität) im Gebäudebestand nicht oder nur sehr schwierig einsetzbar sind, ist die Entwicklung von neuen Materialien für gebäudebestandsgerechte thermische Sanierungen ein sich rasch entwickelndes Gebiet geworden. Aerogel-basierte Dämmputze stellen eine neue Alternative zu althergebrachten Dämmstoffen dar, die eine hohe Dämmleistung mit dem Erhalten der prinzipiellen Erscheinungsform von Fassaden kombinieren.

In dieser Diplomarbeit wird der Effekt eines Hochleistungs-Aerogel-Putzsystems auf typische Details von historischen Fassaden untersucht. Oftmals sind Anschluss- oder Ornamentdetails solcher Fassaden thermisch kritische Wärmebrücken, die im Zuge einer Sanierung besonderes Augenmerk benötigen. Daher werden in dieser Arbeit mit Hilfe eines numerischen Simulationsprogramms für Wärmebrücken verschiedene Sanierungsszenarien dieser Details unter Verwendung des Aerogel-Putzsystems untersucht, mit anderen Sanierungsvarianten verglichen und evaluiert. Betrachtete Indikatoren sind hierbei die sich ergebenden Innenoberflächentemperaturen, der lokale Wärmestrom im Bereich der Details und das Kondensations- und Schimmelrisiko. Zusätzlich wird der Effekt von Sanierungen mit den verschiedenen Varianten auf die energetische Gesamtperformance eines Gebäudes beispielhaft anhand eines typischen Wiener Gründerzeithauses illustriert.

SUMMARY

This thesis presents a study which refers to an impact of application of aerogel-based insulating plaster system on historical building facades. Considering European cutting-edge 20-20-20 strategy there is an urgent need of improving thermal performance of new and already existing buildings with the use of high-performing materials. In this regard, aerogel-based plaster is one of the most potential alternatives to current traditional building insulation materials, combining the benefits of traditional building insulation materials and enhanced thermal performance. The aim of this research is to address an issue of application of aerogel-based plaster, its thermal properties and thus its contribution to mitigating a heat loss through the building envelope and a thermal bridging effect. This work aims to evaluate performance of aerogel-based insulating plaster system, specifically interior surface temperatures, heat flow through a wall construction, condensation risk and mould growth via advanced computer tools. Additionally, an influence of thermal bridging effect on a calculation of annual energy demand of a typical Viennese historical building is analyzed.

Keywords

Thermal insulation, aerogel plaster, building envelope, energy performance, thermal bridge evaluation.

ACKNOWLEDGMENTS

Writing this master thesis has been an amazing journey that has taken me across two thousand miles away from home. It has also been a time of fantastic intellectual and personal growth, fostered by a wonderful learning environment.

First and foremost, I would like to express my sincere gratitude to my supervisor, Professor Ardeshir Mahdavi for his offered assistance and guidance at all levels of this work and for training me in this scientific field. His support and inspiring suggestions have been precious for the development of this thesis content.

This thesis was developed in a framework of AGelFa project (project number FFG-ID) at the Department of Building Physics and Ecology in cooperation with EMPA and Röfix AG. I would like to thank my co-advisor Dr. DI Ulrich Pont for his valuable support through this work.

I would like to express my gratitude to Erasmus Mundus MULTIC Mobility Scholarship for making this study possible with its generous financial support throughout whole period of study.

Finally, and most importantly, my deepest gratitude goes to my dear family, whose unflagging love and unconditional support encouraged me throughout my live and studies.

for my everloving family

TABLE OF CONTENTS

Kurzfassung	II
Summary	IV
Acknowledgments	VI
Notations	XII
1 Introduction	1
1.1 Motivation	1
1.2 Background	2
1.3 Thermal building insulation materials	3
1.4 Conventional insulation materials	4
1.5 Advanced insulation materials	8
2 Silica aerogel	12
2.1 Structure of silica aerogel	12
2.2 Synthesis of silica aerogel	12
2.2.1 Gel preparation	13
2.2.2 Aging of the gel	13
2.2.3 Drying of the gel	14
2.2.4 Building applications of silica aerogel	14
3 Theoretical and technical framework	16
3.1 Theoretical basis	16
3.2 Legal framework for building renovation	18
3.3 Fundamentals of building physics for evaluation of thermal bridges	19
3.3.1 Types of thermal bridges	20
3.3.2 Numerical calculation of thermal bridges	21
3.4 General principles of numerical modelling of thermal bridges	23
3.5 Numerical calculation software	25
3.5.1. Implementation of the simulation	27

4	Methodology	29
4.1	Modelled scenarios and set of junctions	29
4.2	Evaluation of annual energy demand of a building	32
	Calculation of each scenario is implemented with two different options: approximate calculation of thermal bridges and detailed calculation of thermal bridges	34
4.3	Characteristics and application of aerogel-based plaster	34
5	Technical evaluation of details	38
5.1	Brick wall with natural stone cornice	39
5.2	Wooden slab with a gravel filling	44
5.3	Natural stone cornice with steel anchoring	50
5.4	Ventilated attic with retrofitted ceiling slab	55
5.5	Double-box window	62
6	Calculation of annual energy demand	73
7	Discussion	77
8	Conclusion	81
9	References	83
10	List of figures	87
11	List of tables	91
12	Appendix	93
A.	Heat transfer coefficient of double-box windows	93
B.	Building matrix	95
C.	Documentation of a building in Habichergasse 20, Vienna	97

NOTATIONS

Roman upper case letters

Q	Heat flow rate, [W]
R	Thermal resistance, [$\text{W}\cdot\text{m}^{-2}\cdot\text{K}^{-1}$]
RH	Relative Humidity, [%]
T_i, T_e	Temperature of external and internal environment, [$^{\circ}\text{C}$]
U	Heat transfer coefficient, [$\text{W}\cdot\text{m}^{-2}\cdot\text{K}^{-1}$]
L^{2D}	Thermal coupling coefficient, [$\text{W}\cdot\text{m}^{-1}\cdot\text{K}^{-1}$]
H_{total}	Total heat loss of the building, [$\text{W}\cdot\text{K}^{-1}$]
HWB	Annual energy demand of a building, [$\text{kWh}\cdot\text{m}^{-2}\cdot\text{a}$]

Roman lower case letters

c_p	Specific heat capacity, [$\text{J}\cdot\text{kg}^{-1}\cdot\text{K}^{-1}$]
d	Thickness, [m]
m	Mass, [kg]
l	Length, [m]

Greek lower case letters

λ	Thermal conductivity, [$\text{W}\cdot\text{m}^{-1}\cdot\text{K}^{-1}$]
μ	Vapor diffusion resistance factor, [-]
ρ	Density, [$\text{kg}\cdot\text{m}^{-3}$]
ψ	Linear heat transmittance value, [$\text{W}\cdot\text{K}^{-1}$]
f_{Rsi}	Temperature factor, [-]

1 INTRODUCTION

Managing acceptable temperatures in the borders of building envelope by heating and cooling requires a significant amount of energy. This energy load is responsible for high greenhouse emissions. For instance, CO₂ emissions from residential, commercial and public service buildings in Austria comprised 9.94 million metric tons in 2010, according to the indicators from the World Bank. Therefore, there is an urgent need to improve thermal performance of buildings in order to decrease CO₂ emissions from residential, commercial and public service buildings, produced by fuel combustion for heating.

It is well-known that a building has to be properly planned and insulated to be thermally and structurally sound. Proper planning can decrease the amount of energy used for maintaining the interior climate of the house by minimizing the heat transfer through the envelope. Main weak points of such heat transfer are thermal bridges, parts of the building envelope which represent an area of a relatively high heat flow compared to the rest of the building envelope. Avoiding thermal bridges or rather minimizing the effect of already existing thermal bridges can be reached with an adequate and accurate use of insulation, which must be placed through the whole external surface. This rule seems a very simple one, but it is not followed on many construction sites either because of neglecting it or due to the lack of sufficient skills.

Retrofit of historical facades of the building stock has grown in importance due to energy efficiency considerations in the building sector. Consequently, a considerable attention is drawn to older buildings with strongly-articulated, as historical meaningful facades require sophisticated approaches. Along recent new construction technologies, aerogel-based plaster systems with high thermal insulation have been developed in the past few years by the AEC-industry. Although still rather expensive, these systems offer opportunities to insulate highly-articulated historical facades in compliance with the principles of heritage protection.

1.1 Motivation

Heating and cooling load studies have concluded that heat transfer through wall structures is an influential factor in energy loss in residential buildings, 8 % greater than the heat transfer through windows, and 39 % greater than transmission through roofs (Kosny 2008). Major part of heat transfer through the wall structure is passed directly through the building envelope, whether it is masonry, block or stud frame. This process is known as "thermal bridging". Aerogel can be an ultimate solution in building construction and energy efficiency

retrofits, considering that it has extremely low thermal conductivity value of $0.014 \text{ W}\cdot\text{m}^{-1}\cdot\text{K}^{-1}$ (AAAMSA 2001) and accordingly extremely high thermal resistance. Even though the price of such a technically advanced material is normally five times more expensive than of traditional type of insulation, the cost is expected to decrease with a currently growing volume of production.

Majority of scientific studies focused on aerogel thermal conductivity qualities and its synthesis process. Methods of its commercial application such as thermal window insulation, acoustical barriers, supercapacitors and catalytic supports have been suggested, but so far a little has resulted in the way of its actual application (Hrubesh and Pekala 1994, Schmidt and Schwertfeger 1998, Fricke and Tillotson 1997, Pierre and Pajonk 2002). Additionally, there is a lack of research in application of those materials in a construction industry and especially retrofit methodologies.

1.2 Background

Plenty of research has been carried out on a topic of aerogel production and characterization. Graham (1864) has proven in his research that water in silica gel could be potentially replaced by such organic liquids, as alcohol, xylene and paraffin. The final product that biologists reached was a gel, in which the organic part of the composed elements is a disperse phase instead of water.

These discoveries have led Kistler (1932) to understanding that gel, which once was created, has a structure independent from the liquids in its pores and that the liquid can be as well replaced by a gas. The main challenge consisted in removing the liquid without deconstructing the gel structure. Normally, as liquid is removed from gel, surface tension of a liquid causes significant shrinkage and forces the structure to collapse. A method for solving this problem is drying the gel at high temperature and high pressure conditions, so that the liquid is found in its supercritical state. The main feature of such state is that the difference between liquid and gas is minimal. This fact leads to a little effect on surface tension. Hence, liquid molecules can be removed from the gel without deconstructing the porous structure.

Kistler's method of aerogel production was relatively complicated and time-consuming, thus could take several weeks to be accomplished. A considerable improvement was done by the team of Stanislaus Teichner at Universite Claud Bernard, Lyon, France. They have been asked by French Government to develop a method of storing oxygen and rocket fuels in porous materials. The team succeeded in developing a better synthetic process, which replaced the sodium silicate used by Kistler with alkoxysilane.

After this discovery, new developments in aerogel science and technology rapidly took place as a high number of researchers joined this field. In 1985 the first International Symposium on Aerogels was organized by Professor Jochen Fricke in Wurzburg, Germany. Twenty-five scientific papers were discussed by researchers from around the world at this event.

In the late 1980s, the world's lowest density silica aerogel (and the lowest density solid material) was produced by researchers at Lawrence Livermore National Laboratory lead by Hrubesh. A density of this aerogel comprised 0.003 g.cm^{-3} , three times that of air (Open Source Nanotech 2013).

1.3 Thermal building insulation materials

Thermal insulation plays a significant role in meeting the energy demand of a building. With that purpose, a big amount of new state-of-the-art insulation materials and systems are being developed, along with the use of common traditional materials with an increasing thickness in building envelopes. Nevertheless, a high thickness of building envelopes should be avoided due to a number of foregoing primary reasons, along with parameters of specific conditions, e.g. interior volume, economical issues, architectural prohibitions, use of building materials etc.

Many primary reasons for using a proper thermal insulation can be listed, the main are:

- Conservation of energy
- Decreasing heat loss or gain
- Providing a comfortable environment
- Maintaining temperature conditions
- Preventing condensation and mould

Transfer of heat through insulation materials occurs by the means of conduction, while heat loss or gain from the environment occurs by the means of convection and radiation. Effectiveness of insulation is commonly evaluated by its key property R-value [$\text{m}^2 \cdot \text{K} \cdot \text{W}^{-1}$], resistance to conductive heat flow. The R-value depends on the type of insulation, its thickness, and its density. This measure is established in a laboratory under specific conditions but these are not necessarily real world conditions, other factors influence the effectiveness of insulation. In general words, the higher the density of the insulation, the greater the thermal conductivity is, i.e. metals obtain a high density and high thermal conductivity. Other corresponding parameters - thermal conductivity λ [$\text{W} \cdot \text{m}^{-1} \cdot \text{K}^{-1}$], which evaluates material's ability to conduct heat and thermal transmittance U-value [$\text{W} \cdot \text{m}^{-2} \cdot \text{K}^{-1}$], which measures the rate of heat transfer through a building element over a given area

under standardised conditions. For a well-performing insulation, it is important to obtain a high thermal resistance R-value, and consequently a low thermal transmittance U-value. Materials, which obtain a low thermal conductivity, are characterized with a high amount of small voids, filled with gas or air. Their size is too small for transmitting heat by the means of convection or radiation. Hence, they facilitate decreasing heat flow. Other criteria for comparison are important as well: weight, porosity, density, flammability, high resistance to chemical corrosion as well as water absorption and impermeability. Comparison of the main characteristics of insulating materials is presented in Table 1 of this chapter.

1.4 Conventional insulation materials

This chapter provides an overview of the properties of the most traditional insulation materials nowadays used in construction industry. They have been chosen for the reason of their comparatively low thermal conductivity values.

Mineral wool

There are different types of mineral wool which are named after its primary products, used in production, i.e. glass wool, sand limestone and soda or rock wool made of different minerals like e.g. basalt, binders and lubricant/spinning oil. Along with heat, cold and noise insulating function, they serve as fire protection due to their high temperature resistance, up to 700-1000 °C (Saint Gobain Group 2008). Notwithstanding the fact that mineral wool is water-repellent, adherence of water is possible. A proper installation is of high importance for preventing a change in thermal resistance due to shrinkage. The schema of material is presented in Figure 1. Its thermal conductivity ranges between 0.030- 0.050 W·m⁻¹·K⁻¹. Due to durability of several decades (up to ca. 80 years) and amortization period of 3 to 8 months, it is a very popular insulation material despite the high energy consumption within the production (Saint Gobain Group 2008). There are processes which integrate shredded mineral wools into bricks to recycle used insulations. However it should be mentioned that extremely old mineral wools have to be disposed separately and marked because of their potentially carcinogenic fiber dusts. Alike, newly installed mineral wools have to be biodegradable.

Expanded polystyrene

Expanded polystyrene (EPS) is a lightweight material that can be manufactured from oil. The process is called polymerization, in which small spheres of styrene with an expansion agent join at their contact areas and form large molecules of polystyrene. Typical thermal

conductivity of EPS varies in a range of $0.033 \text{ W}\cdot\text{m}^{-1}\cdot\text{K}^{-1}$ at $30 \text{ kg}\cdot\text{m}^{-3}$ and $0.038 \text{ W}\cdot\text{m}^{-1}\cdot\text{K}^{-1}$ at $15 \text{ kg}\cdot\text{m}^{-3}$, depending on its claimed density and moisture content (AAAMSA 2001).

Polystyrene foams are used for a wide range of applications because of their highly insulating properties. They represent a good thermal insulation, have a high resistance to moisture and are extremely lightweight and portable. Expanded polystyrene do not result into chemical reactions because of its passive nature, thus it can be easily used in the construction industry. Application can also be found in insulated panel systems, insulation for facades, walls, roofs and floors in buildings. Schema of material is presented in Figure 2.

Extruded polystyrene

Extruded polystyrene (XPS) is produced by a continuous process of extrusion. The plastic granules are added into an extruder, where the mixture is melted into a plastic fluid under the strict conditions of high temperature and pressure, which is then forced through a die into the desired shape. Further, plastic fluid expands to a foam, which is shaped, cooled, and cut to required dimensions. XPS consists of closed cell structure and provides good surface roughness, stiffness and lower thermal conductivity. Typical thermal conductivity values of XPS are in a range of $0.027 \text{ W}\cdot\text{m}^{-1}\cdot\text{K}^{-1}$ at $28 \text{ kg}\cdot\text{m}^{-3}$ to $0.036 \text{ W}\cdot\text{m}^{-1}\cdot\text{K}^{-1}$ at $45 \text{ kg}\cdot\text{m}^{-3}$, depending on its claimed density and moisture content (AAAMSA 2001).

The closed cell structure of the XPS foam ensures absence of capillary water absorption though water vapour movement is possible. XPS is very weather- resistant, but can be supported by at least 5 cm of gravel under the board, to ensure the protection from hail and wind forces, as well as UV radiation. XPS boards have a resistance to construction materials such as plasters, cements, bitumen and acids, while they are non-resistant to fuels and lacquer solidifiers. XPS products can be trimmed and adjusted to a desired size at the construction site without losing a good value of thermal conductivity. Schema of material is presented in Figure 3.



*Figure 1. Scheme of mineral wool
(Knaufinsulation 2011)*



*Figure 2. Scheme of expanded polystyrene
(Finehomebuilding 2008-2011)*

Polyurethane

Polyurethane (PUR) is a flexible foam, produced by reaction of a polyol (an alcohol with two or more reactive hydroxyl groups per molecule) with a diisocyanate or a polymeric isocyanate provided that suitable catalysts and additives are added. Polyurethane has a density of $40\text{--}60\text{ kg}\cdot\text{m}^{-3}$, and thermal conductivity of $0.035\text{ W}\cdot\text{m}^{-1}\cdot\text{K}^{-1}$ at $10\text{ }^{\circ}\text{C}$, according to Ochs and Muller-Steinhagen (2005), which varies with temperature, its density and moisture content. Polyurethane is characterized with light weight depending on its density, high-performing thermal and sound insulation properties, high resistance to chemical elements and low water absorption. Polyurethane products are used for thermal insulation as well as sound insulation materials in high-rise buildings. It can also be used as expanding foam at the construction site, for sealing the openings of doors and windows; as a shockproof package and filling material.

Even though PUR is a harmless material for its intended purpose, it is extremely harmful in a case of high temperatures and fire. While burning, polyurethane releases poisonous cyanide (HCN) and isocyanites. Typically, hydrogen cyanide is released with a smoke from burning plastics. Scheme of material is provided in Figure 4.

Cellulose

Cellulose (polysaccharide) is thermal insulation material made of 80 % post-consumer recycled newsprint or wood fibre mass. The fibre is chemically processed with boric acid (H_3BO_3) and borax to resist fire, insects and mould. In fact, many specialists describe cellulose as more fire-safe than fiberglass. This claim is based upon the fact that cellulose fibers are tightly packed, which stop fire spreading through the cavities. Typical thermal conductivity values of cellulose vary between $40\text{--}50\text{ W}\cdot\text{m}^{-1}\cdot\text{K}^{-1}$. Cellulose may serve as a filling material for different cavities and spaces, while it can also be produced as insulation boards and mats. Cellulose products are used in wall and roof cavities for division of the inside and outside space, for thermal and acoustical insulation, fire prevention and moisture barrier. In addition, cellulose is an ecological and recycled insulation material for increasing the sustainability of the construction. Scheme of the material is represented in Figure 5.

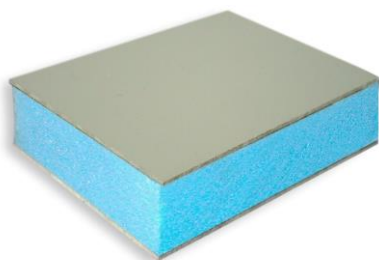


Figure 4. Scheme of extruded polystyrene (Archiexpo 2001)



Figure 3. Scheme of polyurethane foam (Directindustry 2008)



*Figure 5. Scheme of cellulose
(Abemiddleton 2006)*



*Figure 6. Scheme of perlite plaster
(Yougigypsum 2013)*



Figure 7. Scheme of cork material (Wikimedia 2014)

Perlite plaster

Perlite plaster consists of a mixture of expanded perlite with either gypsum or portland cement. In a well-fitting proportion perlite plaster can be applied to walls and ceilings or to metal and gypsum lath for fireproofing structural steel. It is characterized as a very lightweight material, which also decreases transportation costs, very fire-retardant, as it provides up to 5-hour fire protection with a thin layer of material and its minimum weight. It is also very noise-isolating, reducing sound transmission through partition walls. Thermal conductivity of perlite plaster comprises $0.08 \text{ W}\cdot\text{m}^{-1}\cdot\text{K}^{-1}$ (Reichel et al. 2004), its resistance to heat transmission is 4 times higher than sand plaster. Schema of material is in Figure 6.

Cork

Cork insulation is generally made out of cork oak tree, which can be seasonally obtained from it. It is a renewable material with thermal conductivity value of $0.45 \text{ W}\cdot\text{m}^{-1}\cdot\text{K}^{-1}$ at 25°C and thermal diffusivity of $1\times 10^{-6} \text{ m}^2\cdot\text{s}^{-1}$ (Sliva 2005).

Moreover, cork is barely permeable to liquids, it is highly compressible, chemically stable and durable. For mentioned above qualities, its products have been used as bottle sealants, as well as for thermal insulation for buildings. Cork is produced as a filling material as well as in cork boards. Its insulation products can be drilled and cut on the construction site to reach the required dimensions, without any change in thermal resistance. Schema of the material can be seen in Figure 7.

1.5 Advanced insulation materials

At present times, traditional insulation materials are still the most widely used materials in a building insulation. Though, there are multiple disadvantages in case of highly insulated envelopes with traditional materials, such as bulk envelope, limited interior area, architectural regulations for retrofit of heritage buildings. Advanced thermal insulation materials are perspective solutions of today with the lowest conductivity. Below, descriptions of state-of-the-art materials are given.

Gas-filled panels

Gas-filled technology was developed by Lawrence Berkeley National Laboratory. Gas-filled panel (GFP) is a panel consisting of thin polymer films of low-e metalized aluminium. These baffled pockets are filled with low-conductivity gas or air, i.e. Argon (Ar), Krypton (Kr), Xenon (Xe), which retard air flow through the wall. GFPs are completely hermetic panels, which are flexible in shape and are produced in variety of shapes and dimensions. Schema of the material can be seen in Figure 8. Thermal conductivity of gas-filled panels is quite high in the range of $0.0074\text{--}0.0281\text{ W}\cdot\text{m}^{-1}\cdot\text{K}^{-1}$, depending on a type of a gas (Oak Ridge National Laboratory 2006).

Though, it can lose a significant part of its insulating ability in case of puncture, when air will gradually replace existing low-conductivity gas with time. GFP's R-value with various gas fillings can be seen in Figure 9.

With its low thickness and excellent thermal insulation properties, GFP technology is perfectly applicable in new and already constructed residential and commercial buildings. GFP insulation is also relevant for cavity-filling applications. It could be installed into walls, ceilings, floors, as well as doors, radiators, refrigerators, and other appliances. GFP has a



Figure 8. Scheme of gas-filled panel
(Builderonline 2009)

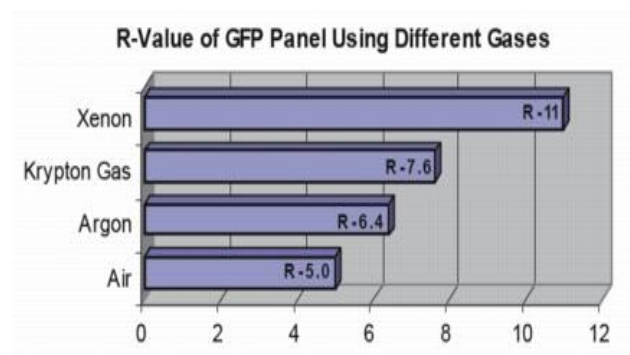


Figure 9. R-value of GFP (Buildinggreen
2006)

possibility to be combined with phase-change materials and other products of building thermal insulations.

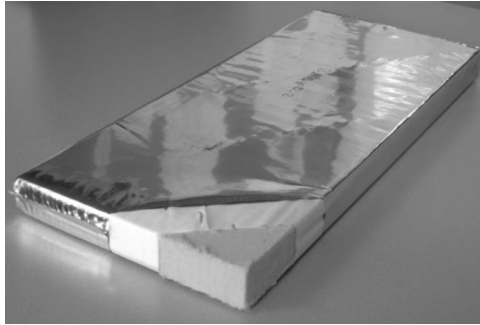
Vacuum insulation panels

Vacuum insulation panels (VIP) are technologically advanced thermal insulation products, which combine a low thermal conductivity value and a thin layer of envelope. A vacuum insulation panel consists of three parts: walls of the membrane, isolating a panel from outside air; a panel made of highly-porous material for protecting the membrane walls from atmospheric pressure when panel is under the vacuum conditions; chemical materials, used for sealing the panel walls. There are panels with a wide variety of barrier types, made of metal sheeting, metal foil, polymer films, and combinations of polymer films and metal foils with metalized layers which are composited into single films. VIP panels provide much more effective insulating value in comparison with other insulation materials, such as foam boards, wool or fiber blankets. Panels can be produced in virtually any dimensions, what makes their application easy. They are generally installed directly on the construction site. The most widespread case is insulation of flat roof terraces with vacuum panels. This provides a simple solution of avoiding big difference in thickness of the construction between the room and the terrace.

At the same time, the main disadvantage of using VIP is its fragility: it loses the main part of its insulating capacity in case of puncture, as well as GFP, which might happen during the installation or use of the panel. Moreover, another weak point is sealing: it might considerably increase its conductivity, especially with age, depending on the design of installation. VIP should be installed in the construction in a way of providing a future possibility of replacing them without much effort. The quantitative wide use of vacuum insulation is still restrained by mainly two factors: high price and low confidence in VIP technology and in its use in building applications. Overall thermal conductivity of VIPs comprises $0.0056 \text{ W}\cdot\text{m}^{-1}\cdot\text{K}^{-1}$ (AAAMSA 2001). Schema of the material is in Figure 10.

Aerogel

Aerogel is a thermal insulation material, representing the highest potential of all at the moment. It is claimed to be the lightest solid material in the world with very low density of $3 \text{ kg}\cdot\text{m}^{-3}$ and extremely low conductivity value of $0.014 \text{ W}\cdot\text{m}^{-1}\cdot\text{K}^{-1}$, which may be reached at a pressure of 50 mbar (AAAMSA 2001).



*Figure 10. Vacuum insulation panels
(Emeraldinsight 2012)*



*Figure 11. Scheme of aerogel (Illumina-
Chemie 2008)*

A range of potential building applications is very wide, provided by the fact that aerogels can be produced as opaque and translucent material. Nevertheless, production cost is the main factor, which restricts a scale of production and application of aerogel at present time. More detailed information about this material will be elaborated in the next chapter of this work. Schema of the material is presented in Figure 11.

Phase-change materials

Phase-change materials (PCM) are substances, which have a high ability of storing and releasing big amounts of energy. They change its state from solid to liquid in case of heating up. Conversely, when the temperature drop happens again, material will solidify, while radiating back earlier absorbed amount of heat into the building. Therefore, they represent a smart thermal mass, able to contribute a lot to building performance. Several characteristics of PCM are especially exceptional: phase change melting temperature range of 25 °C, low cost of various paraffins, they are non-hydroscopic and non-corrosive. Those are important qualities for choosing certain PCMs for building application. They are not included into comparison table due to variety of PCM components and its different characteristics.

Table 1. Physical and thermal properties of typical insulation materials (AAAMSA 2001; FIXIT AG 2013; Gulf Perlite Manufacturers 2009; Griffith 1995)

Insulation material	Density [kg·m⁻³]	Thermal conductivity λ [W·m⁻¹·K⁻¹]	Vapor diffusion resistance factor μ [-]
Glass mineral wool	10 to 80	0.018-0.022 (at 10 °C)	n/a
Expanded Polystyrene (EPS)	30	0.033 (at 10 °C)	25
Extruded Polystyrene (XPS)	100-150	0.027-0.036 (at 10°C)	0.15 to 0.075
Cork	120-200	0.038	20 to 40
Perlite Plaster	70-80	0.08	1
Aerogel plaster	220	0.028	4 -5
Vacuum Insulation Panels (VIP)	110-145	0.0056 (at 13 Pa or 25 °C)	n/a
Gas-filled panels (GFP)	10-14	0.028 for air 0.020 for argon 0.012 for krypton	n/a
Silica aerogel	3	0.013-0.016 at atmospheric pressure	33

2 SILICA AEROGEL

Aerogel is the lightest solid material known in the world, which is composed of 98 % air. Its physical and thermal properties are undoubtedly remarkable, especially its low density and conductivity value. It might be mistakenly thought that aerogels are the products of a recent technological progress. In reality, research on aerogel started by Kistler (1931), as it was described in a previous chapter. The name “aerogel” refers to the way of its production: it is technically a gel, with a gas or vacuum filling its pores instead of a liquid. Silica aerogel is the most widely used type of aerogel, which has the chemical formula SiO_2 . It is insulating glassy material widely used in high-tech and building applications (Open Source Nanotech 2013). Schema of the material is presented in Figure 12.

2.1 Structure of silica aerogel

Silica aerogel is characterized by 3-dimensional network of molecules, containing solid state and pore structure, filled with air or vacuum. This solid framework consists of nanoparticles of silica – the oxide of silicon. The way that these nanoparticles connect together in order to create a network differs and mostly depends on a process of gel production. Primary nanoparticles of silica aerogel, sized 2-50 nm in its diameter, are connected together into bigger spherical particles of a size 50 nm-2 μm (2000 nm) in its diameter. As the next step, they are linked together and result as cross-linked polymers resembling a string of pearls. In case of acid-catalysed gel production process, smaller nanoparticles do not connect together into bigger structures and thus form a structure resembling a leaf-like shape (Open Source Nanotech 2013). Structure of silica aerogel is schemed in Figure 13.

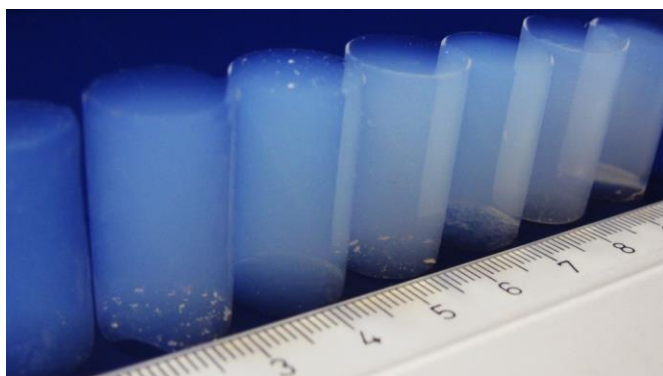


Figure 12. Scheme of silica aerogel (AEROCOINs 2014)

2.2 Synthesis of silica aerogel

Generally, synthesis of aerogel is divided into three main steps: gel preparation, aging of the gel and drying of gel under special conditions. They are dried by the method of supercritical

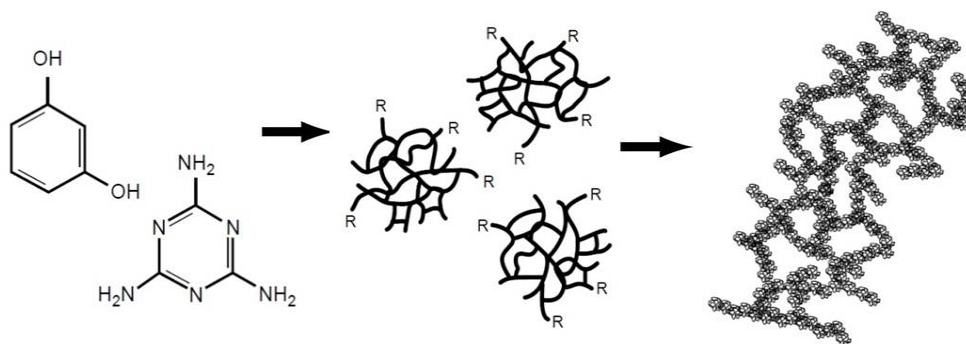


Figure 13. Structure of silica aerogel (LLNL 2006)

drying, so that high porosity of a wet gel state is also kept in dried samples.

2.2.1 Gel preparation

Firstly, the gel is prepared by using a sol-gel process, in which the solid components of the gel are spread in a dissolvent liquid and after some chemical reactions the mixture reaches the gel point. Typical precursors for silica aerogel production are tetramethylorthosilicate (TMOS), tetraethylorthosilicate (TEOS), polyethoxydisiloxane (PEDS), methyltryethoxysilane (MTES), silicon alkoxide etc (Shukla et al. 2012). Process of hydrolysis requires a catalyst, i.e. acid or base catalysis reaction. The sol changes its state to a gel, when distributed nanoparticles group together and form rigid SiO_2 network of particles after their collision. Silicon alkoxides are very specific materials of a high price and represent a challenge in a way of aerogel commercialization. This fact forces replacing silicon alkoxides with water glass or sodium silicate Na_2SiO_3 , as they represent a cheaper raw material.

2.2.2 Aging of the gel

After a sol reaches the gel state, its aging process begins. It might be kept in a solvent for a sufficient amount of time till hydrolysis and condensation processes are finished. Meanwhile strengthening of a gel continues, its mechanical and permeability properties can be improved by controlling the water content and concentration of the solvent and its pH level (see Figure 14). This process was researched by Smitha et al. 2006, who found that bulk density and shrinkage decreased, in addition to the expansion of surface area, pore dimensions and its volume with the increase of TEOS concentration in a solvent. During the process of aging, two mechanisms take place, which affect properties and structure of aerogel: transport of the material to the neck region and dissolution of smaller particles into bigger ones (Soleimani and Abbasi 2008). Transport of material is not affected by the process of convection due to solid state of the gel, while diffusion itself is influenced by the thickness of gel. At the end, required time for each mechanism increases with aging of gel, which makes production of aerogels less practical.

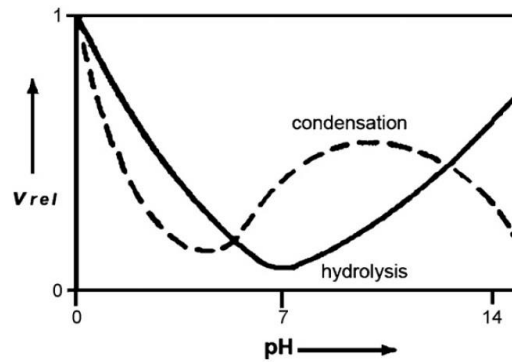


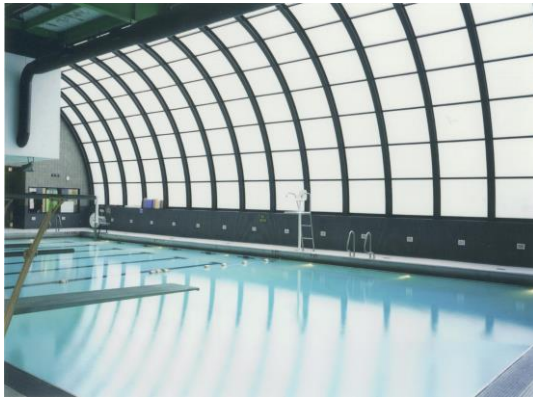
Figure 14. Relative aging rate as function of time for two aging mechanisms (Strom 2007)

2.2.3 Drying of the gel

Drying is the final stage in the production process of aerogel. In this step, the liquid inside the gel acquires a state of a gas and is removed from the gel network. Though, due to the surface tension of the liquid, it might damage the structure of gel network along with the process of evaporation. As a result, gel volumetric shrinkage and network collapse might happen. To avoid this scenario, the aged gel is placed under the supercritical conditions. These conditions facilitate the absence of surface tension, as distinct liquid-vapor phase boundary is absent. Supercritical conditions suppose low or high temperatures depending on a respective liquid (mainly alcohols, some water and catalyst), but high pressure is a necessary condition. As a result, big surface area of silica aerogel with high porosity and low density is produced.

2.2.4 Building applications of silica aerogel

Due to its exceptional thermal performance, silica aerogels represent innovative solution to conventional insulation materials. The only constraint on a way to its massive applicability is a high cost of a material, especially for such cost-sensitive industries as building construction. Multiple researches currently address this issue and attempt to decrease production costs of silica aerogel. Presently, two different application types can be marked for aerogel-based products: insulation materials with thermal properties and translucent aerogel-based insulation. An example of translucent aerogel insulation is depicted in Figure 15a. It is a good solution for combining daylighting purpose with high thermal performance glazing. Figure 15b depicts aerogel lime-based plaster, being applied to an experiment building of industrial partner of Empa Insitute. Such materials as Spaceloft® by Aspen Aerogels, Inc. (Northborough, MA, US), Nanogel® Compression Pack™ by Cabot Aerogel (Massachusetts, US), granular aerogel based window by ZAE Bayern (Germany), monolithic aerogel-based window by HILIT+ project for EU.



(a) Translucent Lumira aerogel glazing in Coleman Park Community Center, Nashville



(b) application of aerogel plaster in experiment building of Empa

Figure 15. Application of silica aerogel in buildings (Duo-Gard 2011; European Coatings 2013)

3 THEORETICAL AND TECHNICAL FRAMEWORK

3.1 Theoretical basis

Apparently, most energy-efficient technologies that have been developed are mostly suitable for new, but not historical buildings. Due to retrofit specifics, application of these measures might appear too challenging and risky. Because of improperly applied retrofit measures the moisture balance of walls may be disturbed considerably and as deleterious consequences may cause mould and fungi growth. Along with that, energy retrofit measures that are commonly used for new buildings are often aesthetically not satisfying for historical buildings. Therefore, new methods of retrofitting historical buildings are currently being developed. Researchers concentrate their scientific research efforts on development of new materials and its application, as well as methods of handling existing thermal bridges in envelopes.

Even though the urban growth of the last century was very extensive and major part of European dwelling stock was built before 1945, a few measures of retrofitting and improving energy performance were taken. For instance, in the Netherlands the annual percentage of newly built dwellings comprises approximately 1 % of the existing residential building stock (Meijer and Thomsen 2007). According to Frits Meijer and Thomsen (2009), currently existing building stock will keep a tendency of domination for the next 5 decades of century. According to Rammerstorfer (2012), major part of the apartments in Vienna was constructed during the so-called “Grunderzeit” period, referring to the construction period before 1919 (see Figure 16). In other words, each 3rd apartment in Vienna was constructed

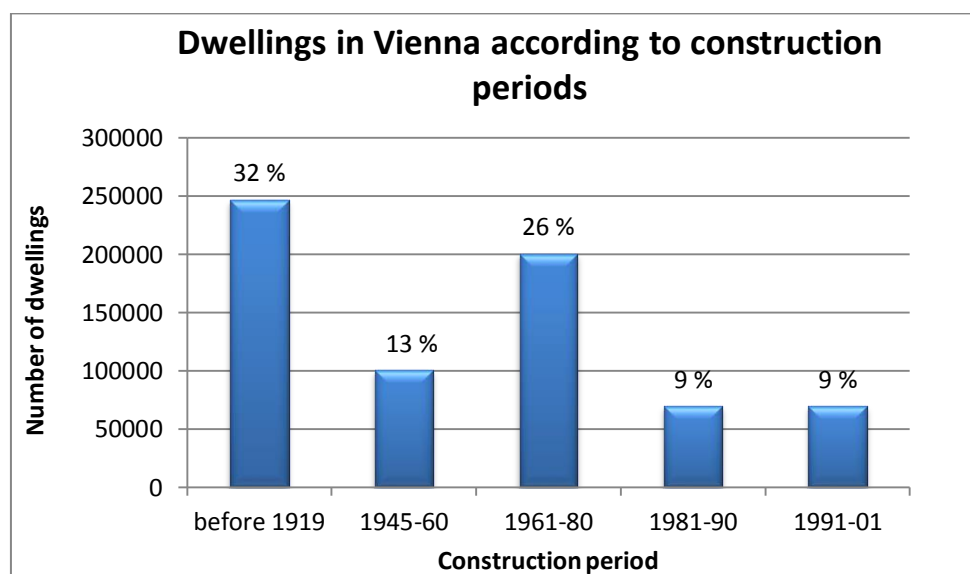


Figure 16. Dwellings in Vienna in construction periods (Rammerstorfer 2012)

before 1919. These dwellings are normally characterized with a typical heating demand of 120-160 kWh·m⁻², which is 5 to 10 times worse than modern low-energy buildings, such as Passivhaus standard buildings (Huttler and Sammer 2010). Thus, the sector of existing buildings offers broad opportunities for energy conservation as well as creation of healthier, more comfortable work environments. Along with these significant advantages, refurbishment of existing buildings with sustainable building technologies at the same time can ensure ample economic and employment potential, improve energy security.

Moreover, practices in renovation of building stock are already running. One of them is Thewosan Project, Thermal Rehabilitation for Residential Projects (Wohnfonds Wien 2013). A total of 28 000 dwellings with a floor area of 1.9 million square meters have been improved since the start of a project. Worth mentioning, the municipality of Vienna provided one third of the costs from its climate protection programme. Potential cost reductions to be achieved by a substantial drop in energy consumption were also advocated as an incentive for the investment.

Focus of this work is on a material representing the biggest potential in renovation techniques - highly insulating aerogel-based plaster system. First empirical tests have been implemented and thermal conductivity of insulating plaster finish has been proven to be 0.028 W·m⁻¹·K⁻¹ in the laboratory of at BFH AHB and EMPA (Carmeliet and Zimmermann 2011).

The target group of buildings, representing a point of interest for this thesis, is group of historical buildings, constructed at the end of 19th-beginning of 20th century. This building sector consists of heterogeneous buildings. Therefore, a reasonable detailed building typology of this sector in Austria is practically non-existent. Several reference buildings, data of TABULA research project and additional literature were thoroughly considered as information materials (Tabula Web Tool 2013). The main aim of TABULA project is development of a general building typology for EU countries. Building typology of each country consists of a set of reference buildings with specific energy-related and living area-relevant characteristics (envelope areas, U-values, used materials, supply system efficiencies). An online calculation function provides information for all reference buildings about the potential energy savings, which could be reached by undertaking the retrofit measures of different level and quality (see Figure 17).

“Building matrix” presents an overview of existing building types and gives numbers for the amount of each building type in the national dwelling stock (Appendix B). Information derived from project database about building constructions of erecting period till 1919 in Austria is represented in Appendix B.


























Country	Region	Construction Year Class	Additional Classification	SFH Single Family House	TH Terraced House	MFH Multi Family House	AB Apartment Block
	national (Gesamt- Österreich)	... 1919	generic (Standard / allgemein typisch)	 AT.N.SFH.01.Gen	 AT.N.TH.01.Gen	 AT.N.MFH.01.Gen	 AT.N.AB.01.Gen
	national (Gesamt- Österreich)	1919 ... 1944	generic (Standard / allgemein typisch)	 AT.N.SFH.02.Gen	 AT.N.TH.02.Gen	 AT.N.MFH.02.Gen	 AT.N.AB.02.Gen
	national (Gesamt- Österreich)	1945 ... 1960	generic (Standard / allgemein typisch)	 AT.N.SFH.03.Gen	 AT.N.TH.03.Gen	 AT.N.MFH.03.Gen	 AT.N.AB.03.Gen
	national (Gesamt- Österreich)	1961 ... 1980	generic (Standard / allgemein typisch)	 AT.N.SFH.04.Gen	 AT.N.TH.04.Gen	 AT.N.MFH.04.Gen	 AT.N.AB.04.Gen
	national (Gesamt- Österreich)	1981 ... 1990	generic (Standard / allgemein typisch)	 AT.N.SFH.05.Gen	 AT.N.TH.05.Gen	 AT.N.MFH.05.Gen	 AT.N.AB.05.Gen

Figure 17. Building matrix of TABULA project for Austrian building stock (Tabula Web Tool 2014)

3.2 Legal framework for building renovation

Building renovation in Austria is regulated by Federal Heritage Office. Its guidelines cover the principles of energy-efficient retrofit of historical buildings and are available for download on its website (OIB 2011). The main goal is maintenance of historical buildings with minimum altering of original facades.

Generally, historical buildings are characterized with traditional and regional construction methods. It is very important to use traditional materials and methods of retrofit in order to keep an original look of the façade. Exterior wall insulation has to preserve appearance, epoche style, authentic materials, while interior insulation should not affect interior shape and applied original plaster surface. Requirement of Austrian Institute of Building Technology (OIB) states a required U-value for brickwork walls as $0.35 \text{ W} \cdot \text{m}^{-2} \cdot \text{K}^{-1}$. Normally, the use of exterior plaster insulation is incompatible with the goal of preserving an authentic appearance of the building. Application of exterior plaster insulation is acceptable only in the following cases:

- comparable insulating effect cannot be obtained by other types of insulation;
- insulating materials are similar to those used in original structure;
- layer thickness, material properties of the original plastering are close to newly applied insulation; the connections, shapes and dimensions of the architectural elements of the façade must correspond to the historical architectural concept;

- original construction is protected from damage via these measures.

For windows, improvement only of U-value is not sufficient, all other factors should be considered as well, such as sound insulation, solar gains and solar shading. Possible measures of improvement include repair of windows; sealing of windows, though it may be a reason of increased condensation and consequently mould; application of various films; use of coated and insulating glass; arrangement of additional glass layer. Replacement of historical window box may occur only in case of extremely bad condition, or previously altered window box, or if dimensioning and detailing of a new element resembles an original design as much as possible.

A significant part of the Vienna building structure comes from the time before 1945, from the Biedermeier Art Nouveau era and the modernism of the interwar period. The characteristic element of these buildings is the so-called Wiener window - a window box with two window layers, which can be opened separately. A general retrofit practice of this type of windows involves replacement of interior window layer with a modern frame, while an exterior layer is kept in its original state. Thus, window performance improves significantly, while an authentic historical look is preserved.

Such elements as ceilings, floors and vaults are less subject to legal formalities in renovation; therefore their retrofit is relatively popular. For this reason, building physics aspects are often improperly implemented. This can lead, for instance, to damages caused by high humidity level in wooden slabs, which are particularly vulnerable to moisture content.

Maintenance of steel roofs in principle is based on requirement of keeping an original construction and avoiding possible damage to historical roofing. In case of attic conversion, thick insulation and ventilation equipment might occupy significant space and have to be planned in accordance with energy-efficient guidelines. Retrofit of flat roofs is allowed if it doesn't affect initial design and new details are carefully planned.

3.3 Fundamentals of building physics for evaluation of thermal bridges

Thermal bridges are typically building junctions where insulation is not consistent in an area where a relatively more conductive element passes through or bypasses the insulating barrier. They represent a path of smaller resistance through the insulation layer, allowing more heat to escape the thermal envelope and influence surface and interior temperatures.

Examples of typical thermal bridges are wall framing, concrete balcony slabs, parapets, cornices, and windows misplaced within the wall assembly.

3.3.1 Types of thermal bridges

Thermal bridges can be classified into 3 main distinct categories:

- Repeating or quasi-homogeneous thermal bridges
- Non-repeating or linear thermal bridges
- Geometrical thermal bridges

The first type of repeating thermal bridges can be described as those, which occur at regular intervals along the insulation surface. They are included in U-value calculation of particular building element as an additional heat flow. Non-repeating thermal bridges are discontinuous and occur at a specific point in the building construction. They are often caused by thermal breaks in the envelope.

These thermal bridges might be a result of the applied construction method or may also happen due to use of different materials over the thermal envelope. They are normally found around window and door openings and other parts where materials of different thermal conductivities form part of the external envelope. Additional heat flow due to their presence is calculated separately. The amount of heat loss through a non-repeating thermal bridge is referred to as thermal transmittance or Ψ -value and is expressed in $[\text{W} \cdot \text{m}^{-1} \cdot \text{K}^{-1}]$.

Geometrical thermal bridges are results of thermal envelope design, they occur due to a difference between the internal and external area, such as corner of a wall. Occurrence of this type of thermal bridging increases as geometry of a building obtains more complicated shapes. They can be 2-dimensional, where 2 planes intersect, or 3-dimensional, where 3 or more planes intersect. All types are presented in Figure 18.

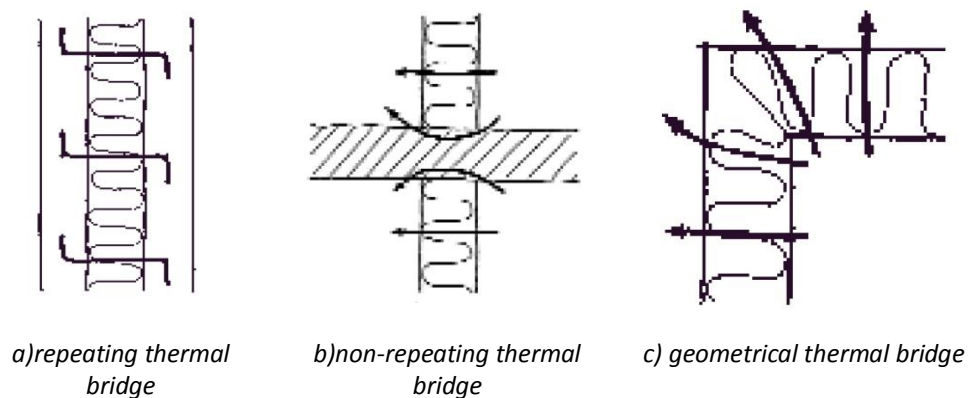


Figure 18. Classification of thermal bridges (OPET 2002)

One of the main consequences of thermal bridging is an increased heat flow. Undoubtedly, it may lead to deleterious consequences. It leads to energy misbalance and increases expenditures for heating. Besides, surface temperatures might decrease considerably by the level of dew point due to low exterior temperatures. As a result, it inevitably leads to moisture and mould growth. The last are proven to have a harmful effect on occupants' comfort and health.

3.3.2 Numerical calculation of thermal bridges

Standard DIN ISO 14683 describes the guidelines and criteria for numerical calculations, implying both for three and two-dimensional models of building details.

Thermal bridging results in heat loss through junctions in building fabric, which is expressed as a linear thermal transmittance Ψ -value. Ψ -values can then be used to arrive at a Υ -value: a factor, which allows calculation of the building's overall heat loss through thermal bridges. Thermal bridge calculations will also determine the temperature factors (f_{Rsi} -values) of each thermal bridge, whilst they are essential to building designers in assessing the risk of condensation and mould growth.

3.3.2.1 Ψ -value

The Ψ -value is an additional heat flow through the linear thermal bridge, multiplied by the length of the occurrence of the construction detail and expressed in $[W \cdot m^{-1} \cdot K^{-1}]$. To calculate it, one needs to subtract the heat flow through the plane elements, expressed by the U -value multiplied by the length of the element, from the total heat flow from the external to internal environment. From BS EN ISO 10211 Ψ -value is determined by the following formula:

$$\Psi = L^{2D} - \sum(U \times l), [W \cdot m^{-1} \cdot K^{-1}] \quad (1)$$

where:

L^{2D} is the thermal coupling coefficient, $[W \cdot m^{-1} \cdot K^{-1}]$

U is the U -value in $W \cdot m^{-2} \cdot K^{-1}$ of the flanking element, $[W \cdot m^{-2} \cdot K^{-1}]$

l is the length over which U applies, $[m]$

From the numerical modelling of a two-dimensional junction, L^{2D} is the thermal coupling coefficient between the internal and external spaces and is calculated from:

$$L^{2D} = Q / T_i - T_e, [W \cdot m^{-1} \cdot K^{-1}] \quad (2)$$

where:

Q is a total heat flow from internal to external environment, $[W \cdot m^{-2}]$

T_i and T_e are temperatures of internal and external environments, [$^{\circ}\text{C}$]

The heat transmission coefficient, H , of a building is derived as the total sum of the heat flows through an area A of all plane building elements plus that through all the thermal bridges:

$$H = \sum A \times U + \sum l \times \Psi, [\text{W} \cdot \text{K}^{-1}] \quad (3)$$

Depending on a method of calculation, Ψ -value can obtain negative numbers in a well-designed detail. In this case, all negative values should be replaced with zeros for calculation of a total sum of heat flow.

It should be noted that areas which have two or more linear thermal bridges, for instance at the junction of two walls and a floor slab, form point thermal bridges, which are characterized with a higher heat loss. However, since the mentioned area is normally small they are ignored in heat flow calculations. Another important guideline to be considered has to do with modelling junctions around the openings. In this case, the boundary of a model has to be taken as adiabatic, meaning that heat flow at the connection of a frame to an opening is equal to zero. Hence, Ψ -value is independent of the frame properties and depends only on frame location and its dimensions. However, for calculation of internal surface temperatures opening details should be modelled together with the window or door, if this information is available.

3.3.2.2 U-value

U-value is a measure of heat flow through a detail due to a difference in external and internal temperatures of environment from both sides of a detail. It is measured on a certain area is expressed in [$\text{W} \cdot \text{m}^{-2} \cdot \text{K}^{-1}$].

A general calculation of U-value is precisely described in standard ISO 6946. It is calculated according to the following formula:

$$U = \frac{1}{R_t} = \frac{1}{R_{se} + \frac{d_1}{\lambda_1} + \frac{d_2}{\lambda_2} + \dots + R_{si}} \quad (4)$$

where:

U is heat transfer coefficient, [$\text{W} \cdot \text{m}^{-2} \cdot \text{K}^{-1}$]

R_t is heat transfer resistance, [$\text{m}^2 \cdot \text{K} \cdot \text{W}^{-1}$]

R_{se} is exterior heat transfer resistance, [$\text{m}^2 \cdot \text{K} \cdot \text{W}^{-1}$]

d_i is thickness of layer i , [m]

λ_i is specific heat capacity of layer i , [$\text{W} \cdot \text{m}^{-1} \cdot \text{K}^{-1}$]

R_{si} is interior heat transfer resistance, [$\text{m}^2 \cdot \text{K} \cdot \text{W}^{-1}$]

U-value is a basic measure that is necessary for determination of thermal bridges and thus it notifies about the amount of energy escaping from the building. Passivhaus standard requires U-value to be below $0.16 \text{ W}\cdot\text{m}^{-2}\cdot\text{K}^{-1}$.

3.3.2.3 Temperature factor, f_{Rsi}

Temperature factors should also be determined in thermal bridge calculations, as they are essential to building designers in assessing the risk of condensation and mould growth of any detail. Current formula is used for calculation of f_{Rsi} under steady state condition:

$$f_{Rsi} = \frac{T_{si} - T_e}{T_i - T_e}, [-] \quad (5)$$

where:-

T_{si} is the surface temperature, [$^{\circ}\text{C}$]

T_i is the internal environmental temperature, [$^{\circ}\text{C}$]

T_e is the temperature of external environment, [$^{\circ}\text{C}$]

Depending on the intended building function, the temperature factor f_{Rsi} of the detail must be greater or equal to the critical factor f_{CRsi} in order to avoid problems of condensation and mould. The appropriate temperature factors are given in BRE Information Paper 1/06. Temperature factor f_{Rsi} does not depend on the imposed environment temperatures, but only on the structure of the element. Once it has been calculated for certain internal and external environment, surface temperature for other conditions can be calculated with this formula:

$$T_{si} = T_e + f_{Rsi}(T_i - T_e), [^{\circ}\text{C}] \quad (6)$$

It should be noted, that in case of modelling three-dimensional details, even well-planned, the internal surface temperature would decrease significantly due to presence of corners. As the area where surface temperature doesn't meet critical value is relatively small, a relaxation factor (g) is usually included in a formula:

$$f'_{Rsi} = g \times f_{CRsi} \quad (7)$$

It applies to all points of the detail that are in distance d or more from the points with the lowest f_{Rsi} . In case of three-dimensional corners located on ground floor, $d=10 \text{ mm}$ and $g=0.93$. These relaxations don't apply for other cases.

3.4 General principles of numerical modelling of thermal bridges

Before the modelling stage, it is important to consider certain rules and guidelines in the design of details in simulation software, which are described in this chapter. Commonly, the building is divided into several parts with an aim of making a feasible model for calculation.

It is usually done by choosing appropriate cut-off planes in a way that no differences in calculation outcome between building itself and a separated part appear. For thermal bridges to be simulated properly, certain guidelines are developed, which are represented in BS EN ISO 10211 as requirements for model development.

First of all, the extent of the model should be designed properly. More specifically, the areas which are adjacent to a thermal bridge should be taken at least 1 meter away from the thermal bridge or 3 times the thickness of the element. If a model contains repeating thermal bridges, it would extend up to a plane of symmetry. In case of any uncertainties in the dimension of a model, surface temperature of the model should be taken into account and has to be recalculated in adiabatic zone with different surface temperature.

If the difference in temperature factor is no more than 0.005, the smaller model would be relevant, otherwise the procedure of recalculation should be repeated until the condition is met.

Specific modelling cases represent thermal bridges, located close to each other. If they are located less than a thickness of a building element away from each other, heat flow from one element might affect the heat flow through another element, therefore heat loss through both of them will be overestimated.

Here, AnTherm programming package is not able to simulate slope lines and only allow the rectangular shapes, parallel to X and Y-axes. In this case, the shape of a sloping element should be approximated with steps of a certain size and number. Parameters that need to be considered in modelling of a sloping element are the angle of the slope β and the thickness d of any thin layers along it. Thin layers are those, whose thickness is less than 4 mm. As it is explained in the paper of Tim Ward and Chris Sanders "Conventions for calculating linear thermal transmittance and temperature factors", β is the angle of the slope and $y/x = \tan(\beta)$. If $\tan(\beta) > 1$, i.e. $\alpha > 45^\circ$, then $x < y$, otherwise $x > y$. The smaller of x or y must be no greater than $2.5 \times$ the thickness, d , of the sloping thin layer. For any sloping part of the geometry that is not a part of a thin layer, the smaller of x or y must be no greater than 10 mm. It should be noted that step size along the whole sloping element may vary, it may decrease or increase from the adjacent step. An easy method of ensuring the correct size of steps is by intersecting each step with a slope line (see Figure 19). The result should be 2 identically similar triangles: one above and one under the intersecting line. In case of multi-layered construction, lower layer stepping line is formed first. After it's completed, the line of upper layer is implemented in a distance of d , thickness, from the line of a lower layer. Because of the connection of the approximated sloping part with the non-

sloping rectangular part of the detail, one or more stepped lines along the slope may need to be extended or shortened to meet with the rest of the rectangular part of the model (see Figure 21). The same principle applies to curves, which have to be approximated in rectangular-modeling software. Successive vertical and horizontal lines forming these steps should intersect with the curve being approximated, with successive intersections of curve and step at a separation on the curve that is no more than 10° apart, as shown in Figure 19 and Figure 20.

3.5 Numerical calculation software

There is a plenty of simulation softwares for evaluation of thermal bridges in construction details. In this work software AnTherm is used for implementation of the tasks. The choice of the software was influenced by a support from authors of the software. License for AnTherm with 1 000 000 equation cells and 8 000 000 evaluated nodes has been kindly provided by Ms. Kornicki. The provided version is also capable of modelling 3D cases. In this work only 2D details are simulated, as there are no available drawings for 3D modelling.

AnTherm is a rectangular-modelling software. In other words, in contrast to CAD-software, it is not capable of modelling sloping lines and curve-shaped details. Thus, sloping lines have to be approximated with steps of precise number and size according to the rules, described

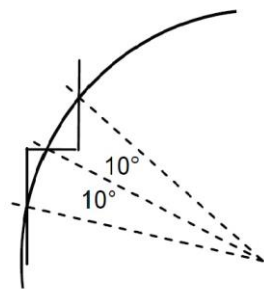


Figure 19. Stepping arrangement of curve element (Ward 2006)

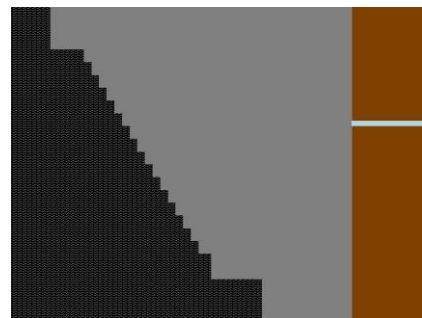


Figure 20. Scheme of approximated stepping slope in AnTherm

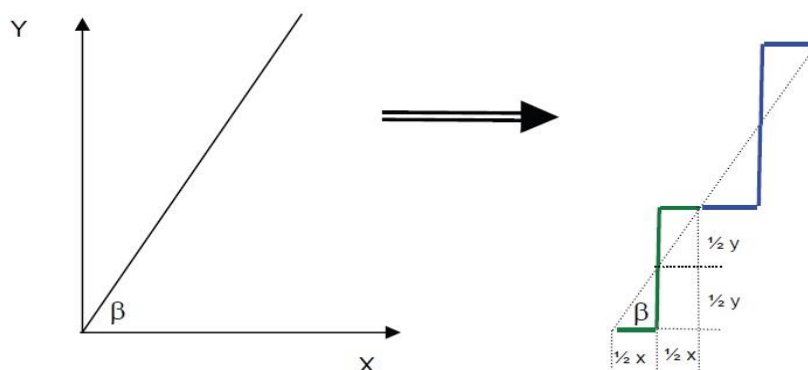


Figure 21. Slope approximation for rectangular modelling software (Ward 2006)

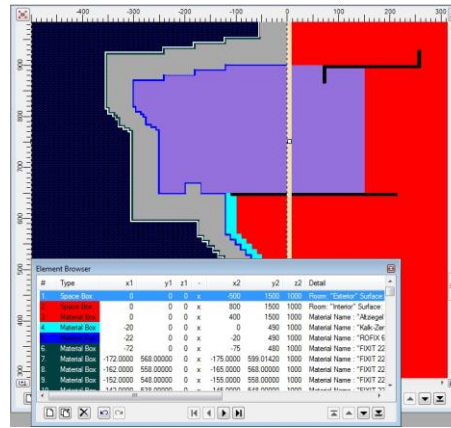


Figure 22. Arrangements of layers in AnTherm

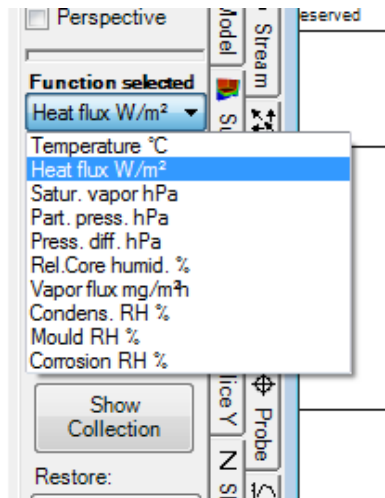


Figure 23. Visual representation of results in AnTherm

in 3.2 chapter. Each rectangular element is characterized with 4 coordinates of X1, X2 and Y1, Y2. Visually visible layers are taken into account for the simulation (see Figure 22). Moreover, exterior and interior space should also be identified and its surface thermal resistance R_s [$\text{m}^2 \cdot \text{K} \cdot \text{W}^{-1}$], depending on the direction of a heat flow.

Along with dimensioning of the elements, it is necessary to identify such values as thermal conductivity and water vapor diffusion resistance factor prior to the start of simulation. It should be noted here that U-value and thermal conductivity are equivalent values, though thermal conductivity is not area-related. AnTherm material choice of materials with many specified characteristics, such as density (ρ), thermal conductivity (λ), thermal conductivity of materials with 50 % and 90 % humidity, thermal conductance (c), minimum and maximum water vapor diffusion resistance factor (μ_{\min} and μ_{\max}). Sources of data are also variable, materials may be chosen from DIN, ISO, IBO, ONORM standards etc.

Simulation outcome should be evaluated by the following results, which can be visualized by the program, as shown in Figure 23:

- Temperature profile of the detail
- Heat flow in the detail
- Saturation vapor and vapor flux
- Partial pressure and pressure difference
- Relative humidity
- Condensation, mould growth, corrosion risk

3.5.1. Implementation of the simulation

Before the next steps are implemented and evaluated in AnTherm, boundary conditions of simulation should be defined. As heat transfer between external and internal environments and the building surfaces is a complicated process, series of standard surface resistances R_{si} and R_{se} is provided in BRE's Information Paper IP 1/06 (Ward 2006) with an aim of application in practical calculations of thermal bridges. These values, R_{si} and R_{se} , are shown in Table 2 below with their reciprocals, h_{si} and h_{se} , the surface heat transfer coefficients. One of these values is usually required in simulation software. In case of not typical surface resistances, such as surfaces with low emissivity values or external surfaces under shelter, the standard values of surface resistances have to be replaced with recalculated values according the equations in Annex A of BS EN ISO 6946. In order to avoid the risk of condensation and mould growth, evaluation result should meet critical temperature factor f_{Rsi} . They are represented below in Table 3 and Table 4 (Ward 2006). In this work for all structural, geometrical and material thermal bridges deviating from DIN 4108 Beiblatt 2, temperature factor f_{Rsi} of evaluated details at the worst location must suffice the requirement of $f \cdot R_{si} \geq 0.70$. Temperature of boundary conditions according to Appendix 2 of DIN4108 should comprise 20 °C for interior and -5 °C for exterior environment. In this work, boundary conditions were altered in order to ensure a reliability of results to +20 °C and -10 °C respectively (see Table 5).

Table 2. Standard surface resistances and heat transfer coefficients (Ward 2006)

Direction of heat flow			
Inside surface	Upwards	Horizontal*	Downwards
R_{si} [$m^2 \cdot K \cdot W^{-1}$]	0.10	0.13	0.17
h_{si} [$W \cdot m^{-2} \cdot K^{-1}$]	10.0	7.69	5.88
Outside surface	Upwards	Horizontal*	Downwards
R_s [$m^2 \cdot K \cdot W^{-1}$]	0.04	0.04	0.04
h_{se} [$W \cdot m^{-2} \cdot K^{-1}$]	25.0	25.0	25.0
*The values under “horizontal” apply to heat flow directions $\pm 30^\circ$ from the horizontal plane, e.g. if a roof slope is greater than 60° , the horizontal values should be used, otherwise the upwards values are used			

Table 3. Critical temperature factors for avoiding mould growth in buildings (Ward 2006)

Type of building	f_{CRsi} [-]
Dwellings; residential buildings; schools	0.75
Swimming pools (including a dwelling with an indoor pool)	0.90

Table 4. Critical temperature factors for evaluating the risk of surface condensation (Ward 2006)

Type of building	f_{CRsi} [-]
Storage buildings	0.30
Offices, retail premises	0.50
Sport halls, kitchens, canteens; buildings heated with un-fueled gas heaters	0.80
Buildings with high humidity, e.g. swimming pools, laundries, breweries	0.90

Table 5. Temperature of boundary conditions

Environment	Temperature [$^\circ C$]
Interior space	+20 $^\circ C$
Outside space	-10 $^\circ C$

4 METHODOLOGY

4.1 Modelled scenarios and set of junctions

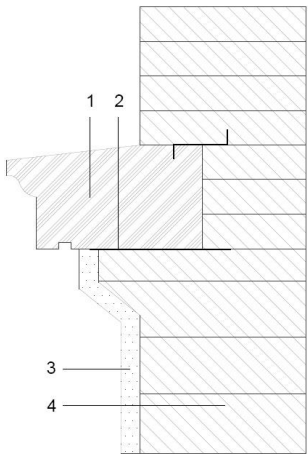
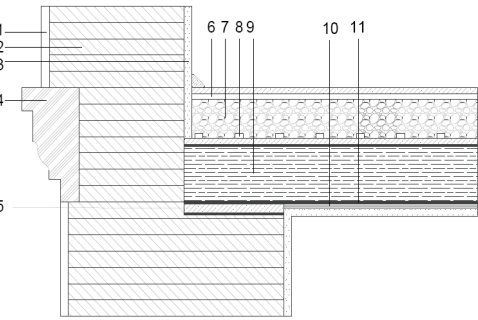
For all five details retrofit scenarios were developed (see Table 6). Scenario A for all details represents the pre-retrofit state. For Details 1-3 five different scenarios were generated and examined, while for Details 4 and 5 a further scenario was considered. For all scenarios the same boundary conditions within the applied linear thermal bridge evaluation were applied ($\theta_i=20\text{ }^{\circ}\text{C}$, $\theta_e=-10\text{ }^{\circ}\text{C}$). Moreover, all details were assessed based on the same calculation settings concerning level of detail and iterative calculation steps in the numeric thermal bridge simulation tool.

Table 6. Simulation scenarios

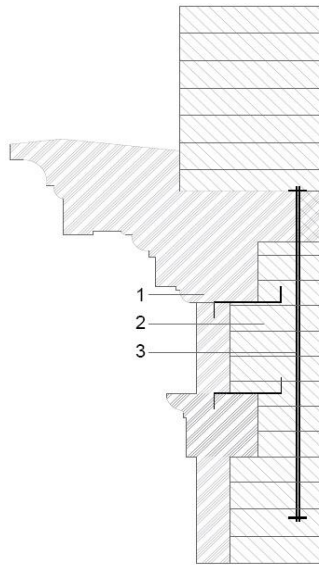
Scenario A	Original detail with no changes in construction
Scenario B	Suggested improvements with applied perlite plaster of 50 mm thickness and original decorative elements
Scenario C	Suggested improvements with perlite plaster, applied with 50 mm on wall surface and 20 mm on decorative elements
Scenario D	Suggested improvements with aerogel plaster of 50 mm
Scenario E	Suggested improvements with aerogel plaster, applied with 50 mm thickness on wall surface and 20 mm on decorative elements

Five typical architectural details (Riccabona and Mezera 2003; Eicke-Hennig et al. 1997) of historical buildings were used for the 2-dimensional thermal bridge evaluation (see Table 7). Details 1-3 represent different cornice variants, including natural stone cornices with and without steel anchor and a junction of a wooden slab next to a masonry cornice. Detail 4 is the attic parapet junction with a ventilated roof. Detail 5 represents a casement window and wall junction. The latter detail was examined both in terms of vertical and horizontal sections. The respective assumed material properties (Kornicki 2014) are summarized in Table 7.

Table 7. Set of analyzed details

Section of the detail	Material	Thermal conductivity λ [W·m ⁻¹ ·K ⁻¹]	Water Vapor Diffusion Resistance μ [-]
1. Brick wall with natural stone cornice			
	1 Natural stone	2.30	35
	2 Reinforced steel	60	100000
	3 Lime cement plaster	0.90	15
	4 Old brick masonry	0.71	8
*Baukonstruktionslehre (Riccabona and Mezera 2003)			
2. Wooden slab with gravel filling			
	1 Lime cement plaster	0.90	10
	2 Old brick masonry wall	0.71	8
	3 Gypsum plaster	0.80	10
	4 Natural stone	2.30	35
	5 Plank flooring	0.13	40
	6 False floor	0.13	40
	7 Gravel filling	0.70	1
	8 Wood	0.15	50
	9 Hard wood	0.1815	125
	10 Fire clay	0.75	1
	11 Cardboard	0.17	50000
* Konstruktionshandbuch (GERTEC Hannover 1997)			

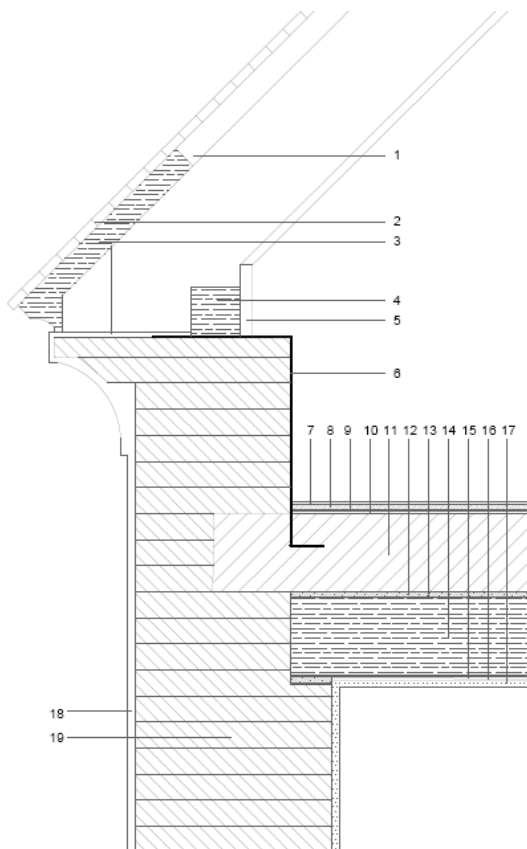
3. Natural stone cornice with steel anchoring



1 Natural stone	2.30	35
2 Old brickwork	0.71	8
3 Reinforced steel	0.60	100000

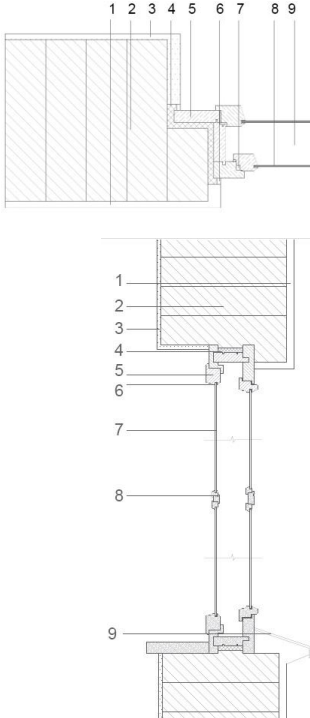
*Baukonstruktionslehre (Riccabona and Mezera 2003)

4. Ventilated attic with retrofitted ceiling slab



1 Air cavity	0.025	1
2 Roofing tile	0.7	10
3 Wood	0.15	50
4 Hard wood	0.1815	125
5 Gypsum cardboard	0.21	10
6 Reinforced steel	0.60	1000000
7 Coating	0.26	1
8 Concrete screed	1.4	50
9 Mineral wool	0.04	50
10 Lime cement plaster	0.90	15
11 Reinforced concrete	2.3	100
12 Plank flooring	0.13	40
13 Cardboard	0.17	50000
14 Hard wood	0.182	125
15 Rough spruce formwork	0.14	50
16 Fire clay	0.75	1
17 Gypsum plaster	0.8	10
18 Lime cement plaster	0.90	15
19 Old brick work	0.71	8

5. Double-box window



1	1 Lime cement plaster	0.9	15
2	2 Old brick masonry	0.71	8
3	3 Gypsum plaster	0.8	10
4	4 PU-foam (R=55)	0.031	50
5	5 Wood (R=800)	0.8	50
6	6 Gluing material	0.001	50000
7	7 Air cavity	0.025	1
8	8 Glass (d=4 mm)	31	1
9	9 Air layer	0.2	1

*Baukonstruktionslehre (Riccabona and Mezera 2003)

4.2 Evaluation of annual energy demand of a building

Theoretically, transmission losses of a building envelope can be calculated in a three-dimensional simulation model, where they have to be considered as shown in Figure 24. Though, practically, a building can be approximated to a scale of a unit, but it is split up as separate structural construction, i.e. walls, slabs, windows. Thermal transmittance of each element is calculated separately, without taking in to account its relation to other components. Total building heat losses are calculated according to the following formula (ISO 14683 2005):

$$\begin{aligned}
 H_{total} = & \sum U_{ext.wall} A_{ext.wall} + \sum U_{roof} A_{roof} \\
 & + \sum U_{basement} A_{basement} + \sum U_{window} A_{window} \\
 & + \sum U_{door} A_{door} + \sum \Psi_k l_k + \sum x_j
 \end{aligned} \tag{8}$$

where:

H_{total} – is the total heat losses of the building, $[W \cdot K^{-1}]$

U – is the total heat transmittance of the building element, [$\text{W}\cdot\text{m}^{-2}\cdot\text{K}^{-1}$]

A – is the surface area of a structural component, [m^2]

Ψ_k – is the linear thermal transmittance of the joint k , [$\text{W}\cdot\text{m}^{-1}\cdot\text{K}^{-1}$]

l_k – is the length of the joint k , [m]

x_j – is the point transmittance, [$\text{W}\cdot\text{K}^{-1}$]

For a general evaluation of annual energy demand (HWB) a typical apartment building was taken as a base sample. It represents a construction period before 1919, originally with brick masonry exterior walls of 400 mm thickness and heat attic space. Calculation for 3 different cases has been carried out, which are:

- Case 1: original state;
- Case 2: : applied perlite plaster with 50 mm thickness on wall surface and 20 mm on decorative elements and improved window box;
- Case 3: applied aerogel plaster with 50 mm thickness on wall surface and 20 mm on decorative elements and improved window box.

Detailed plans of the building can be found in Appendix D. Photos of the building are shown in Figure 25. Calculation is carried out in Archiphysik, energy certificate software with integrated building calculation tools and integrated IBO database of building materials.

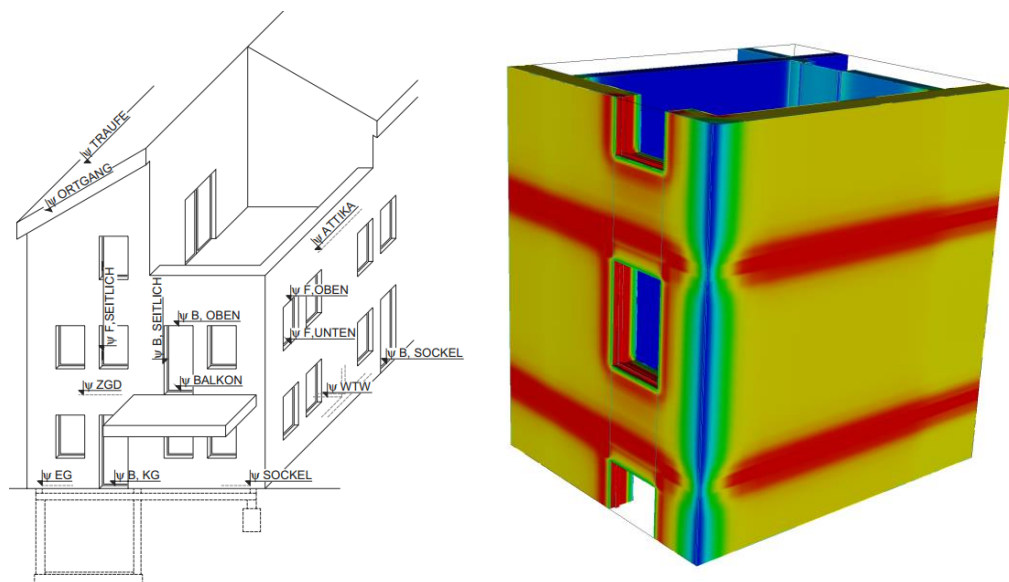


Figure 24. Thermal bridges in a three-dimensional calculation (Wienerberger 2013; Antherm 2008)



Figure 25. Base building of Grunderzeit construction period

Calculation of each scenario is implemented with two different options: approximate calculation of thermal bridges and detailed calculation of thermal bridges.

4.3 Characteristics and application of aerogel-based plaster

In this work, scenario D and E are implemented with ROFIX aerogel insulation plaster system (see Figure 26), which main component is FIXIT 222 Aerogel High Performance Insulating Plaster. It is developed in the framework of R&D project with a support of the Swiss Innovation Promotion Agency (CTI) (see Table 8 for properties of FIXIT 222). In the course of several years of research, EMPA researchers and Fixit product developers have successfully launched this innovative new product onto the market. Complete final plaster system is currently being developed by ROFIX and EMPA project partners and will enter the market in coming time. Its performance in decreasing heat loss and influence on condensation and mould risk is tested in this work. Properties of the insulating system, its components and application method are described further in this chapter. The thermal and technical characteristics and properties of FIXIT 222 Aerogel High Performance Insulating Plaster are given in Table 8 below.

Thanks to aerogel's outstanding properties, Fixit 222 Aerogel high-performance insulating plaster is ideal for use in renovating old buildings to modern standards of energy performance. Fixit 222 Aerogel high-performance insulating plaster is mostly used in combination with other Fixel products. Thus, optimal rigid structure of a system is ensured.

Table 8. Properties of FIXIT 222 Aerogel High Performance Plaster (FIXIT AG 2013)

Characteristic	Value
Maximum application thickness	150 mm
Minimum layer thickness	30 mm
Maximum layer thickness	150 mm
Yield	approx. 5 l·kg ⁻¹
Dry bulk density	approx. 220 kg·m ⁻³
Thermal conductivity coefficient	0.028 W·m ⁻¹ ·K ⁻¹
Water vapor diffusion resistance coefficient	4 - 5
Measured value	0.0261 W·m ⁻¹ ·K ⁻¹ (EMPA report 5214-003132, 6.9.2013)
PH-value	approx. 10.5
Specific heat capacity value	approx. 1 kJ·kg ⁻¹ ·K ⁻¹

According to guidelines provided by FIXIT Gruppe, the following stages are involved into plaster application process:

- 1) As the first step, building surface should be prepared and roughed with an adhesive primer layer, which at the same time reduce absorption capability of the wall. It is done with adhesive primer ROFIX 675 NHL with a thickness d=2 mm.
- 2) As the next step, FIXIT 222 aerogel high-performance plaster is applied with a plastering machine (e.g. PFT G4 or Mai 4ever). Required layer thickness of 50 mm can be easily implemented. After application, surface should be leveled with a wooden or aluminum batten and afterwards a scraper to give a surface an even shape. If a thickness of insulating layer is required, next plaster application can be implemented on the following day, but no later than the third day. As an important notice, plaster surface should be moisturized for at least a week by spraying water in order to exclude a possibility of cracks due to drying process. Normally, drying speed is approximately 3 mm per day, but it strongly depends on local weather conditions. To ensure an adequate structural strength, it is not recommended to apply further coating for at least 3 weeks. Thickness of layer comprises 50 mm.

- 3) Before applying reinforcement mesh, surface should be strengthened with mineral-based undercoat stabilizer Fixit 493. It is recommended to carry out this step 24 hours before embedding the reinforcing fabric mesh. Due to the fact that thickness of this layer is minimal, it has been neglected in simulation model.
- 4) The next step consists in embedding the reinforcement fabric mesh. It is done with a purpose of creating a crack free, solid and level plaster surface. It has to be levelled with the layer of FIXIT 223 special embedding mortar, which thickness comprises 3-5 mm. Drying time for this step takes approximately 10 days.
- 5) As a finishing coat, mineral-based finishing coat ROFIX 380 is applied. Only mineral-based finishing coats can be applied to aerogel insulating plaster components. Thickness of layer comprises 1 mm.
- 6) As the last layer of a system, mineral-based paint coat is applied. The choice can range between FIXIT 783 silicate color, FIXIT 784 silicate color APS or FIXIT 785 evo mineral color. Due to the fact that thickness of this layer is minimal, it has been neglected in simulation model.

Properties of aerogel insulating plaster system are represented in Table 9 below.

Tower of the weather station of Department of Building Physics and Building Ecology is one of several experimental surfaces for application of innovative plaster system. Application was held during the period from April 2014 till June 2014. The process was documented visually by author of thesis and employees of the Department. Photos are represented below in Figure 27, 28, 29, 30.



Figure 26. ROFIX Aerogel Insulating Plaster System (ROFIX AG 2014)



Figure 27. Adhesive primer 675 NHL (on the left), application of FIXIT 222 with a plastering machine (on the right)



Figure 28. Levelling off FIXIT 222 (left), surface of FIXIT 222 (right)



Figure 29. Reinforcement mesh for corners of openings (left), application of reinforcement mesh with FIXIT 223 (right)



Figure 30. Applied reinforcement mesh (left), FIXIT 222 insulating plaster (right)

Table 9. Aerogel Insulating Plaster System Components (FIXIT AG 2013)

Component layer	Thickness d [mm]	Thermal conductivity λ [$\text{W}\cdot\text{m}^{-1}\cdot\text{K}^{-1}$]	Vapor diffusion resistance factor η [-]	Specific heat capacity c [$\text{kJ}\cdot\text{kg}^{-1}\cdot\text{K}^{-1}$]
1. Substrate with adhesive primer ROFIX 675 NHL	2	0.83	12-15	1
2. FIXIT 222 insulating plaster	50	0.028	4-5	1
3. Fixit 493 undercoat stabilizer	-	-	-	-
4. FIXIT 223 special embedding mortar	3	0.035	15-20	Under measurement
5. Finishing coat ROFIX 380	1	0.047	15-20	-
6. Fixit paint coat	-	-	-	-

5 TECHNICAL EVALUATION OF DETAILS

In this chapter modelling cases are presented and the most important results of the simulation are pointed out. The models are written on an enclosed CD and can be viewed and simulated with a low accuracy of results with a free trial version of AnTherm. The results of each case have been documented and are to be found in Appendix B; those results have then been translated into graphs with corresponding legends.

It should be noted that choice of details has been based upon their representative characteristic, meaning they comprise a typical set of junctions of historical buildings of construction period before 1919. Based on the sources described in Chapter 3.3, necessary assumptions have been made concerning material properties of the details.

Before the simulation cases are described, it is important to clarify the properties of certain materials and thicknesses of certain constructions, as they are repeatedly used through the simulation. For instance, wall thickness typically decreases with height, therefore brick masonry wall is simulated with the thickness of 400 mm, 320 mm and 250 mm. Thermal conductivity of bricks is affected by its age, variations in material characteristics, the variations in locally-sourced raw materials, manufacturing processes, as well as by the amount of air cavities. Therefore λ -value of brickwork is assumed to be $0.71 \text{ W}\cdot\text{m}^{-1}\cdot\text{K}^{-1}$, based on the research from Rhee-Duverne and Baker (2013), which investigates the thermal performance of a range of traditional solid brick walls.

Thermal conductivity of static air layer comprises $0.026 \text{ W}\cdot\text{m}^{-1}\cdot\text{K}^{-1}$, which is a relatively low value. As AnTherm is not capable of simulating a convection process, another solution for modelling has to be found. Calculation has to be carried out according to DIN EN ISO 6946, considering the influence of layer thickness, heat flow direction and mounting position. Table 10 shows calculated values for thermal conductivity of various thicknesses of air layers. Original double-box windows are taken as slightly ventilated spaces due to a lack of proper insulation. Newly installed window frames are calculated as non-ventilated air space.

Table 10. Thermal conductivity of air layers (BS EN ISO 6946)

Air layer	Thickness d [mm]	Thermal conductivity λ [$\text{W}\cdot\text{m}^{-1}\cdot\text{K}^{-1}$]
Non-ventilated, horiz.	100	0.55
Slightly ventilated, horiz.	100	1.11
Slightly ventilated, horiz.	135	1.50

5.1 Brick wall with natural stone cornice

The first simulation case includes a natural stone element fixed in an old brick masonry wall with a thickness of 400 mm. A cornice is fixed with 2 steel anchors with a thickness of 5 mm. Section of the detail is presented in Figure 31, material properties are given in Table 11. Generally, five scenarios are analysed:

- scenario A: original state of a detail;
- scenario B: perlite insulating plaster is applied with a thickness of 50 mm only along wall surfaces, thermal conductivity of $0.18 \text{ W}\cdot\text{m}^{-1}\cdot\text{K}^{-1}$;
- scenario C: application of perlite insulating plaster system with 50 mm thickness on wall surfaces and 20 mm on decorative element surfaces. Styrofoam layer is added above the cornice, so that original frontal surface of decorative cornice is kept unaltered and historical look of the façade is preserved as an object of architectural heritage;
- scenario D: application of aerogel insulating plaster system with a thickness of 50 mm only on wall surfaces;
- scenario E: application of aerogel insulating plaster system with 50 mm thickness on wall surfaces and 20 mm on decorative element surfaces. Styrofoam layer is added above the cornice, so that original frontal surface of decorative cornice is kept unaltered.

After the boundary conditions are defined with exterior temperature $T_e = -10^\circ\text{C}$ and interior temperature $T_i = 20^\circ\text{C}$, graphical results are visualized. Figures 32-36 show all simulation models and its temperature profiles. According to them, there is a significant improvement after scenario E has been implemented. Interior surface temperature has increased up to $T_{\min} = 16.9^\circ\text{C}$. Blue arrow represents a location of a point with a minimum interior surface temperature. Temperature profile of an original case showed low interior surface temperature $T_{\min} = 12^\circ\text{C}$, while scenario B reached up to $T_{\min} = 13.1^\circ\text{C}$. Scenario C and D showed minimum surface temperature of $T_{\min} = 13.9^\circ\text{C}$ and $T_{\min} = 13.6^\circ\text{C}$ respectively. Temperature behaviour of the wall was additionally tested by series of simulations with various outside temperatures in a range of -20°C to $+20^\circ\text{C}$. Figure 37 shows a variation of interior surface temperature as a function of exterior temperature. It has to be noted that this simulation is just a static approximation of temperature behaviour. As the next step in further research, dynamic modelling has to be carried out.

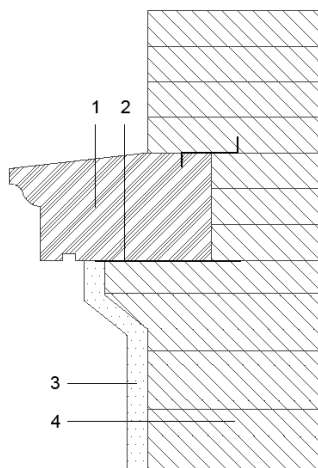


Figure 31. Section of detail 1

Table 11. Material properties of detail 1

Material	λ [W·m ⁻¹ ·K ⁻¹]	μ [-]
1 Natural stone	2.30	35
2 Reinforced steel	60	100000
3 Lime cement plaster	0.90	15
4 Old brick masonry	0.71	8

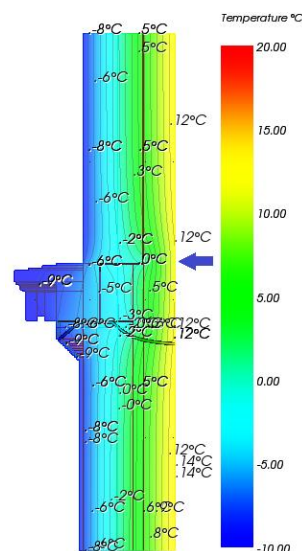
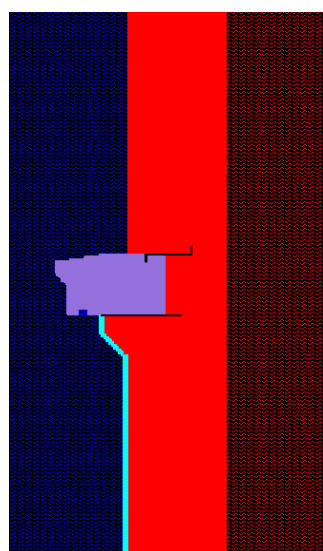


Figure 32. Simulation model and temperature profile of scenario A of detail 1

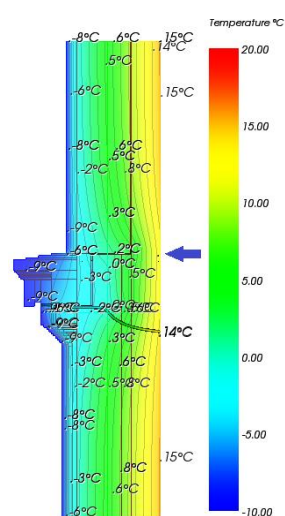
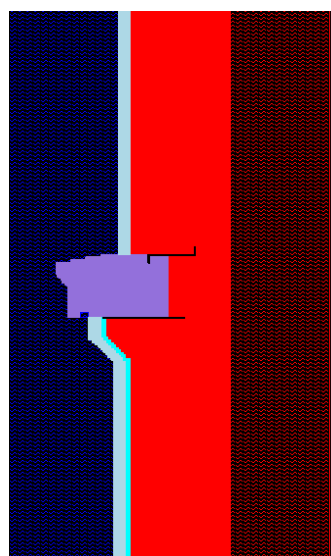


Figure 33. Simulation model and temperature profile of scenario B of detail 1

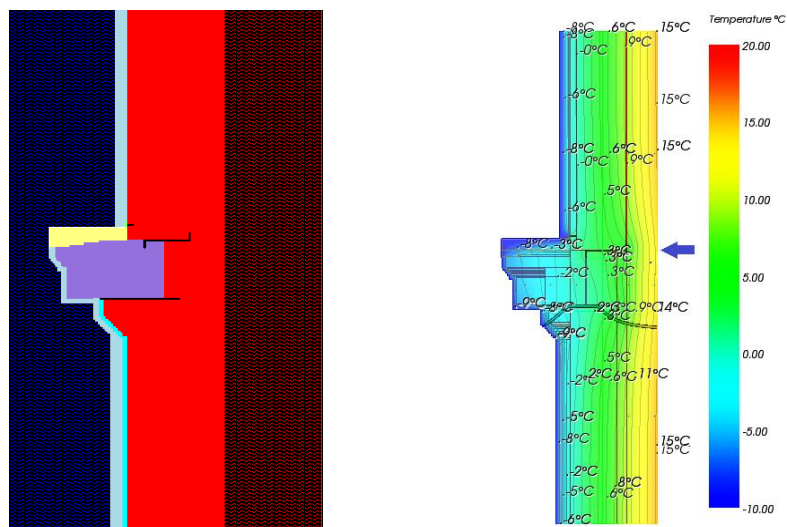


Figure 34. Simulation model and temperature profile of scenario C of detail 1

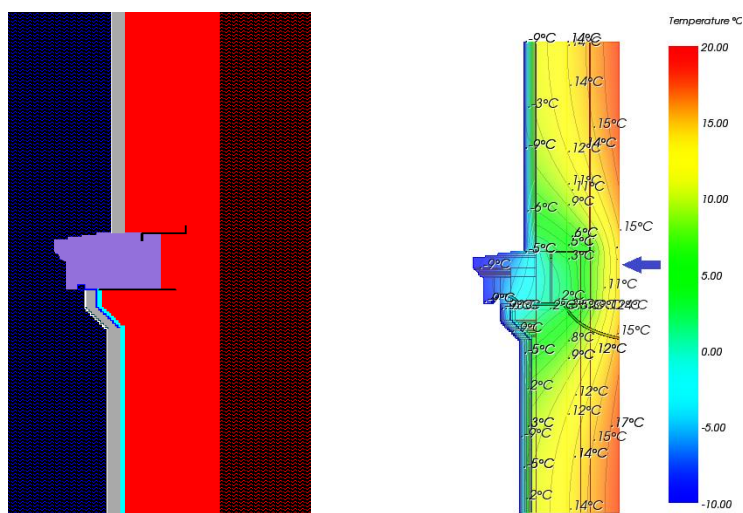


Figure 35. Simulation model and temperature profile of scenario D of detail 1

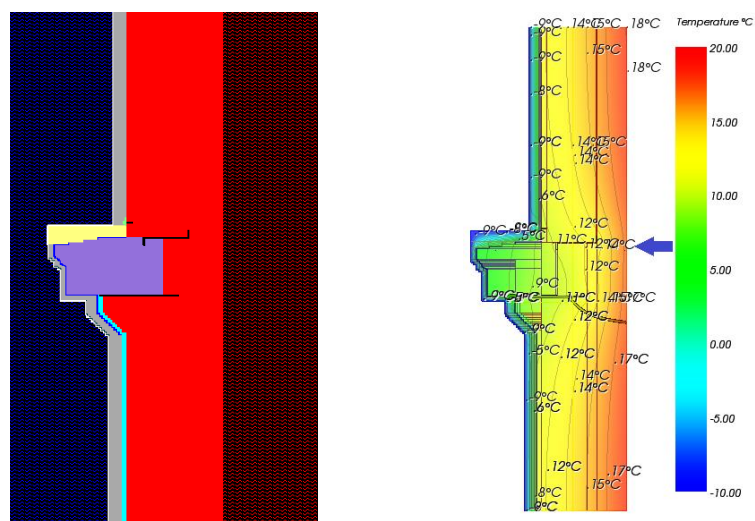


Figure 36. Simulation model and temperature profile of scenario E of detail 1

Next step is analysis of heat flow through the detail. According to temperature profiles, the weakest point of a construction is a decorative cornice, fixed into the wall with 2 anchors. 2 anchors have the highest values of thermal conductivity. In order to decrease a heat flow, a layer of styrofoam has been placed above the cornice. Figure 38 shows heat flux profiles of scenario A and scenario E. Aluminium layer of 2 mm has been added above as a protective element from precipitation impact. Illustrated arrows represent the heat flux distribution. The bigger the arrow is, the stronger is the heat flux at the point of corresponding arrow.

As it has been shown, wall surfaces obtain low temperatures in winter period, therefore it is necessary to determine to which extent humidity in the wall is developed, and consequently how high a risk of mould growth is. Figure 39 shows a pressure difference profile in the connecting area of cornice and brick wall. Result of this investigation indicates no condensation within the brick masonry itself after applied scenario E. Negative values in scenario A indicate a risk of condensation inside the structure.

After a proper insulation of a cornice, vapor flow has considerably decreased, as negative values appear only on outer surface of a construction. After evaluation of temperature factors it was identified that all scenarios have shown satisfactory results above a critical value of 0.70. Table 12 shows U-value improvement in all scenarios. It can be seen that scenario E has significantly improved the U-values of the construction. Total U-value of the wall decreased from $1.26 \text{ W}\cdot\text{m}^{-1}\cdot\text{K}^{-1}$ to $0.37 \text{ W}\cdot\text{m}^{-1}\cdot\text{K}^{-1}$ in case of scenario E and to $0.93 \text{ W}\cdot\text{m}^{-1}\cdot\text{K}^{-1}$ in case of scenario B. Table 13 shows results of retrofit measures in mitigating a thermal bridging effect. The lowest coupling coefficient and highest temperature factor is observed in scenario E. Psi-values depend on uniformity of insulation along the whole detail, therefore higher values are observed in scenario C and scenario D, even though U-values are

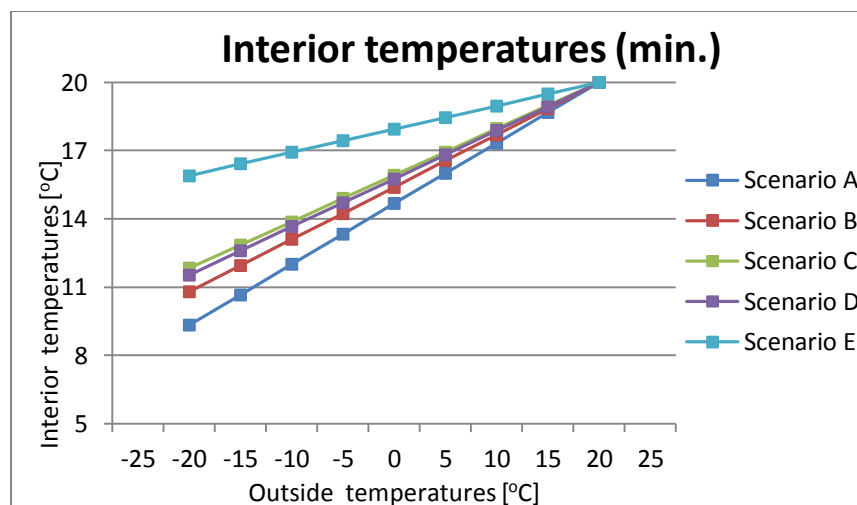


Figure 37. Temperature profiles of the coldest point of interior surface as a function of exterior temperature of detail 1

better in other retrofit scenarios.

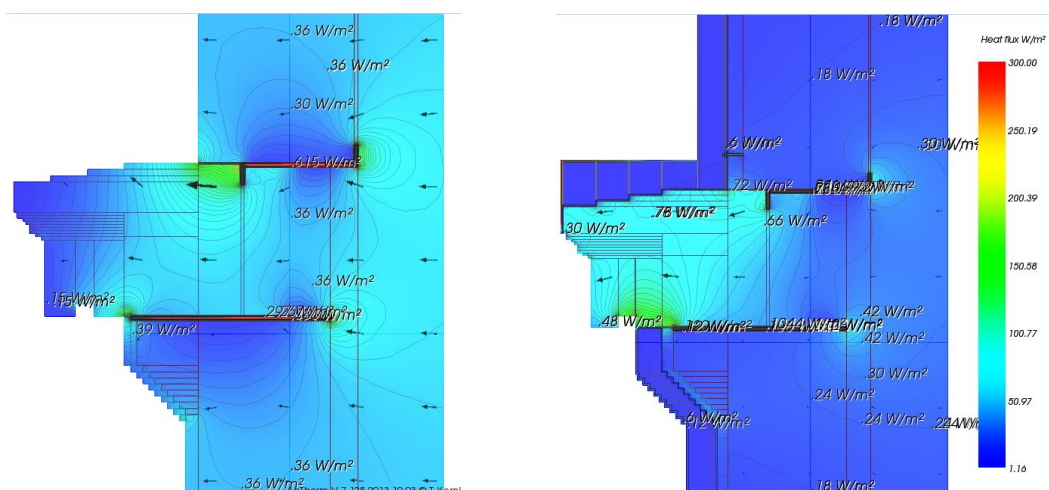


Figure 38. Heat flux profile of detail 1, scenario A and E

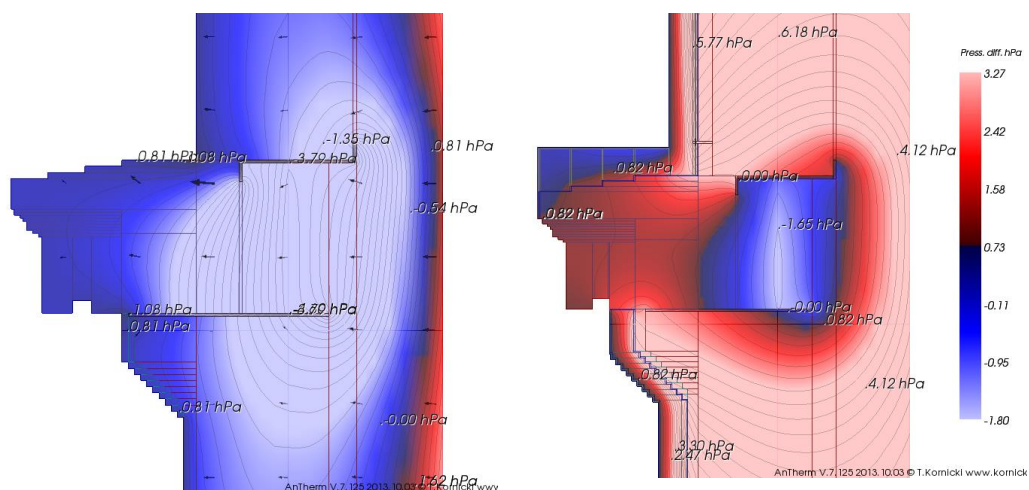


Figure 39. Pressure difference of detail 1, scenario A and E

Table 12. U-values of detail 1 and its improvement after applied retrofit scenarios

	U-value [$\text{W} \cdot \text{m}^{-2} \cdot \text{K}^{-1}$]	Improvement [%]
Scenario A	1.26	-
Scenario B	0.93	26
Scenario C	0.93	26
Scenario D	0.37	71
Scenario E	0.37	71

Table 13. Other values and their improvement after applied measures of detail 1

	L^{2D} [W·m ⁻¹ ·K ⁻¹]	Improvement [%]	Ψ-value [W·m ⁻¹ ·K ⁻¹]	f _{Rsi} [-]
Scenario A	3.39	-	0.19	0.73
Scenario B	2.67	21	0.31	0.77
Scenario C	2.55	25	0.19	0.81
Scenario D	1.63	52	0.71	0.81
Scenario E	1.13	67	0.21	0.9

5.2 Wooden slab with a gravel filling

The second simulation case represents a cross-section of an old brick masonry wall with a natural stone decorative cornice and wooden floor slab with a gravel filling. Thickness of a wall decreases from 400 mm to 250 mm with height of the building. Section of the detail can be seen in Figure 40, material properties are available in Table 14. As in a previous retrofit case, five scenarios are suggested:

- scenario A: original state of a detail;
- scenario B: perlite insulating plaster is applied with a thickness of 50 mm only along wall surfaces, thermal conductivity of 0.18 W·m⁻¹·K⁻¹;
- scenario C: application of perlite insulating plaster system with 50 mm thickness on wall surfaces and 20 mm on decorative element surfaces. Styrofoam layer is added above the cornice, so that original frontal surface of decorative cornice is kept unaltered and historical look of the façade is preserved as an object of architectural heritage;
- scenario D: application of aerogel insulating plaster system with a thickness of 50 mm only on wall surfaces;
- scenario E: application of aerogel insulating plaster system with 50 mm thickness on wall surfaces and 20 mm on decorative element surfaces. Styrofoam layer is added above the cornice, so that original frontal surface of decorative cornice is kept unaltered and historical look of the façade is preserved as an object of architectural heritage.

After the boundary conditions are defined with exterior temperature $T_e = -10$ °C and interior temperature $T_i = 20$ °C, simulation can be proceeded. All five simulation models and their temperature profiles can be seen in Figures 41-45. Due to different wall thickness and

consequently differences in heat flow, 2 spaces are analysed independently: one above and one under the floor slab. Blue arrow represents a location of a point with a minimum interior surface temperature. Detail in its original state showed a poor performance in its surface temperatures, ranging below $T_{\min}=11.97\text{ }^{\circ}\text{C}$. As predicted, scenario E showed the highest temperatures from the suggested options, with $T_{\min}=15.74\text{ }^{\circ}\text{C}$ in the area close to a connection with a floor slab on the upper part of the wall and $T_{\min}=16.12\text{ }^{\circ}\text{C}$ at a lower part of the wall. Simulation result of scenario B and C showed a slight improvement, minimum interior temperature comprises $T_{\min}=12\text{ }^{\circ}\text{C}$ and $T_{\min}=12.21\text{ }^{\circ}\text{C}$, which still keeps a surface relatively cold. Impact of scenario D was relatively similar to the previous and demonstrated interior surface temperature $T_{\min}=12.58\text{ }^{\circ}\text{C}$. Temperature behaviour of the wall was tested by series of simulations with various outside temperatures in a range of $-20\text{ }^{\circ}\text{C}$ to $+20\text{ }^{\circ}\text{C}$. As an outcome of this, Figure 46 shows a variation of interior surface temperature as a function of exterior temperature. It has to be noted that this simulation is just a static approximation

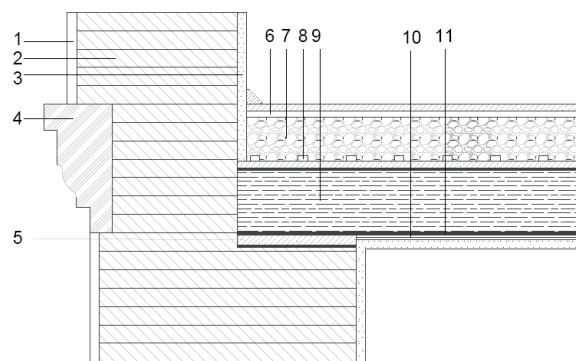


Figure 40. Section of detail 2

Table 14. Material properties of detail 2

	Material	λ [W·m ⁻¹ ·K ⁻¹]	μ [-]		Material	λ [W·m ⁻¹ ·K ⁻¹]	μ [-]
1	Lime cement plaster	0.90	10	7	Gravel filling	0.70	1
2	Old brick masonry	0.71	8	8	Wood	0.15	125
3	Gypsum plaster	0.80	10	9	Hard wood	0.02	100
4	Natural stone	2.30	35	10	Fire clay	0.75	1
5	Plank flooring	0.13	40	11	Cardboard	0.17	50000
6	False floor	0.13	40				

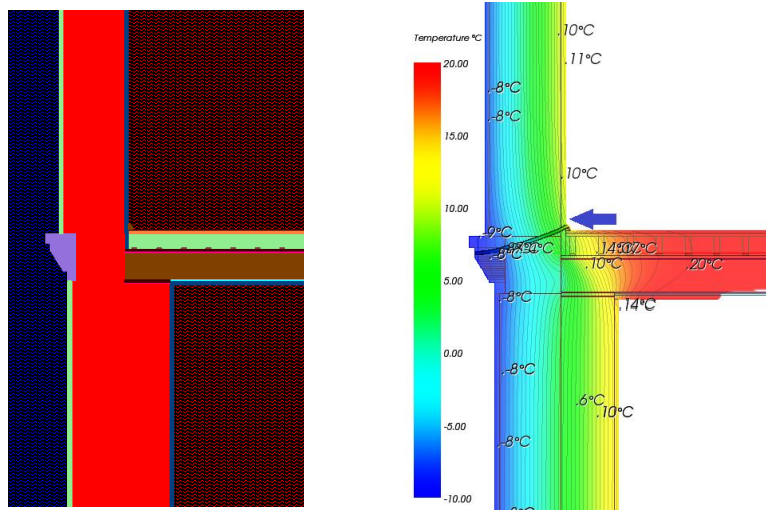


Figure 41. Simulation model and temperature profile of scenario A of detail 2

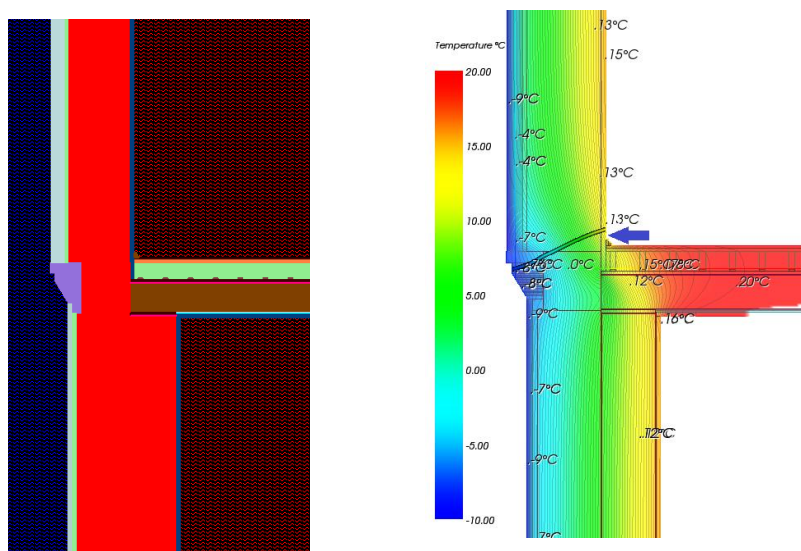


Figure 42. Simulation model and temperature profile of scenario B of detail 2

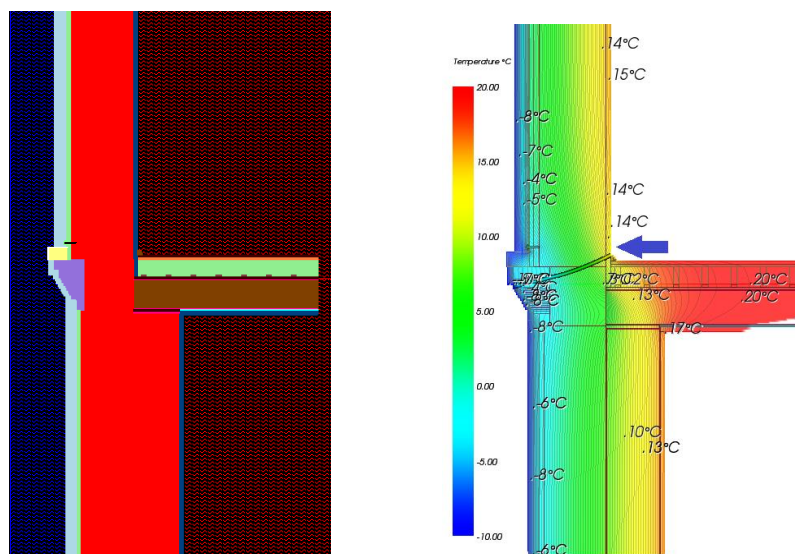


Figure 43. Simulation model and temperature profile of scenario C of detail 2

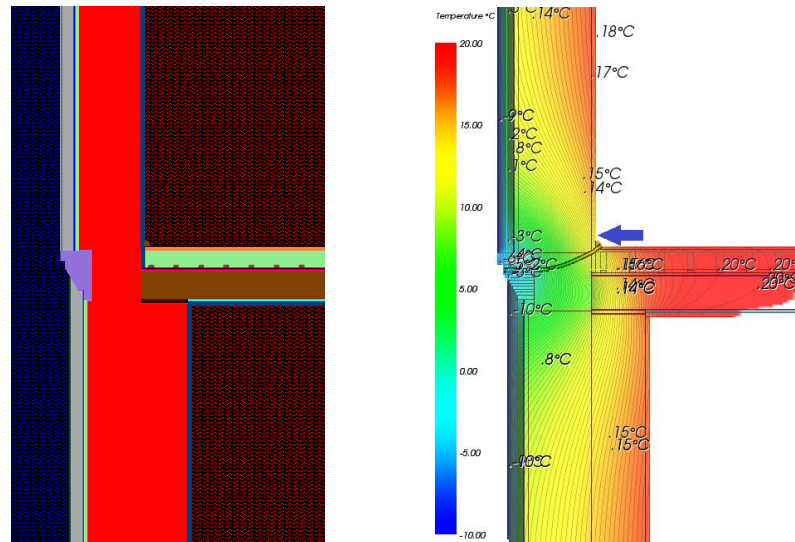


Figure 44. Simulation model and temperature profile of scenario D of detail 2

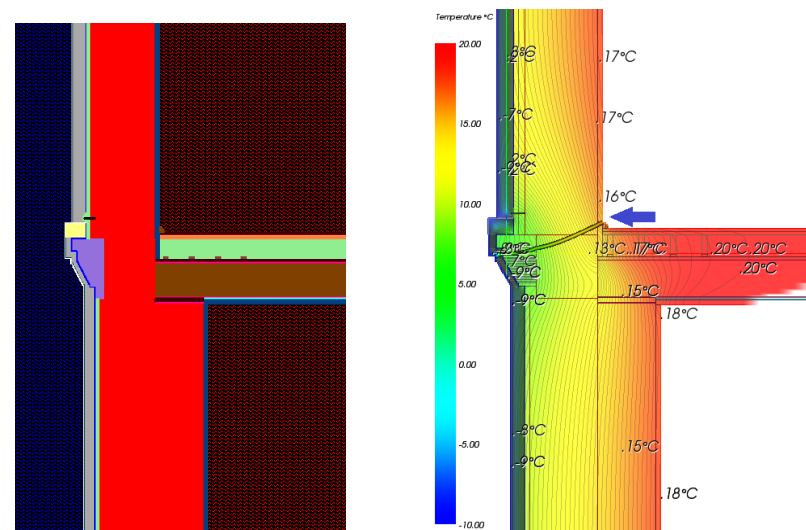


Figure 45. Simulation model and temperature profile of scenario E of detail 2

of temperature behaviour. As the next step in further research, dynamic modelling has to be carried out. As the next stage of analysis heat flow through the detail is tested.

According to temperature profiles, the weakest point of the construction is a decorative cornice. In order to decrease heat flow, a layer of styrofoam has been placed above the cornice. Figure 47 shows heat flux profiles of scenario A and E. Aluminium layer of 2 mm has been added above it with protective function from precipitation impact. Arrows represent the heat flux distribution. Heat flow has considerably decreased in the area of the whole section of the detail.

It is necessary to determine to which extent humidity in the wall and consequently a risk of mould growth is prevented. Figure 48 shows that low condensation risk appears only in a small area of the corner after aerogel insulating plaster system and Styrofoam layer was

applied above the cornice. As aerogel layer keeps the wall performance within the safe values, risk of mould still exists in the fixing area of aluminum cover according to negative values in that area. After the evaluation of temperature factor value f_{Rsi} it was identified that all retrofit scenarios show satisfactory values. Wall heat transmittance values show significant improvement after the implementation of retrofit measures. Total U-value of the detail has decreased from $1.67 \text{ W}\cdot\text{m}^{-1}\cdot\text{K}^{-1}$ at 400 mm wall and $1.23 \text{ W}\cdot\text{m}^{-1}\cdot\text{K}^{-1}$ at 250 mm wall to 0.40 at 400 mm wall and $0.42 \text{ W}\cdot\text{m}^{-1}\cdot\text{K}^{-1}$ at 250 mm wall in case of scenario E.

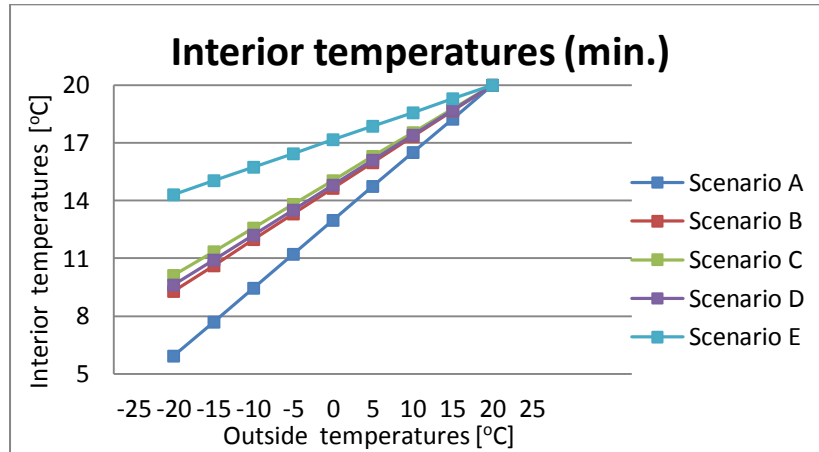


Figure 46. Temperature profiles of the coldest point of interior surface as a function of exterior temperature of detail 2

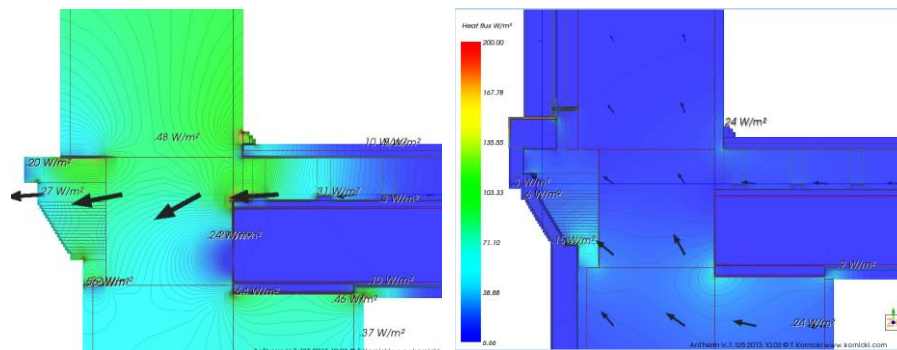


Figure 47. Heat flux of detail 2, scenario A and E

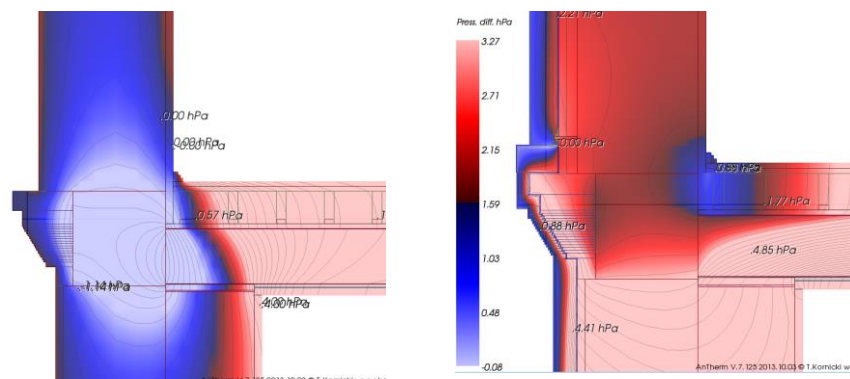


Figure 48. Pressure difference of detail 2, scenario A and E

U-value improvements are represented in Table 15, where number above stands for upper section of a wall, while number under for the section below the floor slab. Other indicators are represented in a Table 16.

Table 15. U-values and its improvement for detail 2

	U-value [$\text{W}\cdot\text{m}^{-2}\cdot\text{K}^{-1}$]	Improvement [%]
Scenario A	1.67	-
	1.23	-
Scenario B	1.19	29
	1.13	8
Scenario C	1.19	29
	1.00	19
Scenario D	0.43	74
	0.37	70
Scenario E	0.40	76
	0.42	66

Table 16. Other values and their improvement after retrofit measures of detail 2

	L^{2D} [$\text{W}\cdot\text{m}^{-1}\cdot\text{K}^{-1}$]	Improvement [%]	Ψ-value [$\text{W}\cdot\text{m}^{-1}\cdot\text{K}^{-1}$]	f_{Rsi} [-]
Scenario A	3.22	-	-0.09	0.65
				0.79
Scenario B	2.71	16	0.07	0.73
				0.85
Scenario C	2.54	21	0.04	0.75
				0.87
Scenario D	1.25	61	0.38	0.79
				0.90
Scenario E	1.07	67	0.13	0.86
				0.92

5.3 Natural stone cornice with steel anchoring

This detail represents a cross-section of an old masonry brick wall with a thickness of 400 mm and historical natural stone cornice. Because of its significant weight, it is fixed with a steel cable throughout the brickwork. In practice, if a load-bearing capacity and durability of decorative elements as cornices do not meet the requirements, they are replaced with new identical details made from such materials as light concrete or plastic. In this work, the original natural stone detail is modelled. Section of the detail can be seen in Figure 49, material properties are to be found in Table 17. As well as in previous cases, five scenarios are suggested for energy-efficient renovation of the detail:

- scenario A: original state of a detail;
- scenario B: perlite insulating plaster is applied with a thickness of 50 mm only along wall surfaces, thermal conductivity of $0.18 \text{ W}\cdot\text{m}^{-1}\cdot\text{K}^{-1}$;
- scenario C: application of perlite insulating plaster system with 50 mm thickness on wall surfaces and 20 mm on decorative element surfaces. Styrofoam layer is added above the cornice, so that original frontal surface of decorative cornice is kept untouched and historical look of the façade is preserved as an object of architectural heritage;
- scenario D: application of aerogel insulating plaster system with a thickness of 50 mm only on wall surfaces;
- scenario E: application of aerogel insulating plaster system with 50 mm thickness on wall surfaces and 20 mm on decorative element surfaces. Styrofoam layer is added above the cornice, so that original frontal surface of decorative cornice is kept untouched and historical look of the façade is preserved as an object of architectural heritage.

After the boundary conditions are defined with exterior temperature $T_e = -10 \text{ }^\circ\text{C}$ and interior temperature $T_i = 20 \text{ }^\circ\text{C}$, the first step of the analysis can be done. All six simulation models and its temperature profiles can be seen in the following Figure 50-54. Blue arrow represents a location of a point with a minimum interior surface temperature. The original scenario A showed that surface temperature of interior surface falls within an extremely low range of $T_{\min} = 8.62 \text{ }^\circ\text{C}$. Such low temperatures are the first signs that mould on the wall surface is likely to grow, because condensation can easily form at this area. Scenario E represents the most effective suggestion, increasing surface temperatures up to $T_{\min} = 12.97$

°C. Scenario B and C performance resembles a similar pattern with values not higher than $T_{\min}=9.59^{\circ}\text{C}$, which is a relatively low temperature and thus is not sufficient for effective energy-efficient renovation. Scenario D demonstrated temperatures in a similar range of degrees with $T_{\min}=10.47^{\circ}\text{C}$. For observation of all scenarios they have been tested by series of simulations with various outside temperatures in a range of -20°C to $+20^{\circ}\text{C}$. Figure 55 below shows a variation of interior surface temperature as a function of outside temperature. Figure 56 below shows a detailed visualisation of the cornice element in scenario A and E, specifically heat flow through a cornice construction before and after it has been insulated with Styrofoam. It shows that heat flow decreased considerably after

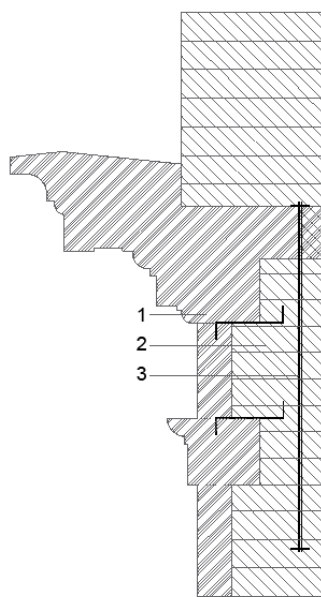


Figure 49. Section of detail 3

Table 17. Material properties of detail 3

	Material	$\lambda [\text{W}\cdot\text{m}^{-1}\cdot\text{K}^{-1}]$	$\mu [-]$
1	Natural stone	2.30	35
2	Old brickwork	0.71	9
3	Reinforced steel	0.60	100000

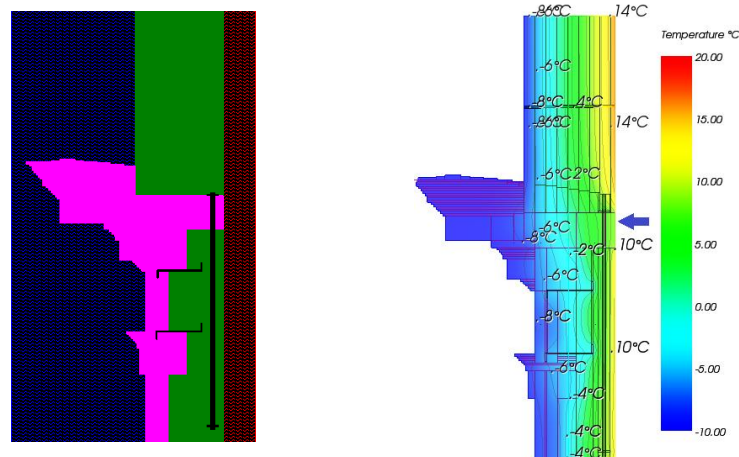


Figure 50. Simulation model and temperature profile of scenario A of detail 3

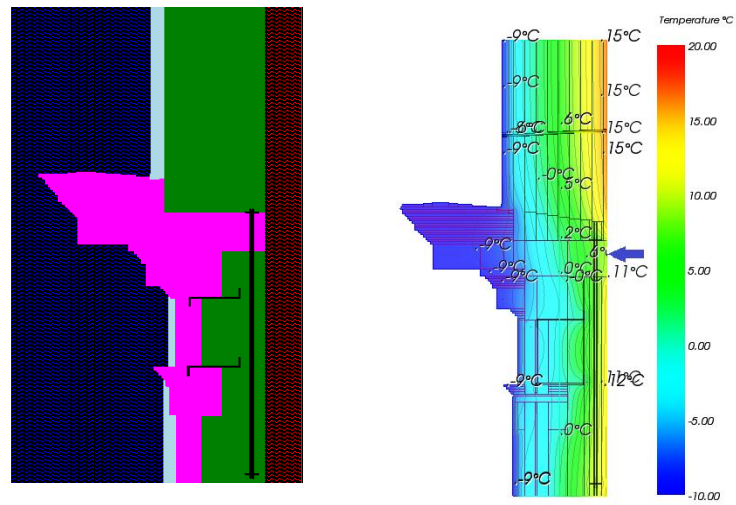


Figure 51. Simulation model and temperature profile of scenario B of detail 3

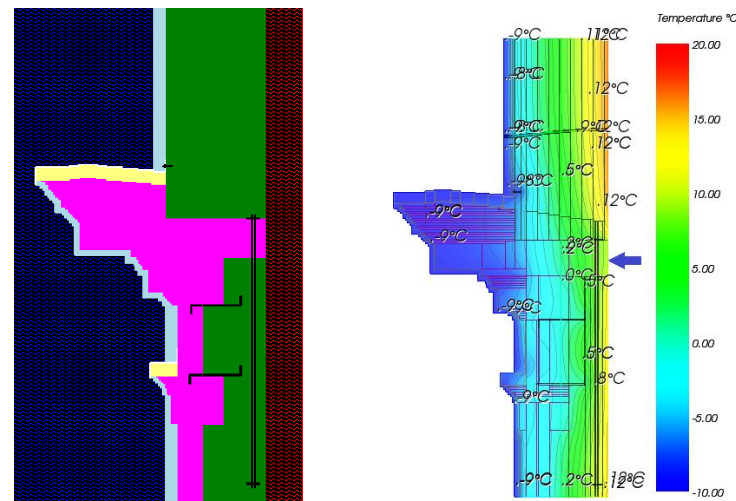


Figure 52. Simulation model and temperature profile of scenario C of detail 3

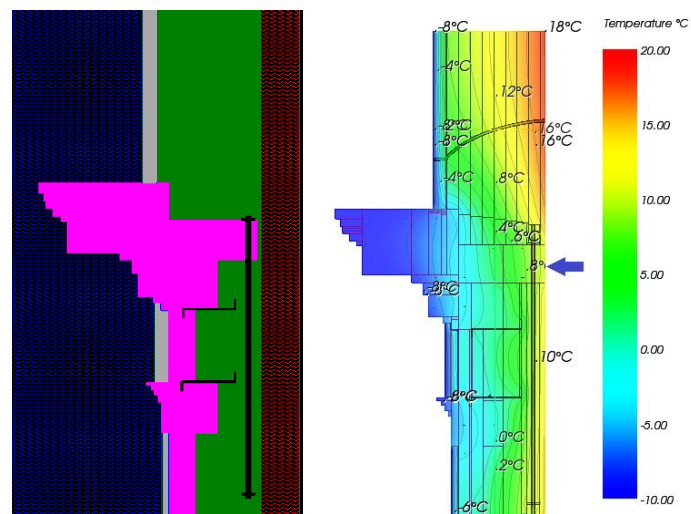


Figure 53. Simulation model and temperature profile of scenario D of detail 3

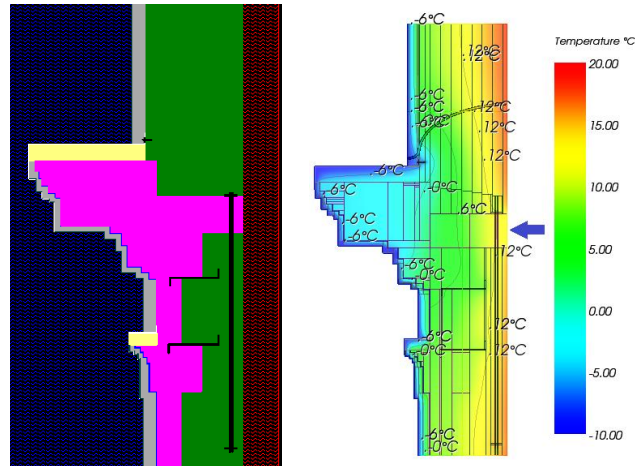


Figure 54. Simulation model and temperature profile of scenario E of detail 3

Styrofoam layer was applied and especially aerogel plaster on cornice surface to $5 \text{ W}\cdot\text{m}^{-2}$.

As important as temperature profiles and heat flows is saturation pressure and humidity level within the wall structure. Figure 57 shows pressure difference profile, from which it is

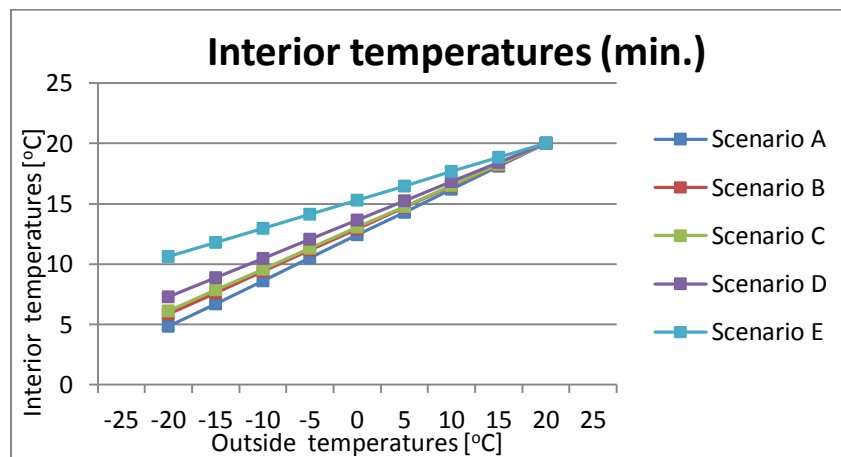


Figure 55. Temperature profiles of the coldest point of interior surface as a function of exterior temperature of detail 3

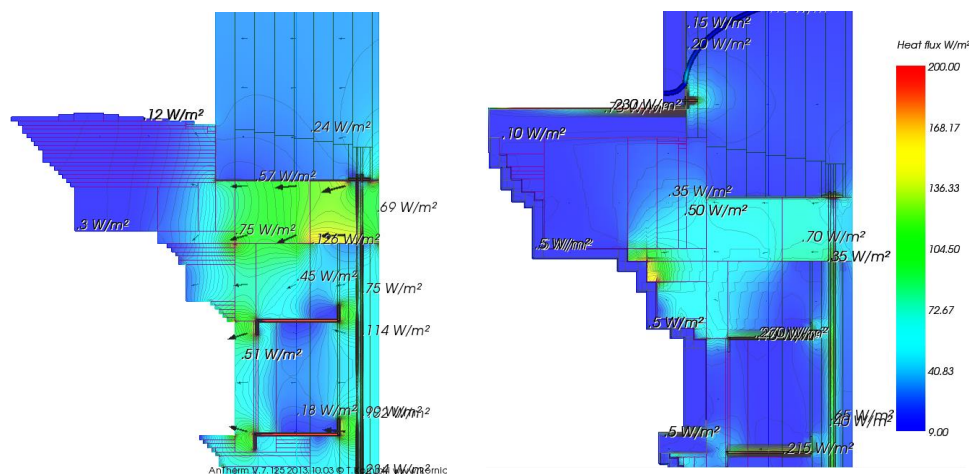


Figure 56. Heat flux profile of detail 3, scenario A and E

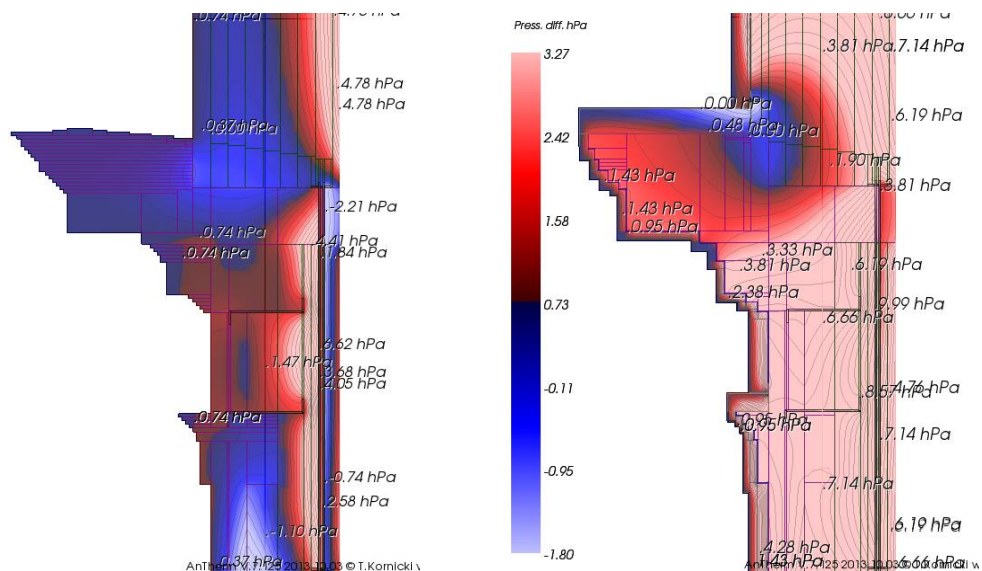


Figure 57. Pressure difference of detail 3, scenario A and E

Table 18. U-values and its improvement after applied retrofit measures for detail 3

	U-value [$\text{W}\cdot\text{m}^{-2}\cdot\text{K}^{-1}$]	Improvement [%]
Scenario A	0.86	-
Scenario B	0.70	19
Scenario C	0.70	19
Scenario D	0.33	62
Scenario E	0.33	62

Table 19. Other values and their improvement after applied retrofit measures of detail 3

	L^{2D} [$\text{W}\cdot\text{m}^{-1}\cdot\text{K}^{-1}$]	Improvement [%]	Ψ -value [$\text{W}\cdot\text{m}^{-1}\cdot\text{K}^{-1}$]	f_{Rsi} [-]
Scenario A	3.03	-	0.69	0.62
Scenario B	2.63	13	0.82	0.65
Scenario C	2.62	14	0.80	0.65
Scenario D	2.18	28	1.18	0.72
Scenario E	1.58	48	1.58	0.77

obvious that risk of condensation significantly decreased within the wall structure after scenario E has been implemented. Nevertheless, area around the cornice and steel anchors

is at risk of higher humidity and consequently risk of mould growth. Judging upon the temperature factors, condensation criteria were not fulfilled in scenarios B, C and D, as temperature factors showed unsatisfactory values below 0.70. Oppositely, scenario E demonstrated positive results, as temperature factors satisfied the condition and comprised $f_{Rsi}=0.77$. These values are represented in Table 19 above.

Wall heat transmittance values demonstrate a significant improvement in analysed scenarios, which can be seen in Table 18 above. Scenario D and E showed an improvement roughly up to 60 % from the original value, while scenario B and C result stayed at 20 % of U-value improvement.

5.4 Ventilated attic with retrofitted ceiling slab

The next detail considered in this work is a cross-section of natural stone decorative element, fixed into an old brick masonry wall with a partial section of a roof. Here, an original slab serves only as a function of a formwork. This method is primarily used in attic extension works to achieve flexibility in wall positioning in the attic space. Thickness of the wall comprises 320 mm and 250 mm, decreasing with a height of the building. The original floor slab is a wooden slab with a thickness of 160 mm, which was retrofitted with an overlaying concrete slab with a thickness of 160 mm. A section and material properties can be seen in Figure 58 and Table 20. Six scenarios are suggested for energy-efficient retrofit of the detail:

- scenario A: original state of a detail;
- scenario B: original state of a detail with improved roof construction;
- scenario C: perlite insulating plaster is applied with a thickness of 50 mm only along wall surfaces and improved roof construction;
- scenario D: application of perlite insulating plaster system with 50 mm thickness on wall surfaces and 20 mm on decorative element surfaces, as well as improved roof construction. Styrofoam layer is added above the cornice, so that original frontal surface of decorative cornice is kept unaltered and historical look of the façade is preserved as an object of architectural heritage;
- scenario E: application of aerogel insulating plaster system with a thickness of 50 mm only on wall surfaces and improved roof construction;
- scenario F: application of aerogel insulating plaster system with 50 mm thickness on wall surfaces and 20 mm on decorative element surfaces, as well as improved roof construction. Styrofoam layer is added above the cornice, so that original frontal

surface of decorative cornice is kept unaltered and historical look of the façade is preserved as an object of architectural heritage.

After the boundary conditions are defined with exterior temperature -10 °C and interior temperature 20 °C, simulation can be proceeded. All six simulation models and its temperature profiles can be seen in the following Figure 59-64. Blue arrow represents a location of a point with a minimum interior surface temperature. Outcome of scenario F

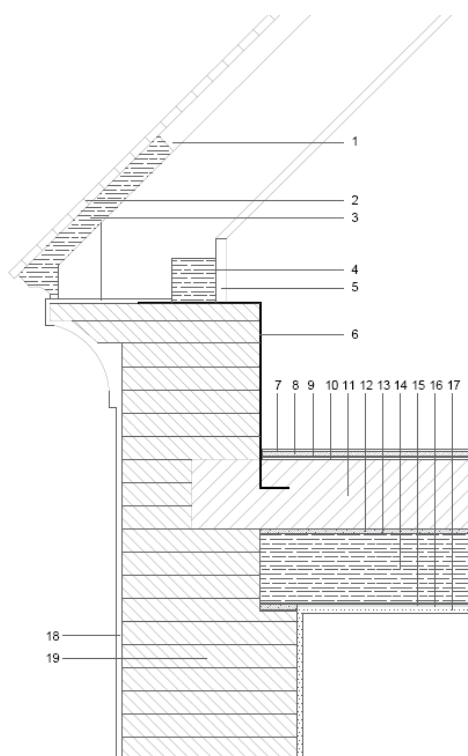


Figure 58. Section of detail 4

Material	λ [W·m ⁻¹ ·K ⁻¹]	μ [-]
1 Air cavity	0.28	1
2 Roofing tile	0.70	10
3 Wood	0.15	125
4 Hard wood	0.02	100
5 Gypsum cardboard	0.21	10
6 Reinforced steel	0.60	100000
7 Coating	0.26	1
8 Concrete screed	1.40	50
9 Mineral wool	0.04	50
10 Cement plaster	1	30
11 Reinforced concrete	2.30	100
12 Plank flooring	0.13	40
13 Cardboard	0.17	50000
14 Hard wood	0.02	100
15 Rough spruce formwork	0.14	50
16 Fire clay	0.75	1
17 Gypsum plaster	0.80	10
18 Lime cement plaster	0.90	15
19 Old brickwork	0.71	4

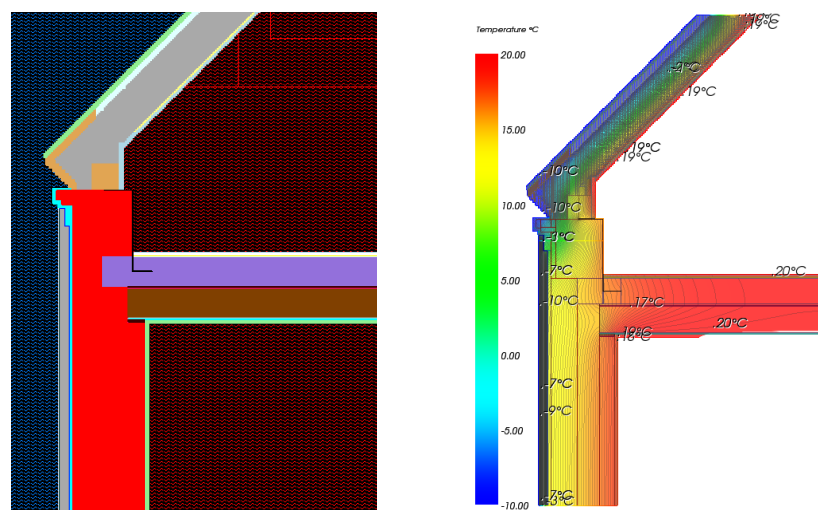
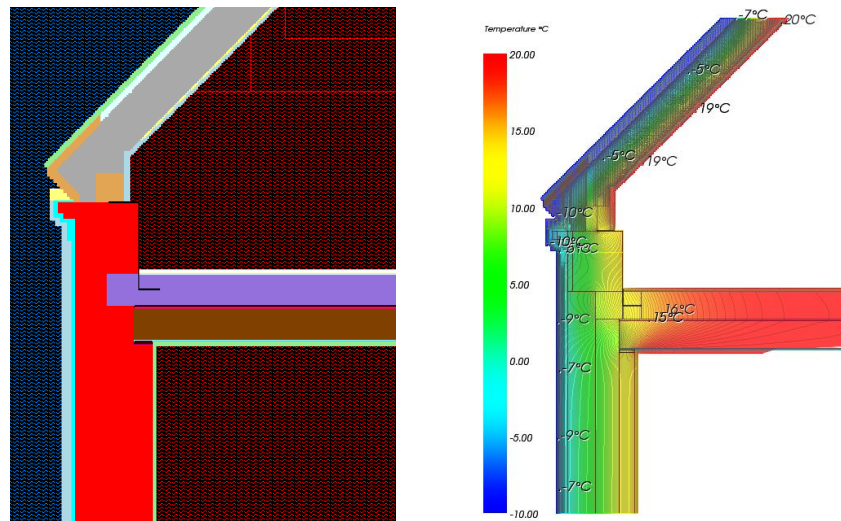
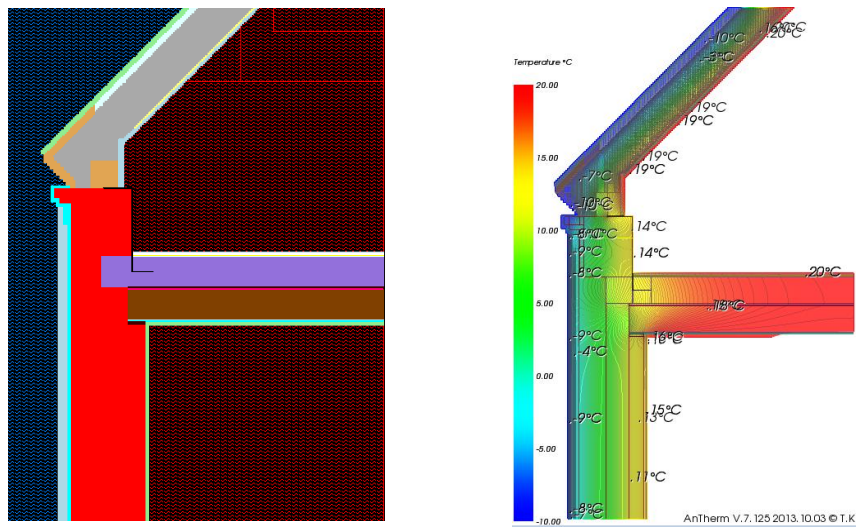
Table 20. List of material properties of detail 4

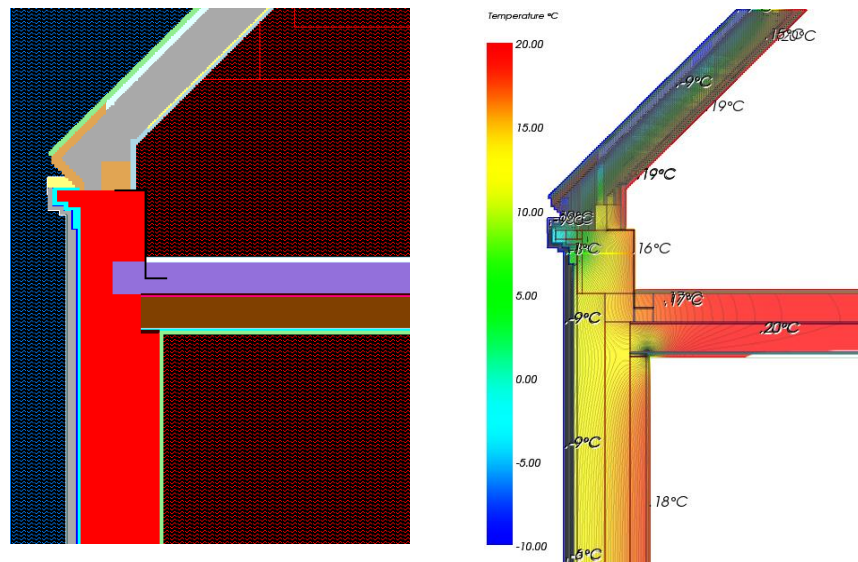
Figure 10 displays the thermal analysis of the roof structure. The left image shows a cross-section of the roof with a color-coded temperature distribution. The right image is a detailed temperature map of the roof structure, showing temperature values in degrees Celsius across different components.

Temperature values (°C) shown in the thermal analysis:

- Roof surface (top right): 14°C, 13°C, 12°C, 11°C, 10°C, 9°C, 8°C, 7°C, 6°C, 5°C, 4°C, 3°C, 2°C, 1°C, 0°C, -1°C, -2°C, -3°C, -4°C, -5°C, -6°C, -7°C, -8°C, -9°C, -10°C.
- Roof edge (left): 19°C, 18°C, 17°C, 16°C, 15°C, 14°C, 13°C, 12°C, 11°C, 10°C, 9°C, 8°C, 7°C, 6°C, 5°C, 4°C, 3°C, 2°C, 1°C, 0°C, -1°C, -2°C, -3°C, -4°C, -5°C, -6°C, -7°C, -8°C, -9°C, -10°C.
- Roof edge (bottom): 19°C, 18°C, 17°C, 16°C, 15°C, 14°C, 13°C, 12°C, 11°C, 10°C, 9°C, 8°C, 7°C, 6°C, 5°C, 4°C, 3°C, 2°C, 1°C, 0°C, -1°C, -2°C, -3°C, -4°C, -5°C, -6°C, -7°C, -8°C, -9°C, -10°C.
- Roof edge (right): 19°C, 18°C, 17°C, 16°C, 15°C, 14°C, 13°C, 12°C, 11°C, 10°C, 9°C, 8°C, 7°C, 6°C, 5°C, 4°C, 3°C, 2°C, 1°C, 0°C, -1°C, -2°C, -3°C, -4°C, -5°C, -6°C, -7°C, -8°C, -9°C, -10°C.

57





thickness. According to the profiles, heat flow through a roof construction has considerably decreased from $90 \text{ W}\cdot\text{m}^{-2}$ to $5 \text{ W}\cdot\text{m}^{-2}$ in case of scenario A and E. During a winter period, surface temperatures of attic space fall to very low values. Hence, it is important to identify the risks of moisture and condensation inside the wall and roof construction. It should be noted that it is irrelevant to evaluate 2 spaces together due to different constructions. Therefore, detail is split up into 2 spaces: under the ceiling slab and above the ceiling slab (attic). Figure 67 shows profiles of pressure difference of scenarios A and E. As it can be seen, amount of vapour considerably decreased after retrofit measures have been applied, in a wall structure as well as it shifted its position in a roof construction. Evaluation of temperature factors showed that space under the floor slab satisfies a condition in its original state and in all retrofit scenarios. As for attic space, values were insignificantly lower and fluctuated from 0.70 up to 0.86, which is satisfactory. Values close to 0.70 might serve as a sign of potential condensation and, as a consequence, mould on a surface.

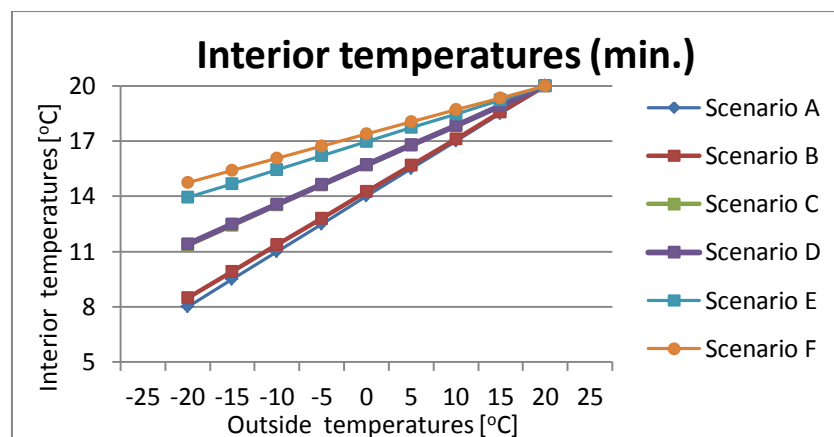


Figure 65. Temperature profiles of the coldest point of interior surface temperature as a function of exterior temperature of detail 4

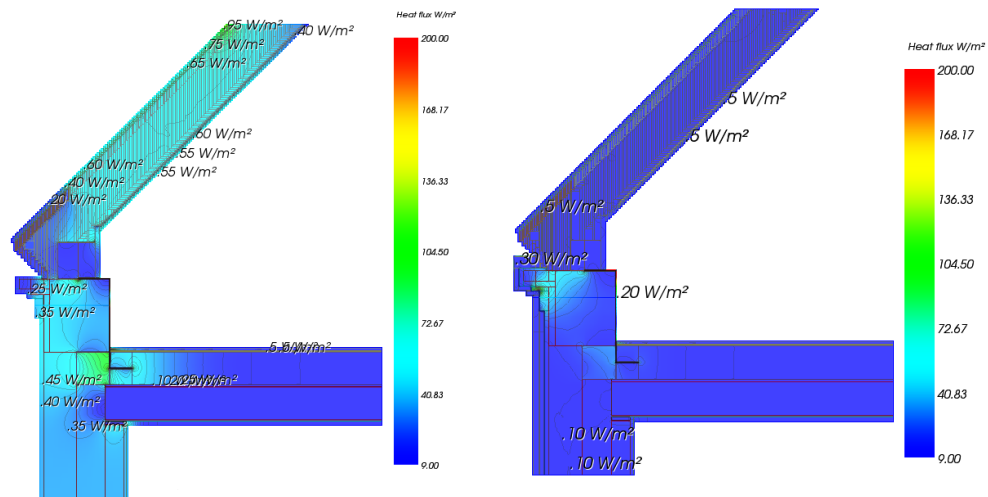


Figure 66. Heat flux of detail 4 of scenario A and E exterior temperature

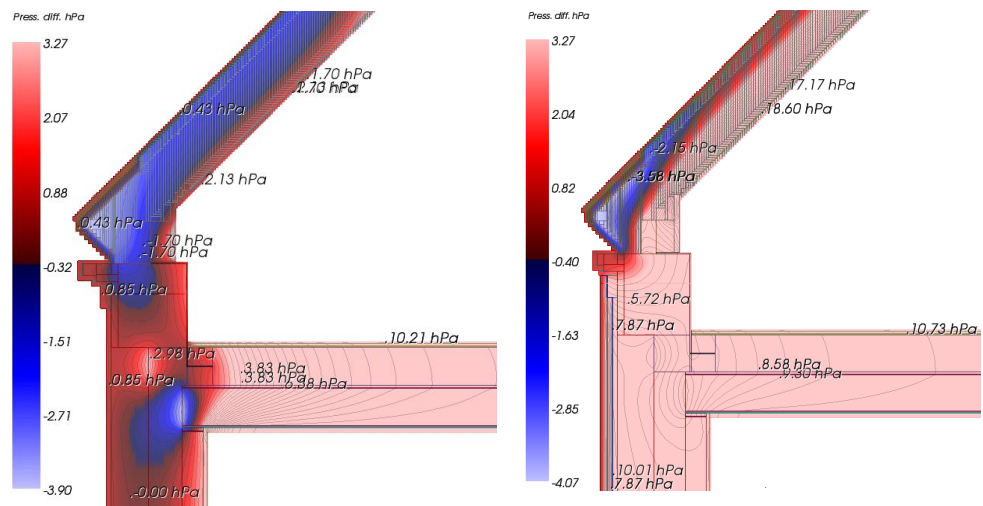


Figure 67. Profile of pressure difference of scenario A and E of detail 4

and, as a consequence, mould on a surface. Though, considering a fact that the space is ventilated, condensation might dry out and the risk of mould might be decreased. Wall heat transmittance values show significant improvement after the implementation of retrofit measures.

Total U-value of the wall in a lower space decreased from $1.24 \text{ W} \cdot \text{m}^{-1} \cdot \text{K}^{-1}$ to $0.37 \text{ m}^{-1} \cdot \text{K}^{-1}$ in case of scenario E and F, thus comprising almost 4 times lower value. Improvements are presented in Table 21. Other indicators are in Table 22.

Table 21. U-value improvement of detail 4

	U-value [$\text{W}\cdot\text{m}^{-2}\cdot\text{K}^{-1}$]	Improvement [%]
Scenario A	1.35	-
	1.24	-
Scenario B	0.11	92
	1.24	0
Scenario C	0.11	92
	0.92	25
Scenario D	0.11	92
	0.92	25
Scenario E	0.11	92
	0.37	70
Scenario F	0.11	92
	0.37	70

Table 22. Improvements due to retrofit measures of detail 4

	L^{2D} [$\text{W}\cdot\text{m}^{-1}\cdot\text{K}^{-1}$]	Improvement [%]	Ψ -value [$\text{W}\cdot\text{m}^{-1}\cdot\text{K}^{-1}$]	f_{Rsi} [-]
Scenario A	5.14	-	1.26	0.70
				0.79
Scenario B	2.63	49	0.62	0.71
				0.79
Scenario C	2.05	60	0.50	0.78
				0.85
Scenario D	2.01	61	0.40	0.79
				0.85
Scenario E	2.02	61	1.31	0.85
				0.94
Scenario F	1.07	79	0.40	0.86
				0.67

5.5 Double-box window

This simulation case assumes an old brick masonry wall with a thickness of 400 mm to be modelled with an originally installed double-box single-layer windows. Double-box single-layer window consists of 2-single glass layers encased in a wooden frame. Section of the material is shown in Figure 68, material properties are provided in Table 23. This type of historical windows is relatively untight in comparison with modern windows and risk of condensation on the inner side of outside glazing is high due to low temperature range between the glazing layers. Age and simplicity of construction is another reason for heat loss through this type of windows. As a consequence, interior space temperatures decrease rapidly and noise protection level doesn't meet sufficient isolation requirement. Six retrofit suggestions are described below, which include:

Table 23. Material properties of detail 5

	Material	λ [W·m ⁻¹ ·K ⁻¹]	μ [-]
1	Lime cement plaster	0.90	15
2	Old brick masonry	0.70	8
3	Gypsum plaster	0.8	25
4	PU-foam (R=55)	0.03	50
5	Wood (R=800)	0.20	125

	Material	λ [W·m ⁻¹ ·K ⁻¹]	μ [-]
6	Gluing material	0.20	50000
7	Air cavity	0.04	1
8	Glass (d=4 mm)	0.80	1
9	Air layer	1.49	1
10	Steel	50	1

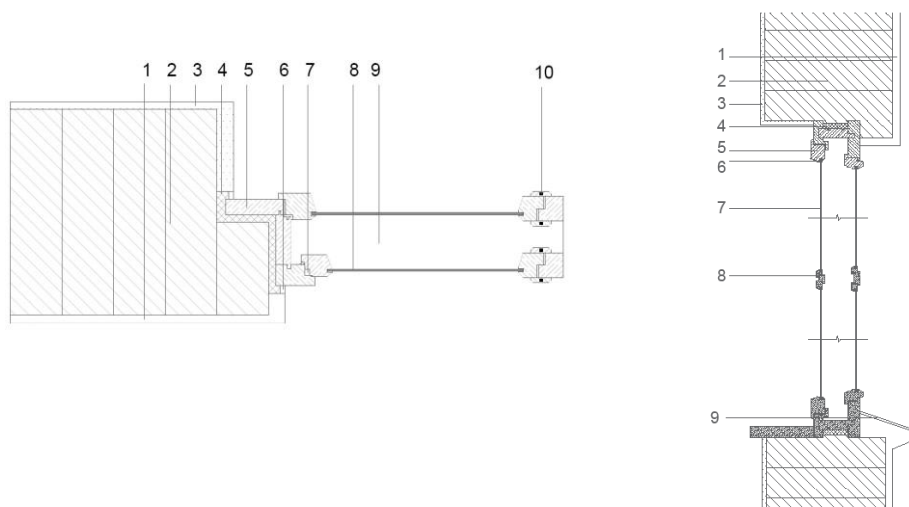


Figure 68. Section of detail 5

- scenario A: original state of a detail;
- scenario B: original state of a detail with an improved window;
- scenario C: perlite insulating plaster is applied with a thickness of 50 mm;
- scenario D: perlite insulating plaster is applied with a thickness of 20 mm;
- scenario E: application of aerogel insulating plaster system with a thickness of 50 mm;
- scenario F: application of aerogel insulating plaster system with 20 mm thickness.

For the reason of heritage protection law, scenario B assumes keeping an original exterior window frame, while replacing interior frame with modern wood frame. Therefore retrofit measures are not visible from the façade viewpoint. This type of renovation of windows is mostly typical for historical buildings, where whole window cannot be replaced. Interior modern wood frame contributes to minimizing heat losses and energy consumption. In this model, new window construction consists of 2 layers of low-e coating insulating glass of 4 mm and 12 mm layer of Xenon, it was selected from AnTherm material database and its total thermal conductivity is $0.018 \text{ W}\cdot\text{m}^{-1}\cdot\text{K}^{-1}$. In addition, a fixing point of glazing and window frame is strengthened with a silicon cover. Scenario F is included as an attempt to reduce the cost of material and maintain sufficient wall performance. After the boundary conditions are defined with exterior temperature -10°C and interior temperature 20°C , simulation can be proceeded. All six simulation models and its temperature profiles can be seen in the following Figure 69-74 for horizontal section and in Figure 75-80 for vertical section. Blue arrow represents a location of a point with a minimum interior surface temperature. Scenario A showed that the highest heat flow occurs through a window construction. As a measure for its improvement, after analysis of scenario B, heat flow decreased and temperature profiles of the original window box improved from 3°C up to 12°C .

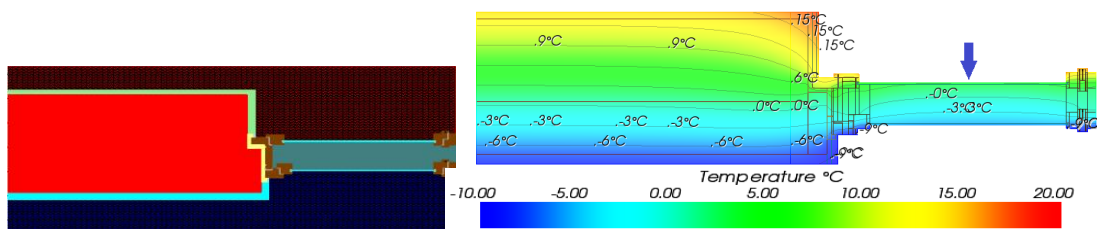


Figure 69. Model and temperature profile of scenario A of detail 5, horizontal section

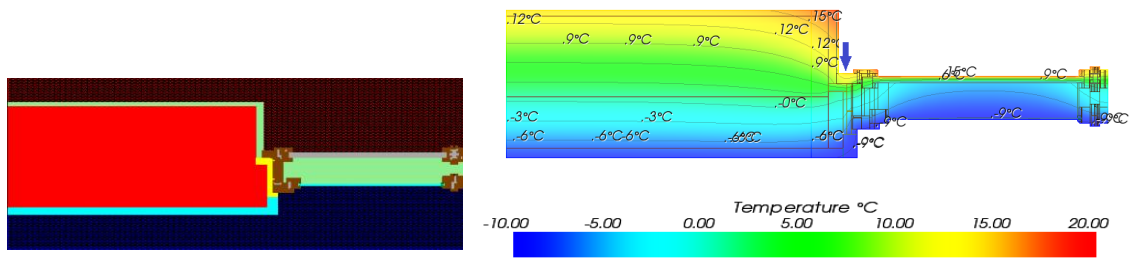


Figure 70. Model and temperature profile of scenario B of detail 5, horizontal section

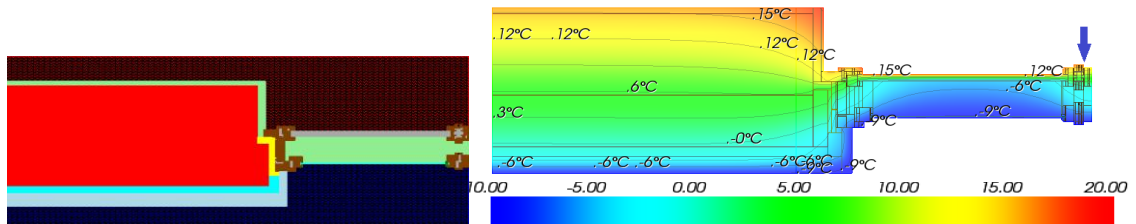


Figure 71. Model and temperature profile of scenario C of detail 5, horizontal section

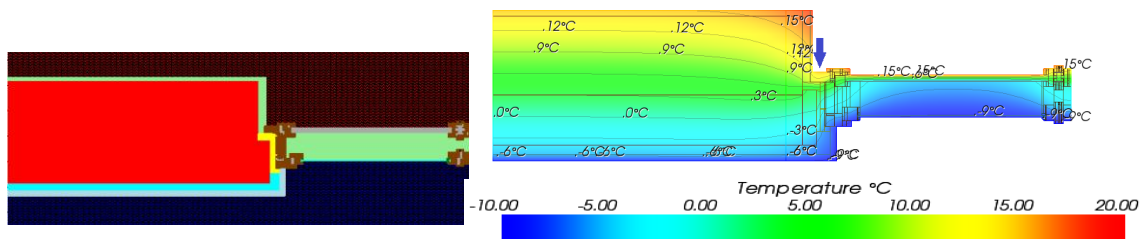


Figure 72. Model and temperature profile of scenario D of detail 5, horizontal section

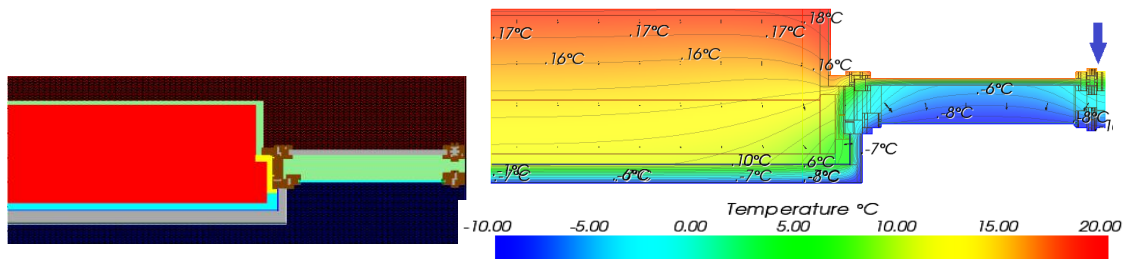


Figure 73. Model and temperature profile of scenario E of detail 5, horizontal section

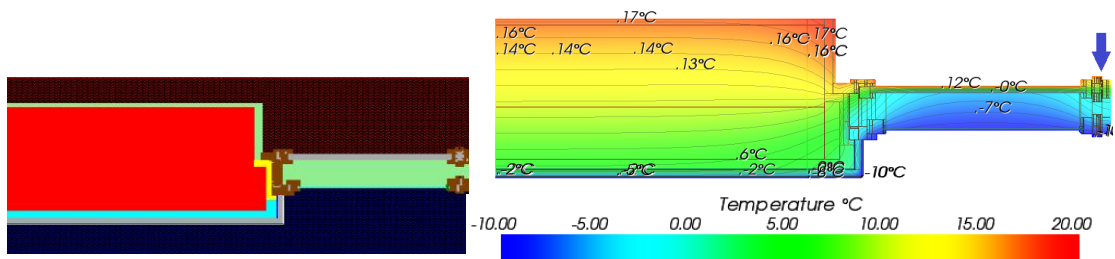


Figure 74. Model and temperature profile of scenario F of detail 5, horizontal section

The rest of scenarios contributed only to performance of a wall structure. As predicted, scenario E and F showed highest temperature values in a range of $T_{\min}=18\text{ }^{\circ}\text{C}$ and $T_{\min}=17\text{ }^{\circ}\text{C}$ respectively. Values of scenarios B, C and D varied in between $12\text{--}15\text{ }^{\circ}\text{C}$. Temperature behaviour of double-box window was tested by series of simulations with various outside temperatures in a range of $-20\text{ }^{\circ}\text{C}$ to $+20\text{ }^{\circ}\text{C}$. Figure 81 shows a variation of interior surface temperature as a function of outside temperature. Such low interior temperatures of scenario A are located in the joint area of the wooden frame, not on interior wall surface (see Figure 82 and Table 24). Heat flow through a construction is shown in Figure 83 for horizontal section and Figure 84 for vertical section. It has demonstrated that a newly installed interior window frame filled with 12 mm Xenon significantly decreased a heat flow through the window. This fact raises a conclusion that consideration of all compound details of a construction is an important issue. Otherwise, if some of them are overlooked, it may disregard other implemented retrofit measures. After it has been shown that heat flow through a window with a modern wooden frame is minimum, it is important to analyse how this type of retrofit influences a formation of condensation in a whole structure. In Figure 85 and 86 it is visible that an area with a negative pressure difference increased. It is explained with a fact that temperature between the frames also decreased due to a reduction of a heat flow from the interior space and therefore cannot keep the same amount of moisture. As a consequence, temperature of the wall surface between the frames decreased too. It should also be noted that highly-insulating glass can be a main cause of the high risk of condensation on a window surface and points of connection of glazing and a frame. This issue can be avoided by means of proper ventilation of interior space, especially during a winter time period, thus level of humidity should reduce significantly. Accumulated moisture during a summer time might also be a reason for condensation. Therefore, this issue might be solved out in the first weeks of heating season, as soon as building materials dried out.

Heat transmittance of the wall showed significant improvement after the implementation of retrofit measures, which decreased from $1.20\text{ W}\cdot\text{m}^{-1}\cdot\text{K}^{-1}$ to $0.36\text{ W}\cdot\text{m}^{-1}\cdot\text{K}^{-1}$ at 400 mm wall in case of scenario E. U-value improvements are represented below in Table 25. As follows, results, closest to U-value of energy-efficient renovation is obtained by scenario E. Results for coupling coefficients, psi-values and temperature factors are to be found in Table 26 below.

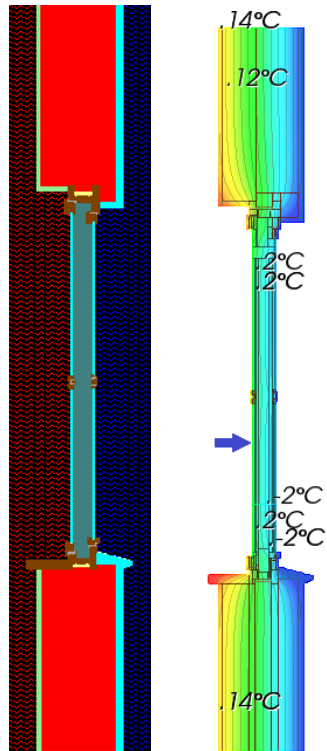


Figure 75. Model and temperature profile of scenario A of detail 5, vertical section

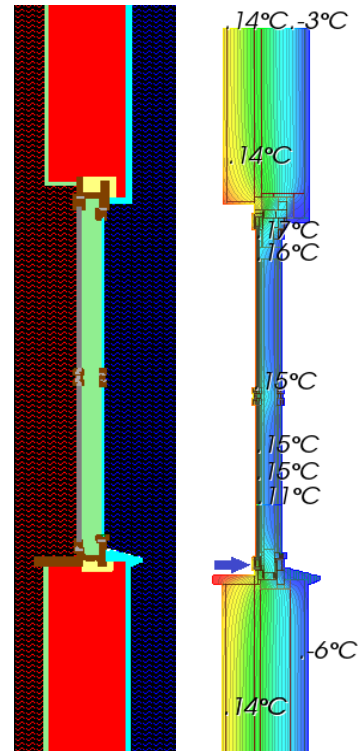


Figure 76. Model and temperature profile of scenario B of detail 5, vertical section

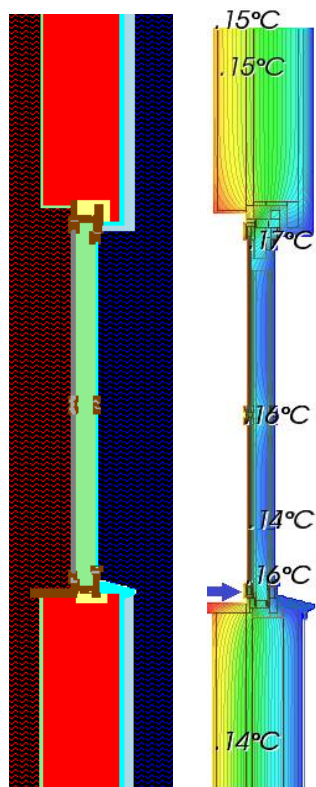


Figure 77. Model and temperature profile of scenario C of detail 5, vertical section

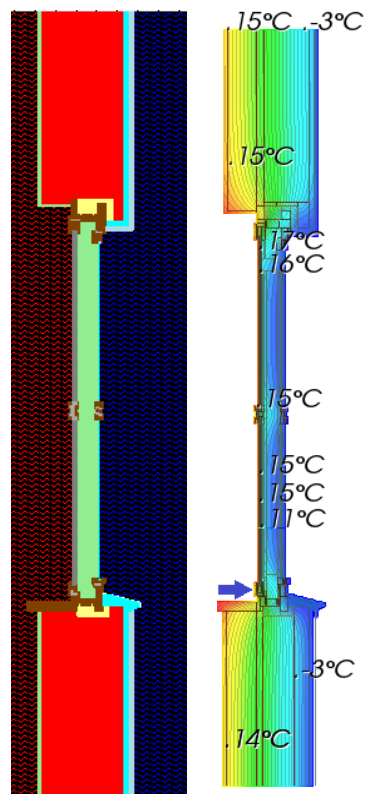


Figure 78. Model and temperature profile of scenario D of detail 5, vertical section

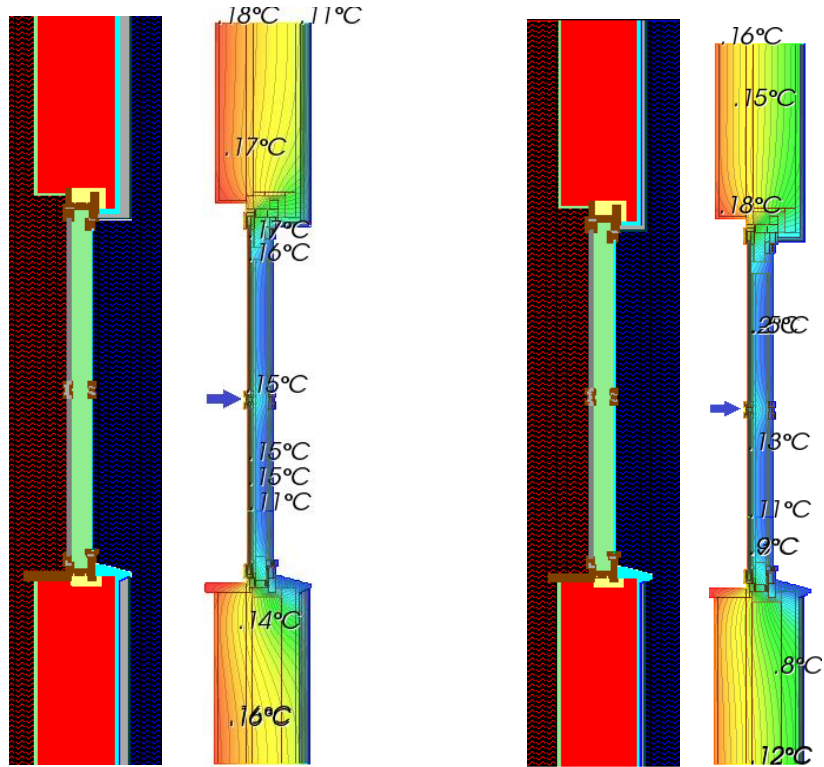


Figure 79. Model and temperature profile of scenario E of detail 5, vertical section

Figure 80. Model and temperature profile of scenario F of detail 5, vertical section

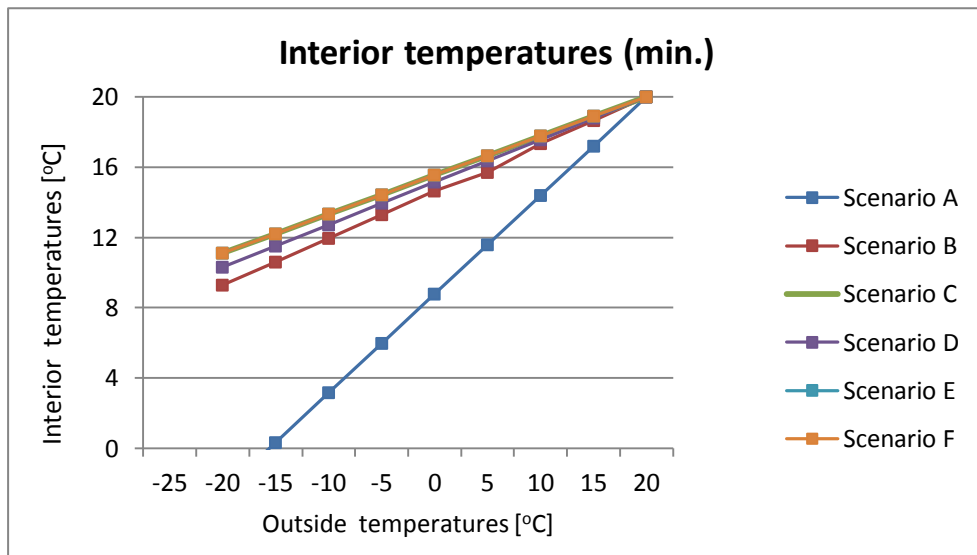


Figure 81. Temperature profiles of the coldest point of interior surface as a function of exterior temperature of detail 5

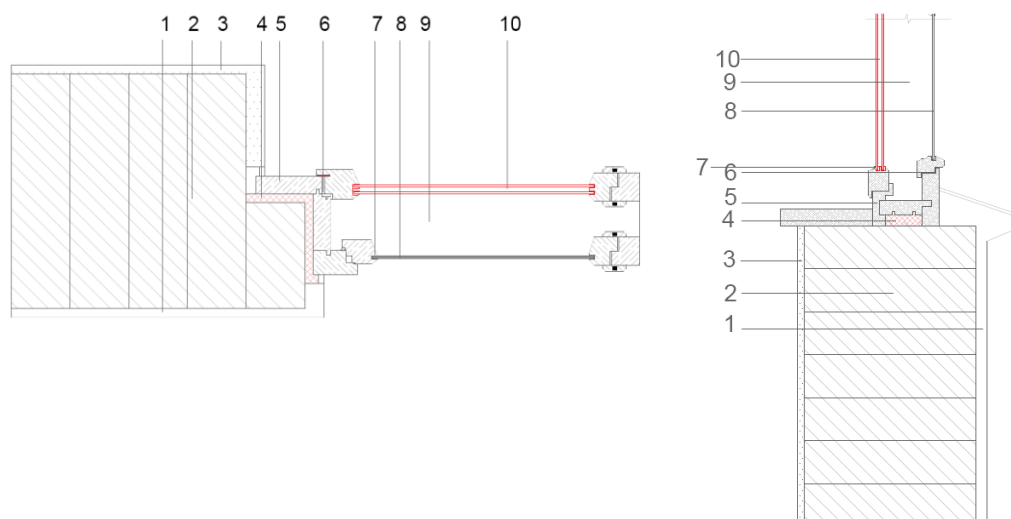


Figure 82. Suggested scenario C: horizontal and vertical section of detail 5

Table 24. Material properties of detail 5

	Material	λ [W·m ⁻¹ ·K ⁻¹]	μ [-]
1	Lime cement plaster	0.90	15
2	Old brick masonry	0.70	8
3	Gypsum plaster	0.80	25
4	PU-foam (R=55)	0.03	50
5	Wood (R=800)	0.20	125
6	Air cavity	0.04	1
7	Silikonexpress Pistolenschaum	0.043	1
8	Glass layer	0.80	1
9	Air layer	0.55	1
10	Two-layer modern glass frame	0.02	1

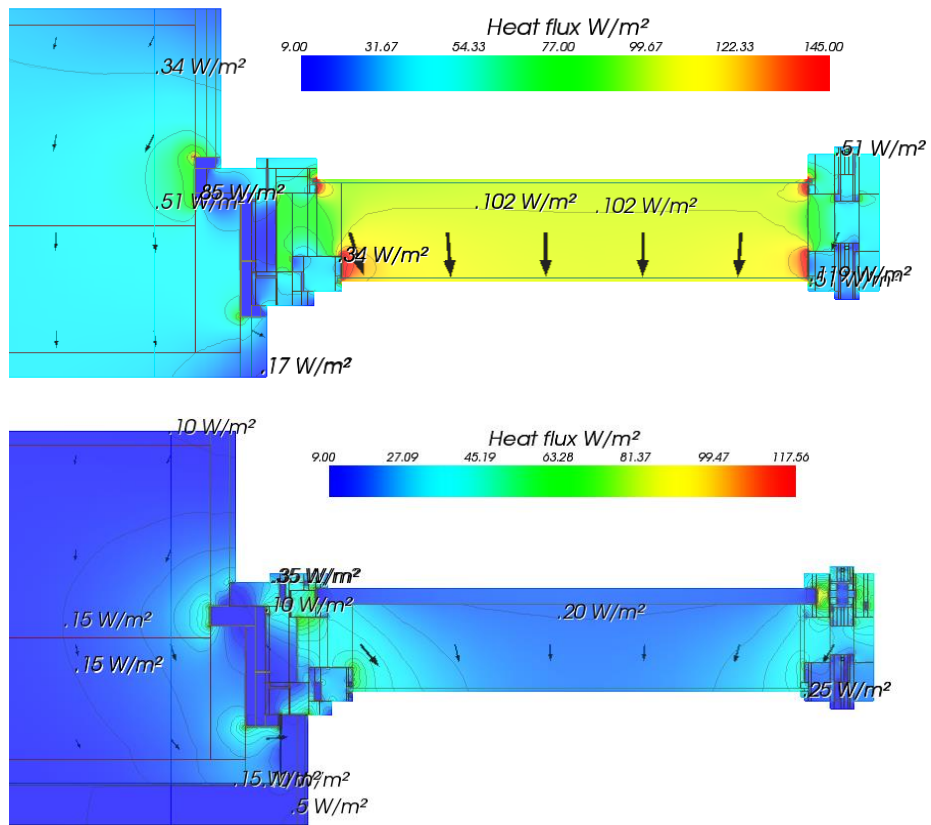


Figure 83. Heat flux of detail 5: scenario A and E, horizontal section

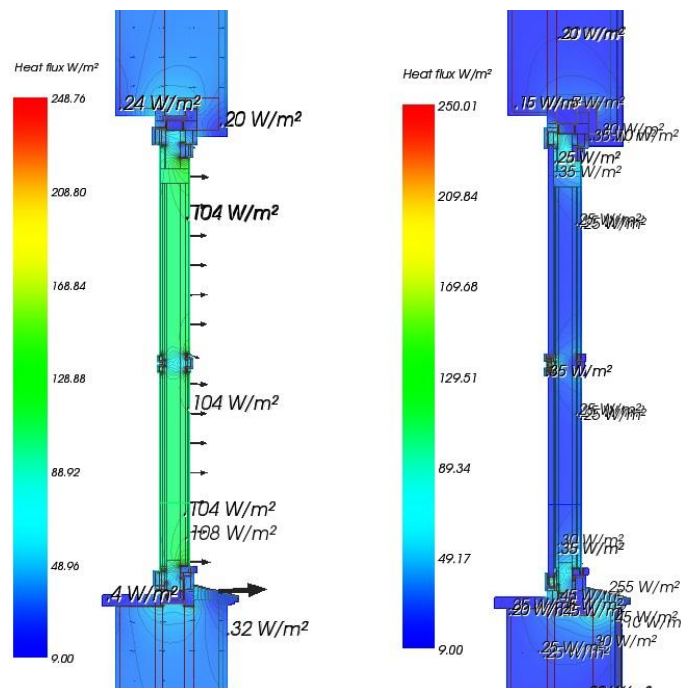


Figure 84. Heat flux of detail 5: original scenario A and scenario E, vertical section

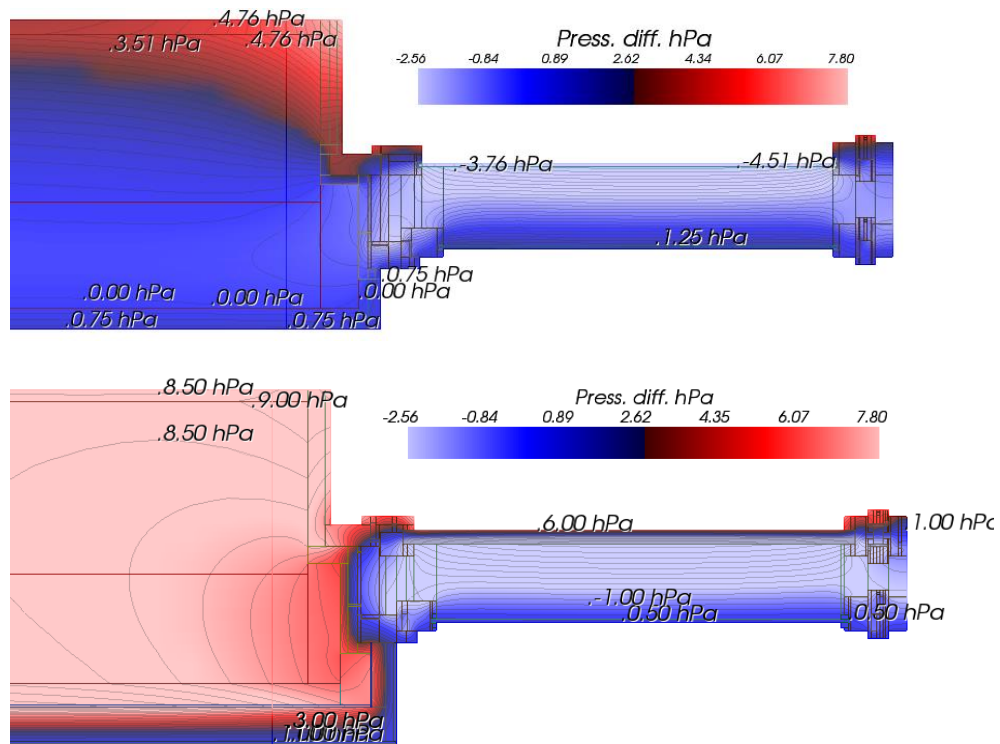


Figure 85. Pressure difference of detail 5, scenario A and E, horizontal section

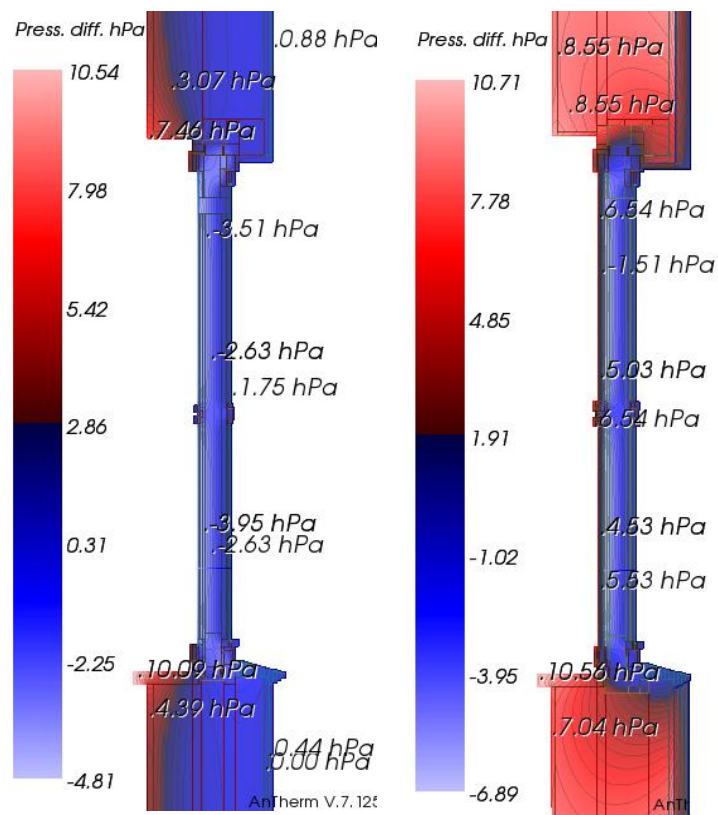


Figure 86. Pressure difference of detail 5, scenarios A and E, vertical section

Table 25. U-values and its improvement after applied retrofit measures of detail 5

	U-value [$\text{W}\cdot\text{m}^{-2}\cdot\text{K}^{-1}$]	Improvement [%]
Scenario A	1.20	-
Scenario B	1.20	-
Scenario C	0.90	25
Scenario D	1.06	12
Scenario E	0.36	70
Scenario F	0.60	50

Table 26. Other values and their improvement after applied retrofit measures, horizontal section

	L^{2D} [$\text{W}\cdot\text{m}^{-1}\cdot\text{K}^{-1}$]	Improvement [%]	Ψ -value [$\text{W}\cdot\text{m}^{-1}\cdot\text{K}^{-1}$]	f_{Rsi} [-]
Scenario A	3.64	-	1.29	0.44
Scenario B	1.94	46	-0.27	0.73
Scenario C	1.62	55	-0.32	0.78
Scenario D	1.79	49	-0.30	0.76
Scenario E	1.06	71	-0.39	0.78
Scenario F	1.29	65	-0.36	0.78

Table 27. Other values and their improvement after applied retrofit measures, vertical section

	L^{2D} [$\text{W}\cdot\text{m}^{-1}\cdot\text{K}^{-1}$]	Improvement [%]	Ψ -value [$\text{W}\cdot\text{m}^{-1}\cdot\text{K}^{-1}$]	f_{Rsi} [-]
Scenario A	8.62	-	3.84	0.43
Scenario B	3.99	54	-0.86	0.74
Scenario C	3.52	59	-0.35	0.76
Scenario D	3.67	57	-0.52	0.76
Scenario E	2.47	71	1.01	0.76
Scenario F	2.86	67	0.46	0.76

Calculation of U-value of original and retrofitted window of scenario C is represented in Table 28 below. Detailed calculation with explained input parameters is to be found in Appendix A. Calculation of retrofitted window with inner insulating glazing is presented in Table 29 below. As an outcome of calculation, heat transfer coefficient of a window has improved by 54 %, specifically from 2.15 to 0.99 $\text{W}\cdot\text{m}^{-2}\cdot\text{K}^{-1}$. Filled cavities with polyurethane foam and decreased heat transfer coefficients of glazing improve room climate, prevent an excess heat loss, increased air flow and energy costs.

Based on above results it is possible to conclude an obvious advantage of retrofitted frame with an applied aerogel insulating plaster system. Interior surface temperature has considerably increased, while heat flow through a window frame has significantly reduced. More detailed calculation is to be found in Appendix A.

Table 28. Input data for calculation of heat transfer coefficient, U_w of an old box window

Interior window frame	$[\text{W}\cdot\text{m}^{-2}\cdot\text{K}^{-1}]$	Exterior window frame	$[\text{W}\cdot\text{m}^{-2}\cdot\text{K}^{-1}]$
U-value of glass U_g	4.72	U-value of glass U_g	4.72
Glazing area A_g	2.26	Glazing area A_g	1.84
U-value of frame U_f	2.80	U-value of frame U_f	2.80
Frame area A_f	0.86	Frame area A_f	0.93
Total U-value	4.73	Total U-value	4.79
U-value: $2.15 \text{ W}\cdot\text{m}^{-2}\cdot\text{K}^{-1}$			

Table 29. Input data for calculation of heat transfer coefficient of a new double-box window with inner insulating glazing

Interior window frame	$[\text{W}\cdot\text{m}^{-2}\cdot\text{K}^{-1}]$	Exterior window frame	$[\text{W}\cdot\text{m}^{-2}\cdot\text{K}^{-1}]$
U-value of glass U_g	0.76	U-value of glass U_g	4.72
Glazing area A_g	2.10	Glazing area A_g	1.84
U-value of frame U_f	2.80	U-value of frame U_f	2.80
Frame area A_f	0.80	Frame area A_f	0.93
U-value	1.32	U-value	4.08
Total U-value: $0.99 \text{ W}\cdot\text{m}^{-2}\cdot\text{K}^{-1}$			

6 CALCULATION OF ANNUAL ENERGY DEMAND

To assess the overall impact of the described retrofit strategies, they were applied virtually to a case study building Figure 87. This building is a typical Viennese residential building from around 1900. For geometry modelling, SketchUp Make was used (SketchUp, 2014). The geometry model was then transferred to Archiphysik. For consideration of the thermal bridges the ψ -values results from AnTherm were added to the default thermal bridges library of Archiphysik. For the whole building evaluation, a set of different cases were calculated. These were based on the scenarios A (original state, referred to as case 1), C (case 2) and E (case 3). All these cases were calculated with two different approaches concerning thermal bridges:

- using the rough default estimation via the Austrian Standard B8110 (ASI, 2014);
- using detailed values for thermal coupling coefficients.

Results of thermal bridge evaluation of details 1-5 were used for this calculation. For thermal bridges of the building envelope that were not evaluated in detail within this study, typical thermal coupling coefficients were used (Hauser & Stiegler 2001; DIN 2008). The evaluations were based on a climate data file for Vienna, Austria. For the detailed calculation of the thermal bridges, the ψ -values illustrated in Table 31 were used. Note that negative ψ -value results of the thermal bridge evaluation were set to zero to avoid inconsistency in heating demand calculation. The other, approximate approach uses an equation from an Austrian Standard (ASI 2014) to derive a cumulative value for all thermal bridges within the building's envelope. This equation uses the conductance values and areas of the building envelope elements as input data.

As an outcome of calculation, following results have been obtained. For case 1, reference annual energy demand with approximated calculation of thermal bridges comprised $316 \text{ kWh}\cdot\text{m}^{-2}\cdot\text{a}$. Detailed calculation of thermal bridges increased the value by 22 %, up to $387 \text{ kWh}\cdot\text{m}^{-2}\cdot\text{a}$. Total heat loss due to linear transmittance in approximate calculation comprised $329 \text{ W}\cdot\text{K}^{-1}$ and in detailed calculation $541 \text{ W}\cdot\text{K}^{-1}$. Energy certificate of detailed calculation of case 1 can be seen in Figure 88. Calculation of case 2 showed a slight improvement in reference annual energy demand and comprised $207 \text{ kWh}\cdot\text{m}^{-2}\cdot\text{a}$ with an approximate calculation of thermal bridges, while detailed calculation showed a value of $229 \text{ kWh}\cdot\text{m}^{-2}\cdot\text{a}$. Total heat loss due to linear in approximate calculation comprised $241 \text{ W}\cdot\text{K}^{-1}$ and in detailed calculation $357 \text{ W}\cdot\text{K}^{-1}$. Energy certificate of case 2 is represented in Figure 89. Calculation of case 3 showed a very satisfactory improvement in building performance.

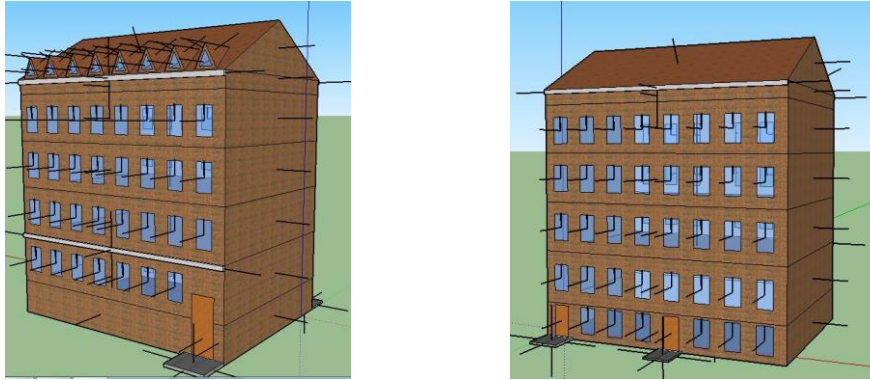


Figure 87. SketchUp model of the analyzed building

Table 30. Assumed values of construction elements

Element	Unit	Scenario A	Scenario C	Scenario E
$U_{\text{ground slab}}$	$[\text{W}\cdot\text{m}^{-2}\cdot\text{K}^{-1}]$	1.20	0.35	0.35
$U_{\text{exterior wall}}$		1.20	0.93	0.37
U_{window}		2.15	0.98	0.98
U_{roof}		1.35	0.11	0.11
U_{door}		2.50	1.70	1.70
g_{glass}	-	0.67	0.67	0.67

Table 31. Psi-values of construction elements in 3 calculation scenarios

	Ψ_{cornice} ($\text{W}\cdot\text{K}^{-1}$)	$\Psi_{\text{window w}}$ (vertical) ($\text{W}\cdot\text{K}^{-1}$)	$\Psi_{\text{window w (horiz.)}}$ ($\text{W}\cdot\text{K}^{-1}$)	Ψ_{roof} ($\text{W}\cdot\text{K}^{-1}$)	$\Psi_{\text{ground slab}}$ ($\text{W}\cdot\text{K}^{-1}$)	Ψ_{door} ($\text{W}\cdot\text{K}^{-1}$)	Ψ_{corner} ($\text{W}\cdot\text{K}^{-1}$)	$\Psi_{\text{floor slab}}$ ($\text{W}\cdot\text{K}^{-1}$)
Case 1	0.19	3.84	1.29	5.04	0.65	0.10	0.00	0.60
Case 2	0.19	0.00	0.00	0.40	0.65	0.10	0.00	0.60
Case 3	0.21	0.46	0.00	0.40	0.65	0.10	0.00	0.60

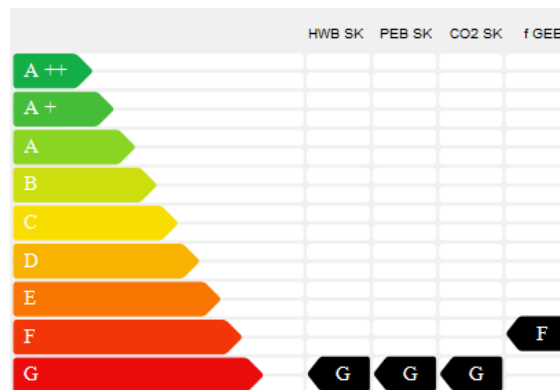


Figure 88. Energy certificate of case 1 with detailed calculation of thermal bridges

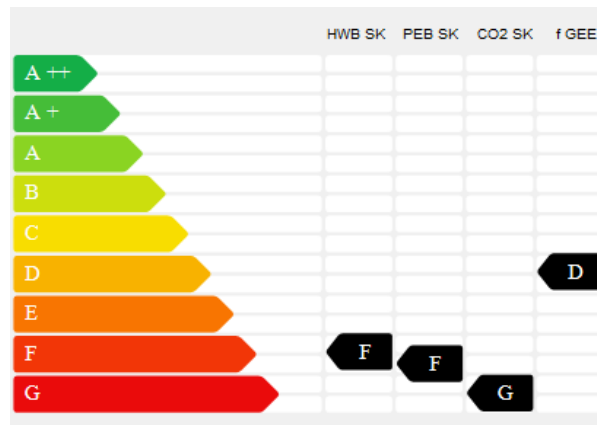


Figure 89. Energy certificate of case 2 with detailed calculation of thermal bridges

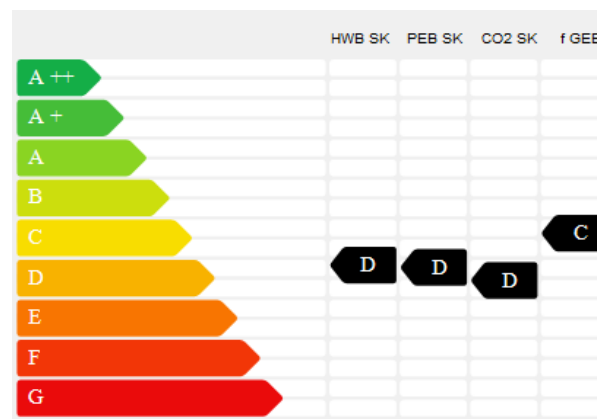


Figure 90. Energy certificate of case 3 with detailed calculation of thermal bridges

Total impact of undertaken retrofit measures, such as aerogel- based plaster insulating system of 50 mm, improvement of original window boxes and added Rockwool insulation of a roof resulted into a significant decrease of annual energy demand. Specifically, it comprised $96 \text{ kWh}\cdot\text{m}^{-2}\cdot\text{a}$ with an approximate calculation of thermal bridges, and $102 \text{ kWh}\cdot\text{m}^{-2}\cdot\text{a}$. Total heat loss due to linear transmittance in approximate calculation comprised $108 \text{ W}\cdot\text{K}^{-1}$ and in detailed calculation $192 \text{ W}\cdot\text{K}^{-1}$. These retrofit measures didn't enhance a building performance to low-energy standards, but contributed to cutting down total energy demand by 75 %. Energy certificate of a building is represented in Figure 90.

Table 32 illustrates the results of the case study building evaluation for heating demand (HWB) and Linear transmittance of the thermal bridges. While the absolute values of the approximation and the detailed calculation show differences, the percentages of improvement, especially for the heating demand, tend to be similar.

The approximation seems to offer sufficient accuracy for benchmarking purposes. However, for detailed thermal bridge evaluation and planning purposes, the detailed values from simulation or catalogues are indispensable.

Table 32. Results of Archiphysik calculation with improvement values (each scenario vs. scenario A)

	HWB [kWh·m ⁻² ·a]		Linear transmittance [W·K ⁻¹]	
	approximated	detailed	approximated	detailed
Case 1	316	387	329	541
Improvement	-	-	-	-
Case 2	207	229	241	357
Improvement	35 %	41 %	27 %	34 %
Case 3	96	102	108	192
Improvement	70 %	74 %	67 %	64 %

7 DISCUSSION

The application of insulation to the outer surfaces of the details results in the following:

- improvement of U-Values of the undistorted “planar” building components;
- changes in the values of indicators related to thermal bridges, i.e., thermal coupling coefficient (L^{2D} according to ISO, 2008), ψ -values, and fRsi-values (ASI, 2014).

While the impact of insulation on the U-Value of the planar components is rather easy to capture, the effects related to thermal bridges require more detailed analysis. Table 33 illustrates all mentioned indicators for all details. Note that some indicators show two instead of one value: This is due to two adjacent building components to outside and two indoor spaces adjacent to the detail (Detail 3 & 4, upper component/upper room), or to results of different sections through the detail (Detail 5, horizontal section mentioned first). Scenarios D and E involve a significant increase in indoor surface temperatures. Table 33 shows the improvement of the detail in terms of U-Value of planar components and thermal bridge indicators. Details 2, 3, 4, and 5 show fRsi-values below the standard thresholds (ASI, 2003) of 0.71 (mould grow) or even 0.69 (surface condensation) in some scenarios. The application of insulation in general seems to improve the thermal performance of the analysed junctions. The scenarios with applied Aerogel plaster insulation significantly decrease the thermal coupling coefficients of the details (28 to 71 % improvement). The application of Perlite plaster in case of detail B does not raise the fRsi above the threshold value. The application of Aerogel plaster raises the fRsi above the threshold of 0.71. This might be due to the fairly large natural stone cornice part. In case of Detail 4, retrofitting only one adjacent building component (roof) might leave the thermal bridge critical. This suggests that treating single components of an existing building's envelope may lead to subpar performance. Rather, a detailed thermal bridge analysis should accompany all projected changes to existing building envelope construction details.

Furthermore, Table 33 illustrates that retrofit strategies that exclude articulated elements of the facades might offer reduce U-values of the planar components, but not necessarily reduce the impact of thermal bridges (this is, for instance, illustrated via the quite large ψ -values in the scenarios without insulation of decorative elements).

Table 33. Results for details 1-5. Bold values in the f_{Rsi} -column imply condensation and/or mould growth risk. Data cells with two instead of one value represent two adjacent building components (Detail 2 and 4), two adjacent indoor spaces (Details 2 and 4), or details with more than one two-dimensional thermal bridge evaluation (Detail 5, horizontal and vertical sections). Values printed in bold letters indicate that they are below the f_{Rsi} -threshold values of 0.69 / 0.71.

Detail&	U-value	U-value	L ^{2D}	L ^{2D}	ψ	f _{Rsi}	
Scenario	[W.m ⁻² .K ⁻¹]	Impr.	[W.m ⁻¹ .K ⁻¹]	Impr.	[W.m ⁻¹ .K ⁻¹]	[-]	
Detail 1	A	1.26	-	3.39	-	0.19	0.73
	B	0.93	26 %	2.67	21 %	0.31	0.77
	C	0.93	26 %	2.55	25 %	0.19	0.81
	D	0.37	71 %	1.63	52 %	0.71	0.81
	E	0.37	71 %	1.13	67 %	0.21	0.90
Detail 2	A	1.67/1.23	- / -	3.22	-	-0.09	0.65 /0.79
	B	1.19/1.13	29 %/8 %	2.71	16 %	0.07	0.73/0.85
	C	1.19/1.00	29 %/19 %	2.54	21 %	0.04	0.75/0.87
	D	0.43/0.37	74 %/70 %	1.25	61 %	0.38	0.79/0.90
	E	0.40/0.42	76 %/66 %	1.07	67 %	0.13	0.86/0.92
Detail 3	A	0.86	-	3.03	-	0.69	0.62
	B	0.70	19 %	2.63	13 %	0.82	0.65
	C	0.70	19 %	2.62	14 %	0.80	0.65
	D	0.33	62 %	2.18	28 %	1.18	0.72
	E	0.33	62 %	1.58	48 %	1.58	0.77
Detail 4	A	1.35/1.24	- / -	5.14	-	1.26	0.70 /0.79
	B	0.11/1.24	92 %/0 %	2.63	49 %	0.62	0.71 /0.79
	C	0.11/0.92	92 %/25 %	2.05	60 %	0.50	0.78/0.85
	D	0.11/0.92	92 %/70 %	2.01	61 %	0.40	0.79/0.85
	E	0.11/0.37	92 %/70 %	2.02	61 %	1.31	0.85/0.94
	F	0.11/0.37	92 %/70 %	1.07	79 %	0.40	0.86/0.67

Detail 5	A	1.20	-	3.64/8.62	-	1.29/3.84	0.44/0.43
	B	1.20	-	1.94/3.99	46 %/54 %	-0.27/-0.86	0.73/0.74
	C	1.06	12 %	1.79/3.67	49 %/57 %	-0.30/-0.52	0.76/0.76
	D	0.90	25 %	1.62/3.52	55 %/59 %	-0.32/-0.35	0.78/0.76
	E	0.60	50 %	1.29/2.89	65 %/67 %	-0.36/0.46	0.78/0.76
	F	0.36	70 %	1.06/2.47	71 %/71 %	-0.39/1.01	0.78/0.76

It has been found that one of the main advantages of aerogel-based plaster is its light weight, which makes its application on weak historical junctions which cannot take additional load possible. In addition, due to its low thermal conductivity, a relatively thin layer is required to ensure a decent wall performance; it makes application of plaster very flexible. For instance, location between the exterior stairs railing and exterior wall surface can be insulated easily; its application on surfaces of decorative elements can be also implemented, while keeping the initial design of the detail.

In historical retrofit, a very important point is maintaining an original look of the historical façade as a measure of architectural heritage protection. Aerogel-based plaster provides broad opportunities in improving a sustainable retrofit methodology by ensuring a high-quality haptic experience in terms of texture and colour. With a mineral-paint colour layer, retrofitted look of the façade resembles an original design to high extent. Moreover, aerogel-based plasters perform satisfactory with other existing plasters on a façade, both physically and aesthetically. It has to be noted that this type of retrofitting technique is more resistant to outside impacts and damages, in comparison with advanced techniques, such as vacuum insulation panels. As aerogel-based plaster provides optimal structural properties, vacuum insulation panels have to be handled carefully and might lose its full performance capacity in case of puncture.

As a main outcome of the AnTherm simulations, it was concluded that aerogel-based plaster significantly contributes to avoiding increased moisture in historical structures due to its permeability to water vapour, low water absorption and water repellent properties. Consequently, it decreases a risk of surface condensation and mould growth, improving the quality of a living environment.

Moreover, application purpose is not limited with exterior insulation, it is also appropriate for interior insulation purposes. That point should make aerogel-based plaster attractive for

architects by providing new possibilities in retrofit without altering an initial look of exterior and interior wall surfaces.

8 CONCLUSION

This contribution explored the application of Aerogel plasters to historical building envelopes. The application of such systems has a high impact on the thermal performance of both planar components and articulated architectural details. If properly planned, it is possible to significantly reduce both the building's heating demand and the impact of thermal bridges, without compromising the building's architectural appearance. Concerning the U-values of the planar surfaces of the examined details, a reduction of 26-71 % could be realized with application of Aerogel plasters (perlite plaster: 19-26 % reduction). The thermal coupling coefficients reduction by application of Aerogel-plasters ranges between 28-79 % for the details (perlite plaster: 13-61 %).

However, an application of aerogel plaster systems on heritage protected architectural buildings still requires specific approval by relevant authorities and might be hampered by the comparatively high price of aerogel plasters and the complexity of application.

During the study, one of the biggest challenges consisted in collecting historical data of architectural drawings of buildings, constructed at the end of 19th and the beginning of 20th century. Thus, necessary assumptions have been made on materials and dimensions of the structures and data sources have been documented.

It is important to mention that this project was carried out considering constant energy consumption of the walls. To get a more complete and concise picture concerning of aerogel insulation, transient simulation of a system may be carried out, as well as life cycle costs can be evaluated.

An important recommendation would consist in strengthening insulation layers in the joints, where the heat fluxes have the biggest rate. An especially important point is to retrofit original old windows that are characterized with the highest heat flow. After all retrofit measures are applied, the structure will resist heat transfer in a new way and will response to the requirements of energy efficiency. Another point to pay attention is keeping the original look of decorative elements, meaning to avoid application of aerogel-based plaster on its surfaces when possible. Care must be taken of the fact that insulation should be highly capillar, so that moisture is released from the insulation and no risk of mould and condensation formation arises.

Future research efforts in this field should address the following aspects:

- broadening the scope of examined details based on typical construction details from different architectural époques that would allow a usage of Aerogel-plaster systems;

- 3D simulations of thermal bridges;
- conducting transient thermal performance simulations of the thermal bridges and comparison with measurements of corresponding details;
- the details illustrated in this contribution were retrofitted following straight-forward approaches. There is, for sure, potential for more sophisticated solutions such as a partial material replacement, and detailing based on traditional techniques. For instance, the application of the plaster without edge profiles and stabilizing net should be explored via long-term-durability tests, as this seems to be important for retrofitting highly-articulated façade profiles;
- currently, the behaviour of the Aerogel-plaster can be modelled in view of parameters such as conductivity, water vapour resistance, and specific heat. However, long-term monitoring of the thermal and hygric behaviour of the aerogel plaster in different scenarios, such as drought stress, high sun exposure, and wind-driven rain should be considered;
- to popularise aerogel plasters in the market, comprehensive efforts in communication, involvement, and coordination of all potential stakeholders of a retrofit processes (clients, craftsmen, and historical preservation officials) is required.

As a conclusion, evaluated energy-efficient refurbishment with an applied highly insulating aerogel plaster system is highly recommended for historical buildings, since indoor environment can be improved and running energy costs of the building for heating and cooling can be reduced without altering an original look of the facade and reducing a volume of interior space.

9 REFERENCES

- AAAMSA, 2001. Thermal Insulation Handbook. <http://www.aaamsa.co.za/images/Technical%20Publications/TIASA/Handbook%20Chapter1.pdf>. Accessed 04.05.2014.
- A-Null, 2014. "Archiphysik 11", www.archiphysik.com. Accessed 11.2014.
- ASI, 2003. Austrian Standard B 8110-2, 2003. "Wärmeschutz im Hochbau, Teil 2: Wasserdampfdiffusion und Kondensationsschutz". <http://www.austrian-standards.at>. Accessed November 2014.
- BDA, 2011. "Richtlinie Energieeffizienz am Baudenkmal". Bundesdenkmalamt (Editor). <http://www.bda.at/documents/944221227.pdf>. Accessed November 2014.
- BS EN ISO 10211, 2009. *Thermal bridges in building construction. Heat flows and surface temperatures. Detailed calculations.*
- Carmeliet, J. and Zimmermann, M., 2011. Annual Report. <http://www.bfe.admin.ch/php/modules/enet/streamfile.php?file=000000010665.pdf&name=000000290447>. Accessed 25.05.2014.
- DIN, 2008. "DIN EN ISO 14683 – Wärmebrücken im Hochbau – Lagenbezogener Wärmedurchgangskoeffizient – Vereinfachte Verfahren und Anhaltswerte (ISO 14683:2007)". Normenausschuss Bauwesen (NABau) im DIN, Deutsches Institut für Normung e.V.
- Eicke-Hennig, W., Siepe, B., & Zink, J., 1997. *Konstruktionshandbuch – Verbesserung des Wärmeschutzes im Wohngebäudebestand*. Darmstadt 1997. <http://www.iwu.de/dateien/Konstruktionshandbuch.pdf>. Accessed 11.2014.
- FIXIT AG, 2013. http://www.fixit.ch/var/fixitgruppe/storage/ilcatalogue/files/pdf/CHDE/Technisches_Merkblatt_Fixit_222_Aerogel_Hochleistungsdc3%A4mmputz_DC0017220.PDF. Accessed 19.04.2014.
- Fricke, J. and Tillotson T., 1997. Aerogels: production, characterization, and applications. In: *Thin Solid Films* (297), pp. 212–223.
- Graham, T. J., 1864. On the properties of silicic acid and other analogous colloidal substances. In: *Journal of the Chemical Society* 17, pp. 318-327.
- Griffith, B. T. and Arasteh, D., 1995. Gas-Filled Panels: An Update on Applications in the Building Thermal Envelope. *Proceedings of the BETEC Fall Symposium "Superinsulations*

- and the Building Envelope*”, November 14, 1995, Washington, DC.
- Gulf Perlite, 2014. <http://www.uaeperlite.com/brochure/GulfPerlitePlastersTDS.pdf>. Accessed 21.04.2014.
- Hrubesh, L.W. and Pekala, R.W., 1994. Thermal properties of organic and inorganic aerogels. In: *Journal of Materials Research*/ Volume 9/ Issue 03/ 1994, pp 731-738. DOI: 10.1557/JMR.1994.0731.
- Huttler, W., Sammer, K., 2010. Innovative Sanierung von Gründerzeitgebäuden – Technische Optionen und rechtliche Fragen. In: *Immolex* (2010), pp. 2037-243.
- Kistler, S. S., 1932. Coherent expanded aerogels. In: *Journal of Physical Chemistry* 36 (1), pp. 52-64. DOI: 10.1021/j150331a003.
- Kornicki, M., 2014 “AnTherm 7.125” www.kornicki.eu. Accessed 11.2014.
- Kosny, J., 2008. R-Value Misconceptions. In: *Better Buildings by Design Conference* (2008), 14th February 2008, Burlington, VT.
- Meijer, F. and Thomsen, A., 2007. Sustainable Housing Transformation; Quality And Improvement; Strategies of the ageing private housing stock in the Netherlands. In: *Sustainable Urban Areas: International Conference*, 25-28 June 2007, Rotterdam, Netherlands.
- Meijer, F., Itard, I. and Sunikka-Blank, M., 2009. Comparing European residential building stocks: performance, renovation and policy opportunities. In: *Building Research and Information* 37 (5-6), pp. 533-551.
- Oak Ridge National Laboratory, 2006. <http://gfp.lbl.gov/>. Accessed 15.05.2014.
- Ochs, F. and Müller-Steinhagen, H., 2005. Institute for Technical Thermodynamics of Stuttgart. http://www.itw.uni-stuttgart.de/dokumente/Publikationen/publikationen_05-11.pdf. Accessed 12.04.2014.
- OIB, 2011. Leitfaden zur OIB-Richtlinie 6. www.oib.or.at. Accessed 11.2014.
- Open Source Nanotech, 2013. <http://www.aerogel.org/?p=822>. Accessed 05.04.2014.
- Organization for the Promotion of Energy Technologies, 2002. Thermal bridges in residential buildings in Denmark. https://www.tc.cz/files/istec_publications/thermal-bridges.pdf. Accessed 07.07.2014.
- Pierre, A. C. and Pajonk, G. M., 2002. Chemistry of aerogels and their applications.

- In: *Chemical Reviews* 102 (11), pp. 4243–4266. DOI: 10.1021/cr0101306.
- Rammerstorfer J., 2012. Modernisierung von Gründerzeitgebäuden. E7 Energie Markt Analyse GmbH. http://www.oegut.at/downloads/pdf/bi_hdz-twsjuni2012_rammerstorfer.pdf. Accessed 05.11.2014.
- Reichel, A., Hochberg, A. and Kopke, C., 2004. Plaster, Render, Paint and Coatings: Details, Products, Case Studies. http://books.google.at/books?id=y6JNRsbjAX4C&printsec=frontcover&hl=de&source=gbs_ge_summary_r&cad=0#v=onepage&q&f=false. Accessed 02.05.2014.
- Rhee-Duverne, S. and Baker, P., 2013. Research into the thermal performance of traditional brick walls. <http://www.helm.org.uk/guidance-library/research-thermal-performance-traditional-brick-walls/1917394/>. Accessed 28.08.2014.
- Riccabona, C. & Mezera, K., 2003. *Baukonstruktionslehre 5, Sanierungen-Industriebau-Fassaden*. Manz, 2003.
- Saint Gobain Group, 2008. <http://www.isover.com/Our-solutions/Insulation-materials/Mineral-wool/Features>. Accessed 06.04.2014.
- Schmidt, M. and Schwertfeger, F., 1998. Applications for Silica Aerogels Products. In: *Journal of Non-Crystalline Solids* (225): pp. 364-368.
- Shukla, N. C., Fallahi, A. and Kosny, J., 2012. Aerogel for thermal insulation of interior wall retrofits in cold climates. In: *Building Enclosure Science & Technology (BEST3) Conference*, 2-4 April 2012, Atlanta, GA.
- SketchUp. 2014. "Trimble SketchUp Make 2014", www.sketchup.com. Accessed 11.2014.
- Sliva, S. P., Sabino, M. A., Fernandes, E. M., Correlo, V. M., Boesel, L. F., Reis, R. L., 2005. Cork: properties, capabilities and applications. In: *International Materials Review* 50 (6), pp. 345-365.
- Smitha, S., Shajesh, P., Aravind, P. R., Rajesh Kumar, S., Krishna Pillai, P., Warriar, K. G. K., 2006. Effect of aging time and concentration of aging solution on the porosity characteristics of subcritically dried silica aerogels. In: *Microporus Mesoporus Mater* 91, pp. 286-292.
- Soleimani, A. D., Abbasi, M. H., 2008. Silica aerogel; synthesis, properties and characterization. In: *Journal of materials processing technology* 199 (2008), pp. 10-26.
- TABULA Web Tool, 2013. <http://webtool.building-typology.eu>. Accessed 04.06.2014.

- Ward, T., 2006. BRE's Information Paper IP 1/06. Assessing the effects of thermal bridging at junctions and around openings. <http://products.ihs.com/cis/Doc.aspx?AuthCode=&DocNum=277903>. Accessed 17.03.2014.
- Werner, E., Siepe, B., Zink, J., 1997. *Konstruktionshandbuch – Verbesserung des Wärmeschutzes im Wohngebäudebestand*. Darmstadt, 1997. ISBN: 3-932074-09-2.
- Wienerberger AG, 2013. Thermal Bridge Catalogue for low-energy house. <http://www.wienerberger.at/downloads-service-und-infomaterial/downloads/energie-effizientes-bauen>. Accessed 5.11.2014.
- Wohnfonds Wien, 2013. Thewosan, Thermal Rehabilitation for Residential Projects. http://www.wohnfonds.wien.at/media/file/Sanierung/erstinfo_thewosan.pdf. Accessed 25.09.2014.
- World Bank, 2011. World Bank Indicators Austria. <http://www.tradingeconomics.com/austria/co2-emissions-from-residential-buildings-and-commercial-and-public-services-million-metric-tons-wb-data.html>. Accessed 20.03.2014.
- WUFI, 2013. "Software for calculation of moisture and heat transfer in building components". <http://www.wufi.de>. Accessed 11.10.2014.

10 LIST OF FIGURES

Figure 1. Scheme of mineral wool (Knaufinsulation 2011)	5
Figure 2. Scheme of expanded polystyrene (Finehomebuilding 2008-2011).....	5
Figure 3. Scheme of polyurethane foam (Directindustry 2008)	6
Figure 4. Scheme of extruded polystyrene (Archiexpo 2001)	6
Figure 5. Scheme of cellulose	7
Figure 6. Scheme of perlite plaster	7
Figure 7. Scheme of cork material (Wikimedia 2014).....	7
Figure 8. Scheme of gas-filled panel	8
Figure 9. R-value of GFP (Buildinggreen.....	8
Figure 10. Vacuum insulation panels (Emeraldinsight 2012)	10
Figure 11. Scheme of aerogel (Illumina-Chemie 2008)	10
Figure 12. Scheme of silica aerogel (AEROCOINs 2014).....	12
Figure 13. Structure of silica aerogel (LLNL 2006)	13
Figure 14. Relative aging rate as function of time for two aging mechanisms (Strom 2007) .	14
Figure 15. Application of silica aerogel in buildings (Duo-Gard 2011; European Coatings 2013).....	15
Figure 16. Dwellings in Vienna in construction periods (Rammerstorfer 2012)	16
Figure 17. Building matrix of TABULA project for Austrian building stock (Tabula Web Tool 2014).....	18
Figure 18. Classification of thermal bridges (OPET 2002)	20
Figure 19. Stepping arrangement of curve element (Ward 2006)	25
Figure 20. Scheme of approximated stepping slope in AnTherm.....	25
Figure 21. Slope approximation for rectangular modelling software (Ward 2006)	25
Figure 22. Arrangements of layers in AnTherm.....	26
Figure 23. Visual representation of results in AnTherm	26
Figure 24. Thermal bridges in a three-dimensional calculation (Wienerberger 2013; Antherm 2008).....	33
Figure 25. Base building of Grunderzeit construction period	34
Figure 26. ROFIX Aerogel Insulating Plaster System (ROFIX AG 2014	36
Figure 27. Adhesive primer 675 NHL (on the left), application of FIXIT 222 with a plastering machine (on the right).....	37
Figure 28. Levelling off FIXIT 222 (left), surface of FIXIT 222 (right)	37

Figure 29. Reinforcement mesh for corners of openings (left), application of reinforcement mesh with FIXIT 223 (right)	37
Figure 30. Applied reinforcement mesh (left), FIXIT 222 insulating plaster (right)	37
Figure 31. Section of detail 1	40
Figure 32. Simulation model and temperature profile of scenario A of detail 1	40
Figure 33. Simulation model and temperature profile of scenario B of detail 1	40
Figure 34. Simulation model and temperature profile of scenario C of detail 1	41
Figure 35. Simulation model and temperature profile of scenario D of detail 1	41
Figure 36. Simulation model and temperature profile of scenario E of detail 1	41
Figure 37. Temperature profiles of the coldest point of interior surface as a function of exterior temperature of detail 1	42
Figure 38. Heat flux profile of detail 1, scenario A and E	43
Figure 39. Pressure difference of detail 1, scenario A and E	43
Figure 40. Section of detail 2	45
Figure 41. Simulation model and temperature profile of scenario A of detail 2	46
Figure 42. Simulation model and temperature profile of scenario B of detail 2	46
Figure 43. Simulation model and temperature profile of scenario C of detail 2	46
Figure 44. Simulation model and temperature profile of scenario D of detail 2	47
Figure 45. Simulation model and temperature profile of scenario E of detail 2	47
Figure 46. Temperature profiles of the coldest point of interior surface as a function of exterior temperature of detail 2	48
Figure 47. Heat flux of detail 2, scenario A and E	48
Figure 48. Pressure difference of detail 2, scenario A and E	48
Figure 49. Section of detail 3	51
Figure 50. Simulation model and temperature profile of scenario A of detail 3	51
Figure 51. Simulation model and temperature profile of scenario B of detail 3	52
Figure 52. Simulation model and temperature profile of scenario C of detail 3	52
Figure 53. Simulation model and temperature profile of scenario D of detail 3	52
Figure 54. Simulation model and temperature profile of scenario E of detail 3	53
Figure 55. Temperature profiles of the coldest point of interior surface as a function of exterior temperature of detail 3	53
Figure 56. Heat flux profile of detail 3, scenario A and E	53
Figure 57. Pressure difference of detail 3, scenario A and E	54
Figure 58. Section of detail 4	56
Figure 59. Simulation model and temperature profile of scenario A of detail 4	57

Figure 60. Simulation model and temperature profile of scenario B of detail 4	57
Figure 61. Simulation model and temperature profile of scenario C of detail 4	58
Figure 62. Simulation model and temperature profile of scenario D of detail 4	58
Figure 63. Simulation model and temperature profile of scenario E of detail 4	58
Figure 64. Simulation model and temperature profile of scenario F of detail 4	59
Figure 65. Temperature profiles of the coldest point of interior surface temperature as a function.....	59
Figure 66. Heat flux of detail 4 of scenario A and E exterior temperature	60
Figure 67. Profile of pressure difference of scenario A and E of detail 4.....	60
Figure 68. Section of detail 5	62
Figure 69. Model and temperature profile of scenario A of detail 5, horizontal section	63
Figure 70. Model and temperature profile of scenario B of detail 5, horizontal section	64
Figure 71. Model and temperature profile of scenario C of detail 5, horizontal section	64
Figure 72. Model and temperature profile of scenario D of detail 5, horizontal section	64
Figure 73. Model and temperature profile of scenario E of detail 5, horizontal section.....	64
Figure 74. Model and temperature profile of scenario F of detail 5, horizontal section.....	64
Figure 75. Model and temperature profile of scenario A of detail 5, vertical section.....	66
Figure 76. Model and temperature profile of scenario B of detail 5, vertical section.....	66
Figure 77. Model and temperature profile of scenario C of detail 5, vertical section	66
Figure 78. Model and temperature profile of scenario D of detail 5, vertical section	66
Figure 79. Model and temperature profile of scenario E of detail 5, vertical section	67
Figure 80. Model and temperature profile of scenario F of detail 5, vertical section	67
Figure 81. Temperature profiles of the coldest point of interior surface as a function of exterior temperature of detail 5	67
Figure 82. Suggested scenario C: horizontal and vertical section of detail 5	68
Figure 83. Heat flux of detail 5: scenario A and E, horizontal section	69
Figure 84. Heat flux of detail 5: original scenario A and scenario E, vertical section	69
Figure 85. Pressure difference of detail 5, scenario A and E, horizontal section	70
Figure 86. Pressure difference of detail 5, scenarios A and E, vertical section	70
Figure 87. SketchUp model of the analyzed building	74
Figure 88. Energy certificate of case 1 with detailed calculaiton of thermal bridges.....	74
Figure 89. Energy certificate of case 2 with detailed calculation of thermal bridges.....	75
Figure 90. Energy certificate of case 3 with detailed calculation of thermal bridges.....	75
Figure 91. Vertical sections of a building in Habichergasse 20, Vienna	97
Figure 92. Facades of a building in Habichergasse 20, Vienna	98

Figure 93. Roof plan of a building in Habichergasse 20, Vienna.....	98
Figure 94. Plan of the first floor of a buiding in Habichergasse 20, Vienna	99

11 LIST OF TABLES

Table 1. Physical and thermal properties of typical insulation materials (AAAMSA 2001; FIXIT AG 2013; Gulf Perlite Manufacturers 2009; Griffith 1995).....	11
Table 2. Standard surface resistances and heat transfer coefficients (Ward 2006).....	28
Table 3. Critical temperature factors for avoiding mould growth in buildings (Ward 2006) ..	28
Table 4. Critical temperature factors for evaluating the risk of surface condensation (Ward 2006).....	28
Table 5. Temperature of boundary conditions.....	28
Table 6. Simulation scenarios	29
Table 7. Set of analyzed details	30
Table 8. Properties of FIXIT 222 Aerogel High Performance Plaster (FIXIT AG 2013).....	35
Table 9. Aerogel Insulating Plaster System Components (FIXIT AG 2013).....	37
Table 10. Thermal conductivity of air layers (BS EN ISO 6946)	38
Table 11. Material properties of detail 1	40
Table 12. U-values of detail 1 and its improvement after applied retrofit scenarios.....	43
Table 13. Other values and their improvement after applied measures of detail 1	44
Table 14. Material properties of detail 2	45
Table 15. U-values and its improvement for detail 2.....	49
Table 16. Other values and their improvement after retrofit measures of detail 2.....	49
Table 17. Material properties of detail 3	51
Table 18. U-values and its improvement after applied retrofit measures for detail 3	54
Table 19. Other values and their improvement after applied retrofit measures of detail 3	54
Table 20. List of material properties of detail 4	56
Table 21. U-value improvement of detail 4.....	61
Table 22. Improvements due to retrofit measures of detail 4	61
Table 23. Material properties of detail 5	62
Table 24. Material properties of detail 5	68
Table 25. U-values and its improvement after applied retrofit measures of detail 5	71
Table 26. Other values and their improvement after applied retrofit measures, horizontal section	71
Table 27. Other values and their improvement after applied retrofit measures, vertical section	71
Table 28. Input data for calculation of heat transfer coefficient, U_w of an old box window ...	72

Table 29. Input data for calculation of heat transfer coefficient of a new double-box window with inner insulating glazing	72
Table 30. Assumed values of construction elements	74
Table 31. Psi-values of construction elements in 3 calculation scenarios	74
Table 32. Results of Archiphysik calculation with improvement values (each scenario vs. scenario A)	76
Table 33. Results for details 1-5	78
Table 34. Specification of original window frames.....	93
Table 35. Specifications of original window frames.	94
Table 36. Construction data on Austrian building types (TABULA project)	95

12 APPENDIX

A. Heat transfer coefficient of double-box windows

1. Heat transfer coefficient of original double-box window

Glass layer (d=4 mm)

Heat transfer coefficients for each glazing layer are calculated with a following formula:

$$U_w = \frac{U_f \times A_f + U_g \times A_g + \Psi \times l_g}{A} \quad (7)$$

Table 34. Specification of original window frames.

Outer glass layer			Inner glass layer		
Glass U_g		$4.72 \text{ W} \cdot \text{m}^{-2} \cdot \text{K}^{-1}$	Glass U_g		$4.72 \text{ W} \cdot \text{m}^{-2} \cdot \text{K}^{-1}$
Average frame U_f		$2.80 \text{ W} \cdot \text{m}^{-2} \cdot \text{K}^{-1}$	Average frame U_f		$2.80 \text{ W} \cdot \text{m}^{-2} \cdot \text{K}^{-1}$
Glazing area A_g		1.84 m^2	Glazing area A_g		1.84 m^2
Wooden frame area A_f		0.93 m^2	Wooden frame area A_f		0.93 m^2
U-value of the layer		$4.08 \text{ W} \cdot \text{m}^{-2} \cdot \text{K}^{-1}$	U-value of the layer		$4.73 \text{ W} \cdot \text{m}^{-2} \cdot \text{K}^{-1}$

According to the standard EN ISO 6946, total U-value of a double-box window can be calculated. The formula is presented below:

$$U_w = \frac{1}{\frac{1}{U_{w1}} - R_{si} + R_s - R_{se} + \frac{1}{U_{w2}}} \quad (8)$$

where R_{si} – surface inside resistance

R_{se} – outside surface resistance

R_s – air space resistance

As a result, total U-value of original double-box window comprises:

$$U_w = \frac{1}{\frac{1}{4.079} - 0.13 + 0.179 - 0.04 + \frac{1}{4.7345}} = 2.15 \text{ W} \cdot \text{m}^{-2} \cdot \text{K}^{-1} \quad (9)$$

2. Heat transfer coefficient of retrofitted double-box window with inner insulating window

New insulating glass consists of 2 layers of glazing, each 4 mm thick and gas layer of Xenon 12 mm thick. Outer glazing layer is kept at its original state.

Heat transfer coefficients for each glazing layer are calculated with formula (7). All input parameters are combined in a Table 26 below.

Table 35. Specifications of original window frames.

Outer glass layer		Inner glass layer	
Glass U_g	$4.72 \text{ W} \cdot \text{m}^{-2} \cdot \text{K}^{-1}$	Glass U_g	$1.59 \text{ W} \cdot \text{m}^{-2} \cdot \text{K}^{-1}$
Average frame U_f	$2.80 \text{ W} \cdot \text{m}^{-2} \cdot \text{K}^{-1}$	Average frame U_f	$2.80 \text{ W} \cdot \text{m}^{-2} \cdot \text{K}^{-1}$
Glazing area A_g	1.84 m^2	Glazing area A_g	2.10 m^2
Wooden frame area A_f	0.93 m^2	Wooden frame area A_f	0.80 m^2
U-value of the layer	$4.08 \text{ W} \cdot \text{m}^{-2} \cdot \text{K}^{-1}$	U-value of the layer	$1.32 \text{ W} \cdot \text{m}^{-2} \cdot \text{K}^{-1}$

According to the standard EN ISO 6946, total U-value of a double-box window can be calculated. The formula is presented below:

$$U_w = \frac{1}{\frac{1}{U_{w1}} - R_{si} + R_s - R_{se} + \frac{1}{U_{w2}}} \quad (10)$$

where R_{si} – surface inside resistance

R_{se} – outside surface resistance


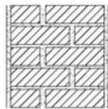
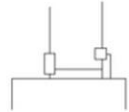

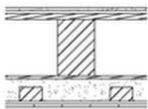
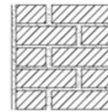
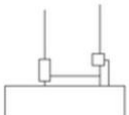
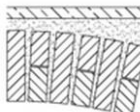
R_s – air space resistance

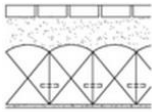
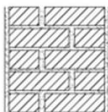
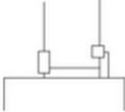

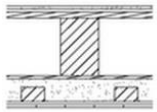
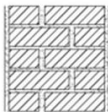
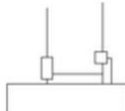
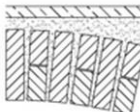
As a result, total U-value of original double-box window comprises:

$$U_w = \frac{1}{\frac{1}{1.321} - 0.13 + 0.179 - 0.04 + \frac{1}{4.079}} = 0.989 \text{ W} \cdot \text{m}^{-2} \cdot \text{K}^{-1} \quad (11)$$

B. Building matrix

Table 36. Construction data on Austrian building types (TABULA project)

Roof		Wall	Window	Floor
SFH (single-family house) Construction time till 1919				
	$U=1.4 \text{ W}\cdot\text{m}^{-2}\cdot\text{K}^{-1}$	$U=1.1 \text{ W}\cdot\text{m}^{-2}\cdot\text{K}^{-1}$	$U=2.2 \text{ W}\cdot\text{m}^{-2}\cdot\text{K}^{-1}$	$U=1.6 \text{ W}\cdot\text{m}^{-2}\cdot\text{K}^{-1}$
	tilted wooden roof, plastered, clay tile	solid brick wall	single glazing box-type windows	concrete ceiling
TH (terraced house) Construction time till 1919				
	$U=0.8 \text{ W}\cdot\text{m}^{-2}\cdot\text{K}^{-1}$	$U=1.1 \text{ W}\cdot\text{m}^{-2}\cdot\text{K}^{-1}$	$U=2.2 \text{ W}\cdot\text{m}^{-2}\cdot\text{K}^{-1}$	$U=0.71 \text{ W}\cdot\text{m}^{-2}\cdot\text{K}^{-1}$
	wooden ceiling with filling, wooden planks	solid brick wall	single glazing box-type windows	brick vault ceiling

MFH (multi-family house) Construction time till 1919				
	$U=1.95 \text{ W}\cdot\text{m}^{-2}\cdot\text{K}^{-1}$	$U=1.1 \text{ W}\cdot\text{m}^{-2}\cdot\text{K}^{-1}$	$U=2.2 \text{ W}\cdot\text{m}^{-2}\cdot\text{K}^{-1}$	$U=1.08 \text{ W}\cdot\text{m}^{-2}\cdot\text{K}^{-1}$
	wooden anchor beam ceiling with filling, wooden planks`	solid brick wall	single glazing box-type windows	Concrete ceiling
AB (apartment block) Construction time till 1919				
	$U=0.8 \text{ W}\cdot\text{m}^{-2}\cdot\text{K}^{-1}$	$U=1.1 \text{ W}\cdot\text{m}^{-2}\cdot\text{K}^{-1}$	$U=2.2 \text{ W}\cdot\text{m}^{-2}\cdot\text{K}^{-1}$	$U=0.71 \text{ W}\cdot\text{m}^{-2}\cdot\text{K}^{-1}$
	wooden ceiling with filling, wooden planks	solid brick wall	single glazing box-type windows	brick vault ceiling

The architectural cross-section shows two adjacent building volumes. On the left, the 'STRASSENTRAKT' features a multi-story structure with a pitched roof. A staircase labeled 'KERNROST MIT SCHUTZBLENDER 3 STÜCKE REINSTEIE Ø 90/60' is shown at the top. Floor levels are indicated by elevations such as DG 76.64, 3. ST 72.94, 2. ST 69.43, 1. ST 65.83, EG 62.07, and KG 59.60. On the right, the 'HOFTRAKT' also has a pitched roof and contains floors at DG 77.92, 3. ST 74.62, 2. ST 71.22, 1. ST 67.65, EG 64.05, and KG 60.60. A note specifies 'ABGEBEN DERLEGE IM BEREICH D. LEITUNGSRUH.' near the ground level. Both sections show vertical dimensions for room heights and overall building height, along with horizontal dimensions for widths.



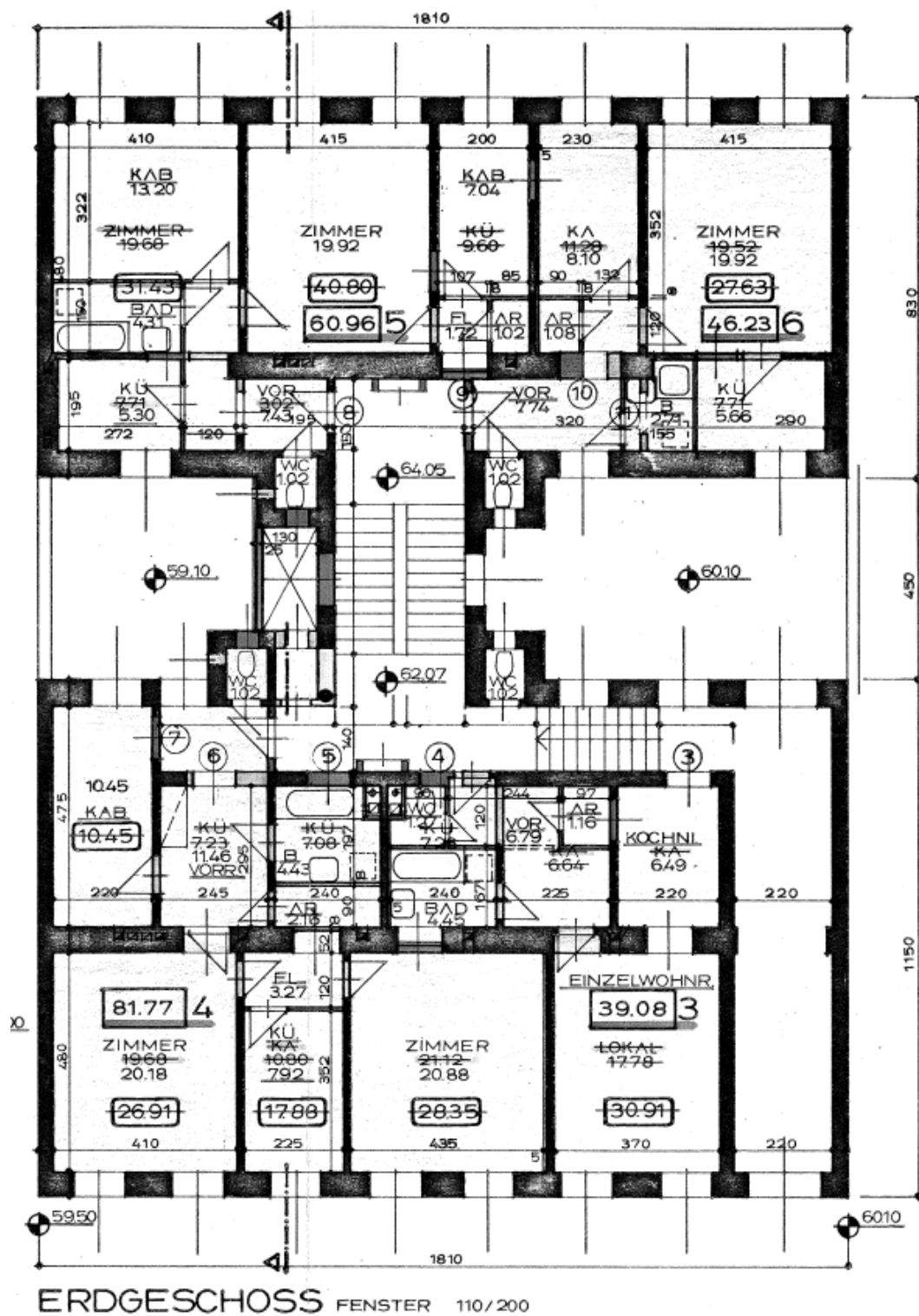


Figure 94. Plan of the first floor of a building in Habichergasse 20, Vienna